FINAL REPORT

PROJECT TITLE: "Nonlinear Optical Characterizations of II-VI Semiconductor Compounds for Device Applications"

PRINCIPAL INVESTIGATOR: Dr. Jin-Joo Song
Oklahoma State University

GRANT NO: MDA972-920J-1039

PROJECT PERIOD: 9/1/92 - 8/30/96

SPONSOR: DARPA

REPORT DATE: 2/18/97

FINAL REPORT

In this AASERT program, graduate students were trained in the area of laser investigations of wide gap semiconductor materials such as ZnSe-based quantum wells and III-nitride heterostructures. The goal of the program was to study nonlinear optical properties for opto-electronic device applications. Blue semiconductor lasers and optical modulators were of particular interest to us. We have recorded several first observations:

- first femtosecond coherent four-wave-mixing spectroscopy in ZnSe/ZnCdSe quantum wells.
- first observation of high order (up to 7th order) optical nonlinearities in ZnSe/ ZnCdSe quantum wells. In fact, this is the highest order susceptibility observed in any semiconductors.
- first observation of two-photon pumped blue lasing in ZnSe.
- first observation of above room temperature (up to 450k) lasing in GaN. The lasing threshold was found to be not very sensitive to temperature.

The reprints on the above work, as well as other publications resulting from the AASERT award, are attached in this report.

We also had extensive collaborations with MBE and MOCVD research groups including the following:

North Carolina State University (Prof. J.F. Schetzina), Notre Dame (Prof. J.K. Furdyna), Eagle-Picher Industries and Hiroshima University (Prof. T. Yao) in II-VI research; and

Honeywell, CREE and the University of Illinois (Prof. H. Morkoc) in III-nitrides work.

This award also resulted in a Ph.D. thesis of John Hays in the Department of Physics: "Linear and nonlinear spectroscopy of selected II-VI compound bulk and quantum-confined structures." In addition, students made numerous presentations at national and international conferences. (See the list of abstracts.)

The following are publications and abstracts related to the project "Nonlinear Optical Characaterizations of II-VI Semiconductor Compounds for Device Applications."

Publications:

"Nonlinear Optical and Transport Properties of CdMnSe and CdMnTe", B. Taheri, A. Munoz, R.C. Powell, J.J. Song, and J.K. Furdyna, Proc. SPIE, Nonlinear Optical Materials for Switching and Limiting, **2229**, 11 (1994).

"Femtosecond Four-wave-mixing Studies of Exciton Localization and Exciton-exciton Interaction in ZnSe/ZnCdSe Quantum Wells", A.J. Fischer, D.S. Kim, J. Hays, W. Shan, J.J. Song, D.B. Eason, J. Ren, J.F. Schetzina, H. Luo, and J.K. Furdyna, Phys. Rev. **B50**, 17643 (1994).

"Femtosecond Coherent Spectroscopy of Bulk ZnSe and ZnCdSe/ZnSe Quantum Wells", A.J. Fischer, D.S. Kim, J. Hays, W. Shan, J.J. Song, H. Luo, J.K. Furdyna, Z.Q. Zhu, T. Yao, J.F. Klem, and W. Schafer, Phys. Rev. Lett. **73**, 2368 (1994).

"Femtosecond Wave Mixing Experiments in ZnSe and ZnCdSe/ZnSe Quantum Wells", D.S. Kim, A.J. Fisher, J.M. Hays, W. Shan, J.J. Song, D.B. Eason, J. Ren, J.F. Schetzina, Z.Q. Zhu, T. Yao, and W. Schafer, Appl. Phys. Lett. **65**, 1534 (1994).

"Room Temperature Blue Lasing of ZnS_xSe_{1-x} Alloy by Photopumping", X.H. Yang, J.M. Hays, W. Shan, J.J. Song, E. Cantwell, and J. Aldridge, Appl. Phys. Lett. **60**, 926 (1992).

"Bound Exciton Luminescence in ZnSe Under Hydrostatic Pressure", W. Shan, J.M. Hays, X.H. Yang, J.J. Song, E. Cantwell, and J. Aldridge, Appl. Phys. Lett. **60**, 736 (1992).

"Optical Investigation of ZnSe Crystals Grown by Seeded Vapor Phase Transport Technique", J.M. Hays, W. Shan, X.H. Yang, J.J. Song, and G. Cantwell, Semicond. Sci. Technol. **7**, 1407 (1992).

"Two-photon Pumped Blue Lasing in Bulk ZnSe and ZnSSe", X.H. Yang, J.M. Hays, W. Shan, J.J. Song, and E. Cantwell, Appl. Phys. Lett. **62**, 1071 (1993).

"Optical Properties of Highly Strained CdSe/ZnSe Quantum Wells", W. Shan, S.J. Hwang, J.M. Hays, and J.J. Song, J. Appl. Phys. **74**, 5699 (1993).

"Determination of the Fundamental and Split-off Band Gaps in Zinc-blende CdSe by Photomodulation Spectroscopy", W. Shan, J.J. Song, H. Luo, and J.K. Furdyna, Phys. Rev. **B50**, 8012 (1994).

"Optical Studies of GaN and GaN/AlGaN Heterostructures on SiC Substrates", W. Shan, A.J. Fischer, J.J. Song, G.E. Bulman, H.S. Kong, M.T. Leonard, W.G. Perry, M.D. Bremser, and R.F. Davis, Appl. Phys. Lett. **69**, 740 (1996).

"Above Room Temperature Near Ultraviolet Lasing From an Optically Pumped GaN Film Grown on Sapphire", X.H. Yang, T.J. Schmidt, W. Shan, J.J. Song, and B. Goldenberg, Appl. Phys. Lett. **66**, 1 (1995).

"Room-temperature Stimulated Emission in GaN/AlGaN Separate Confinement Heterostructures Grown by Molecular Beam Epitaxy", T.J. Schmidt, X.H. Yang, W. Shan, and J.J. Song, Appl. Phys. Lett. **68**, 1820 (1996).

Abstracts:

"Femtosecond Four-Wave-Mixing Studies of Nearly Homogeneously Broadened Excitons in GaN", A.J. Fischer, G.H. Park, J.J. Song, D.S. Kim, D.S. Yee, R. Horning, and B. Goldenberg, QELS (1996).

"Strain Effects on Excitonic Transitions in GaN", W. Shan, R.J. Hauenstein, A.J. Fischer, J.J. Song, W.G. Perry, M.D. Bremser, R.F. Davis, and B. Goldenberg, MRS Fall Meeting, Boston, MA (1996).

"Picosecond Four-Wave-Mixing in GaN Epilayers at 532 nm", B. Taheri, J. Hays, J.J. Song, and B. Goldenberg, Conference on Lasers and Electro-Optics (CLEO), Ahaheim, CA, (1996).

"Optical Studies of GaN Epitaxial Films and GaN/AlGaN Heterostructures Grown on SiC Substrates", J.J. Song, W. Shan, G.E. Bulman, and J.A. Edmond, APS March Meeting, St. Louis, MO (1996).

"Recent Progress in AlGaN/GaN Laser Structures on 6Hi-SiC", G.E. Bulman, J.A. Edmond, V. Dmitriev, H.S. Kong, K. Irvine, and J.J. Song, SPIE Conference: Wide Band Gap Semiconductors: Lasers, LEDs and High-Temperature Devices", San Jose, CA (1995).

"Optically Pumped Near Ultraviolet Lasing in GaN Films Grown on Sapphire Substrates", T.J. Schmidt, X.H. Yang, W. Shan, B. Taheri, J.M. Hays, J.J. Song, and B. Goldenberg, Conference on Lasers and Electo-Optics (1995).

"Femtosecond Coherent Spectroscopy of Bulk ZnSe and ZnCdSe/ZnSe Quantum Wells", A.J. Fischer, D.S. Kim, J. Hays, W. Shan, J.J. Song, D.B. Eason, J. Ren, J.F. Schetzina, H. Luo, J.K. Furdyna, Z.Q. Zhu, and T. Yao, QELS Conference on Quantum Electronics and Laser Science, Anaheim, CA (1995).

"Femtosecond Four Wave Mixing in Bulk ZnSe and ZnCdSe/ZnSe Quantum Wells", A. J. Fischer, D.S. Kim, J. Hays, W. Shan and J.J. Song, APS March Meeting, San Jose, CA, Bull. Am. Phys. Soc. 40, 755 (1995).

"Room Temperature Picosecond Stimulated Emission from GaN Epilayers Grown on Sapphire", J. Hays, B. Taheri, X.H. Yang, T. Schmidt, and J.J. Song, APS March Meeting (1995).

"Femtosecond Coherent Spectroscopy of ZnCdSe/ZnSe Quantum Wells," A.J. Fischer, et al, OSA Annual Meeting Exhibit, 79, Dallas, TX (1994).

"Two-photon Spectroscopy of Homoepitaxy ZnSe/CdZnSe Quantum Wells", J.M. Hays, J.J. Song, J. Ren, and J.F. Schetzina, OSA Annual Meeting Exhibit, 112, Dallas, TX (1994).

"Optical Properties of Homoepitaxy CdZnSd/ZnSe MQW's Grown on ZnSe substrates", J.M. Hays, X.H. Yang, S.J. Hwang, W. Shan, J.J. Song, J. Ren, Z. Yu, and J.F. Schetzina, Bull. Am. Phys. Soc. **39**, 86 (1994).

"Above Room Temperature Optically Pumped Lasing in GaN at 382nm", T.J. Schmidt, X.H. Yang, W. Shan, and J.J. Song, Rare Earth Doped Optoelectronic Materials Workshop, June 16-17, Malibu, California (1994).

"Blue/Green ZnSe-ZnCdSe Light Emitting Diodes and Photo-Pumped Laser Structures Grown by MBE on ZnSe Substrates," X.H. Yang and J.J. Song, to be published in the proceedings of the Sixth International Conference on II-VI Compounds and Related Optoelectronic Materials, Newport, Rhode Island (1994).

"Nonlinear Optical and Transport Properties of CdMnSe and CdMnTe", B. Taheri, A. Munoz F., R.C. Powell, J.J. Song, and J.K. Furdyna, submitted to Nonlinear Optical Materials for Switching and Limiting, SPIE Conference, Los Angeles, CA (1994).

PROCEEDINGS REPRINT

SPIE–The International Society for Optical Engineering

Reprinted from

Nonlinear Optical Materials for Switching and Limiting

7–8 April 1994
Orlando, Florida

Volume 2229

Nonlinear Optical and Transport Properties of CdMnSe and CdMnTe

Bahman Taheri, A. Munoz F.*, Richard C. Powell** and Jin Joo Song
Center For Laser Research, Oklahoma State University
Stillwater, OK 74074

and

J.K. Furdyna
Department of Physics, University of Notre Dame
Notre Dame, IN 46556

ABSTRACT

Nonlinear optical and carrier dynamics of CdMnSe and CdMnTe were studied using picosecond pulses from a mode-locked, Q-switched Nd:YAG laser operating at 1064 nm. The study of the effects of free carriers on the refraction and absorption of a delayed probe beam resulted in the determination of the magnitude and sign of these nonlinearities for different Mn concentrations. It was found that at high carrier concentrations the magnitude of the nonlinear refraction coefficient is not constant and decreases with an increase in the electron concentration. The carrier dynamics were studied using forward propagating pulsed probe degenerate four wave mixing. The study was done for a number of different pump beam irradiances. A saturation in the diffraction efficiency was found at higher carrier concentrations. The lifetime of the electrons in the conduction band was determined by monitoring the lifetime of the free carrier absorption.

1 INTRODUCTION

II-VI semiconductors containing Mn belong to classification of the materials known as Diluted Magnetic Semiconductors (DMS). What sets these materials apart from other semiconductors containing transition metal ions is the large solubility of the Mn in the host. This leads to a continuous change in the lattice parameter and bandgap of these materials[1,2] . The enhanced magneto-optical properties of these materials have been extensively studied and for the most part understood. Their nonlinear optical properties, however, are less known. With this in

0-8194-1533-2/94/$6.00

mind, experiments were performed to determine the nonlinear optical and carrier dynamics of $Cd_{1-x}Mn_xTe$ and $Cd_{1-x}Mn_xSe$ samples with several Mn concentrations.

The nonlinear optical properties of semiconductors can be categorized as those arising from the bound electrons and those due to free carriers. The nonlinearities due to the bound electrons are instantaneous and will follow the temporal shape of the pulse. In the case of the third order susceptibility tensor, these result in the two photon absorption, β, and the bound electron nonlinear refraction, γ, coefficients. To a good approximation, these parameters have shown to be material bandgap dependent and their expected values have been estimated for a range of semiconductors[3,4] . Therefore, we shall focus on the effects of free carriers on the optical nonlinearities.

The paper will be divided into two sections; the first dealing with the nonlinear optical properties and the second with the carrier dynamics. The study was done using a mode-locked, Q-switched, Nd:YAG laser operating at 1.06 μm with a FWHM of 27 ps.

2 NONLINEAR OPTICAL PROPERTIES

The photon energy at this wavelength is smaller than the bandgap of the materials under investigation, and therefore free carrier generation takes place via two photon absorption. The generated carriers will then modulate the absorption coefficient and index of refraction of the material. Since these effects persist while the electrons remain in the conduction band, it is possible to monitor their effects after the excitation pulse has passed. If the number of generated carriers were known, it would be a relatively simple task to determine the changes induced by them. In particular, if the excitation pulse has a Gaussian intensity profile, the spatial profile of the generated electrons will be radial and the material will behave as an absorptive lens. The post sample spatial profile of a delayed probe beam can then be used to determine the effect of the carriers.

Figure 1 shows the experimental setup used to study the third order nonlinearities in our samples. The probe beam is delayed 100 ps from the pump beam to insure that there are no interactions between the beams. Both beams are passed through a $1m$ focal length lens and have the same beam radius of $590\mu m$ at the front surface of the sample. Each sample was placed 29cm behind the focal plane of the lens. The samples were 'thin' compared to the Rayleigh range of the beams ($\sim$30 times smaller) to insure applicability of the thin medium formalism.[5] The energy of the pump beam was varied by a waveplate-polarizer combination and that of the probe was kept fixed at a level where no self-induced optical nonlinearities were measurable. The apertures placed in front of the detectors are to monitor the total and the on-axis transmission of each beam. The detected energy at each meter was stored in a computer as a function of the input energy of the pump beam.

The amplitude, I, and the phase changes, ϕ, of the incident pump beam are given by[3]:

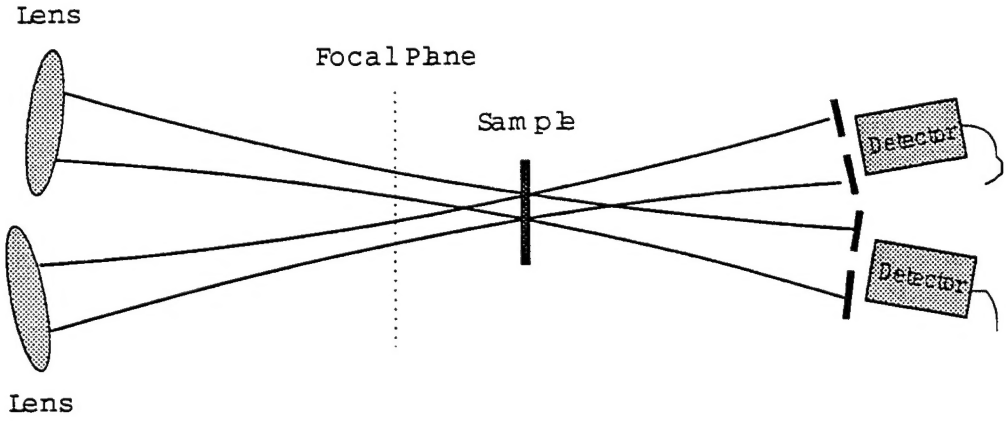

Figure 1: Experimental setup for measuring the nonlinear optical properties.

$$\frac{dI}{dz} = -\alpha I - \beta I^2 - \sigma N I \tag{1}$$

$$\frac{d\phi}{dz} = k(\gamma I + \sigma_r N) \tag{2}$$

where for the laser photon energies ($\hbar\omega < E_{gap}$) the carrier concentration, N, is given by:

$$\frac{dN}{dt} = \beta \frac{I^2}{2\hbar\omega} \tag{3}$$

Here, k is the wave vector of the incident pump beam, α is the absorption coefficient of the material, σ is the free carrier absorption cross section, and σ_r is the nonlinear refraction coefficient of the free electrons. In Eq. 3 any recombination of the carriers is neglected since the lifetime of the carriers are much greater than the 27 ps pulsewidth of the laser. A similar set of equations can be used for the delayed probe beam. However, any changes of the probe beam amplitude and phase are a result of the pump beam generated free carriers. In terms of the above equation, this means contributions from the σN and $k\sigma_r N$ terms only. From Eq. 2 we see that the concavity of the induced absorptive lens is given by the sign of the phase change. In general, these coupled equations have to be solved numerically. The field at any plane past the sample can, then, be calculated by a zeroth order Hankel transform of the field at the exit plane.[6]

Figures 2 (a) and (b) show the transmission coefficients of the pump and probe beams obtained in a fully open aperture experiment performed on CdTe. In this case, changes in the phase front will not affect the results and the changes in the transmission coefficients are solely due to the two

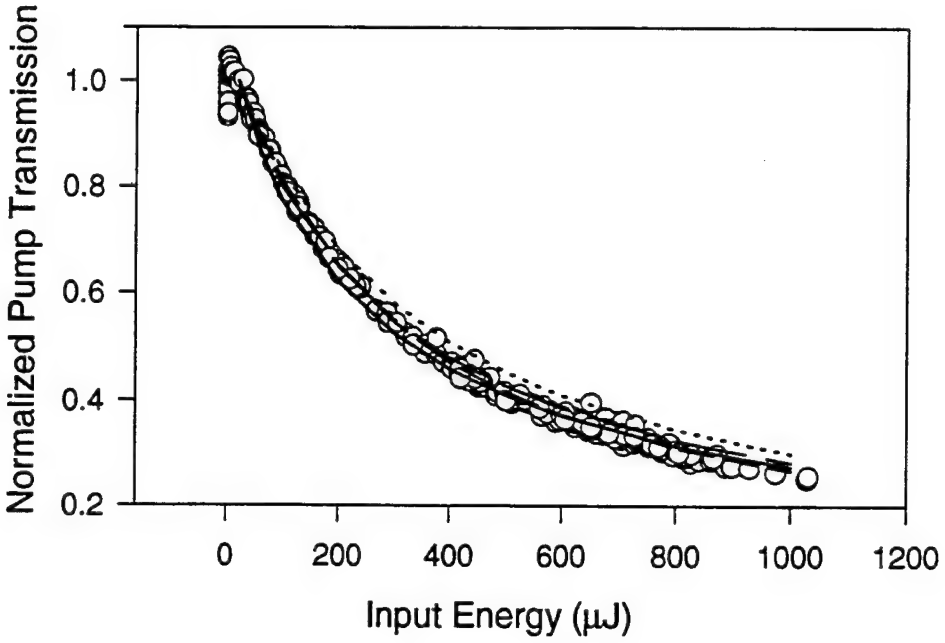

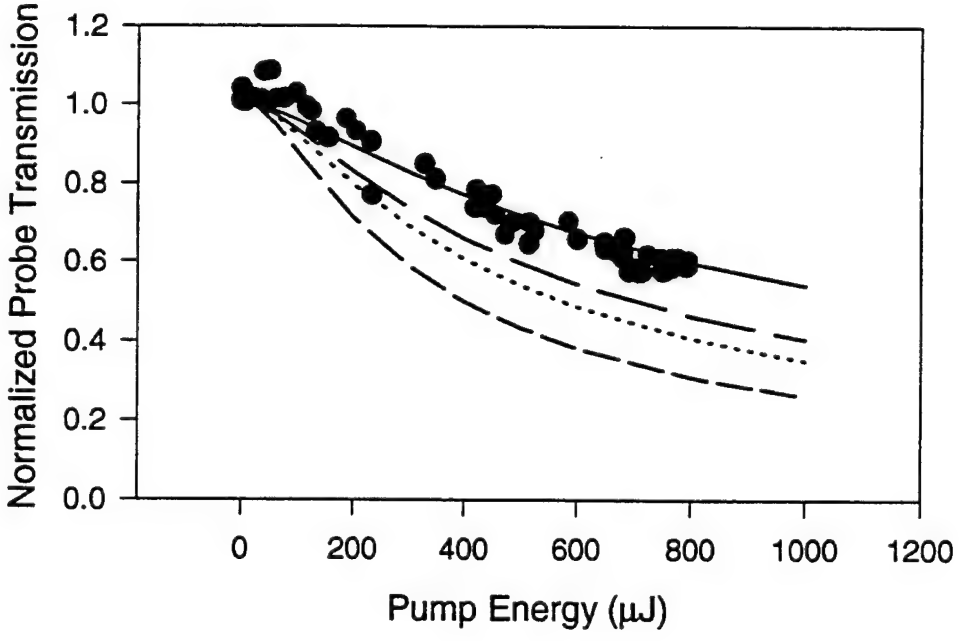

Figure 2: Results of the open aperture experiment on CdTe for (a) Pump beam and (b) Probe beam. The circles are the data points and the lines are the solutions of Eqs. 1-3 at the detectors.

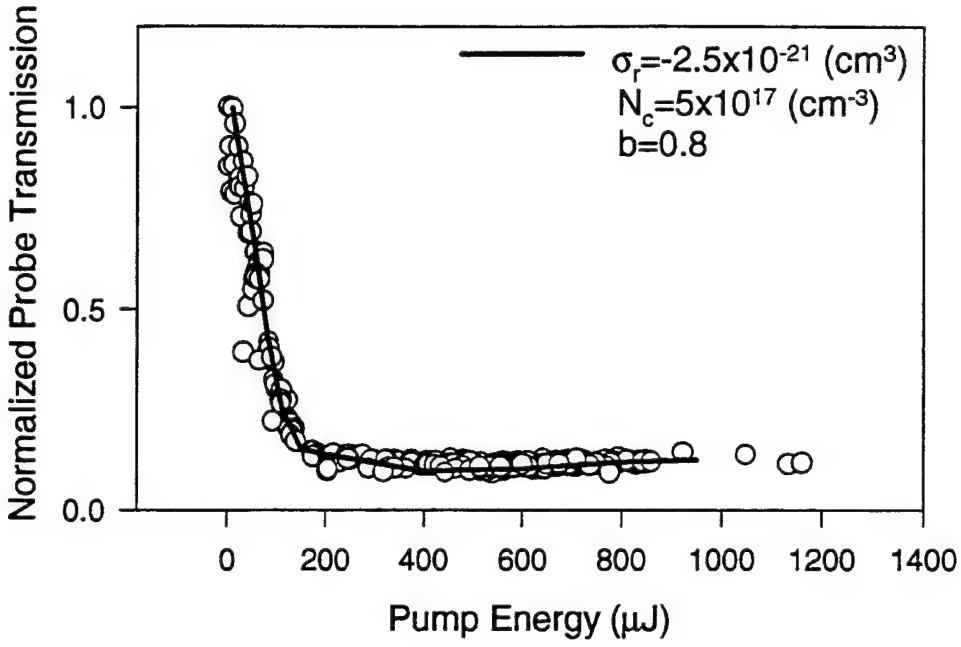

Figure 3: Results of the closed aperture experiment on CdTe for the probe beam. The fit was obtained using Eq. 6 for σ_r.

photon and free carrier absorption coefficients. For the probe beam, these changes are a result of the free carrier absorption only. The lines in the graphs correspond normalized transmission of the pump and probe beams for various values of β and σ. While it is apparent that a "fit" to the pump beam transmission can be obtained for a number of β and σ values, use of both graphs will uniquely determine each coefficient.

Figure 3 shows the normalized transmission coefficient of the probe beam obtained in a small aperture experiment performed on CdTe. Here, the relevant parameters for the probe beam are σ (which was determined earlier) and σ_r. Comparing the probe transmissions in figures 3 and 2 , we see that the probe transmission decreases more rapidly in the small aperture experiment than in the case of an open aperture experiment. This suggests that the free carriers induced lensing behaves as a negative lens. However, the sharp saturation in the transmission coefficient could not be described by Eq. 1 - 3. In particular, a fit could only be obtained if the value of σ_r were to decrease with an increase in the pump beam energy or, in other words with carrier concentration. We believe that this is due to the dependence of the effective mass on the carrier concentration. This is to be expected since at high electron concentrations, states higher than the bottom of the conduction band are occupied. It has been shown that the effective mass of the electrons has an energy dependence given by[7]:

$$m^* = m_o^*(1 + 2\frac{E - E_c}{E_{gap}}) \tag{4}$$

with $E - E_c \approx E_f$, where E_f is the Fermi energy. When carrier concentrations exceed a critical value, N_c, the quasi-Fermi level will be within the conduction band and thus the effective mass of the carriers will differ from the dilute case. In general, the location of the Fermi level with respect to the bottom of the band is dictated by the Fermi integral[8] but for our case it can be approximated by $E_f \approx a(\ln(N/N_c))^2$. This means that the effective mass of electrons are given by:

$$m^* = m_o^*(1 + b(\ln(N/N_c))^2) \tag{5}$$

which implies that:

$$\sigma_r = \left\{ \begin{array}{ll} \sigma_{ro} & for\ N < N_c \\ \frac{\sigma_{ro}}{1+b(\ln(N/N_c))^2} & for\ N \geq N_c \end{array} \right\} \tag{6}$$

Using the above, we noticed that the slope of the transmission coefficient for $N < N_c$ was dictated by σ_{ro} and the saturation level was determined by b and N_c values. The values for b and N_c obtained using the fit correspond well to the expected values for these parameters.

3 CARRIER DYNAMICS

The decay of the nonlinear optical behavior described above is dictated by the electron recombination time and diffusion coefficient. To study these properties, we used a forward propagating laser induced grating technique. The probe beam was at an angle of 2^o to the plane of the pump beams. The scattered and the transmitted probe will, therefore, be out of the plane of the pump beams which allows for the detection of the total energy in them. The energy ratio between the two pump beams was kept at 1:1 and they were focused to a $1mm$ radius and crossed at the sample. The crossing angle for the two pump beams, 2θ, was 9.5^o, which corresponds to a grating spacing of $6.5\ \mu m$. The probe beam energy was kept constant and had a beam radius of $0.3mm$ at the sample. The smaller radius of the probe helps minimize any effects arising from the Gaussian nature of the pump beam spatial profile. The energy of the transmitted and the scattered probe beam was monitored by two LaserPrecision energy meters. This was done as a function of the pump beam energy and the probe beam delay.

The scattering efficiency, η, of a light, scattering from a sinusoidal grating is given by[9]:

$$\eta = e^{-(\alpha+\Delta\alpha)z/\cos\theta}\{\sin^2(\frac{\pi z}{\lambda\cos\theta}\Delta n_o) + \sinh^2(\frac{z}{4\cos\theta}\Delta\alpha_o)\} \tag{7}$$

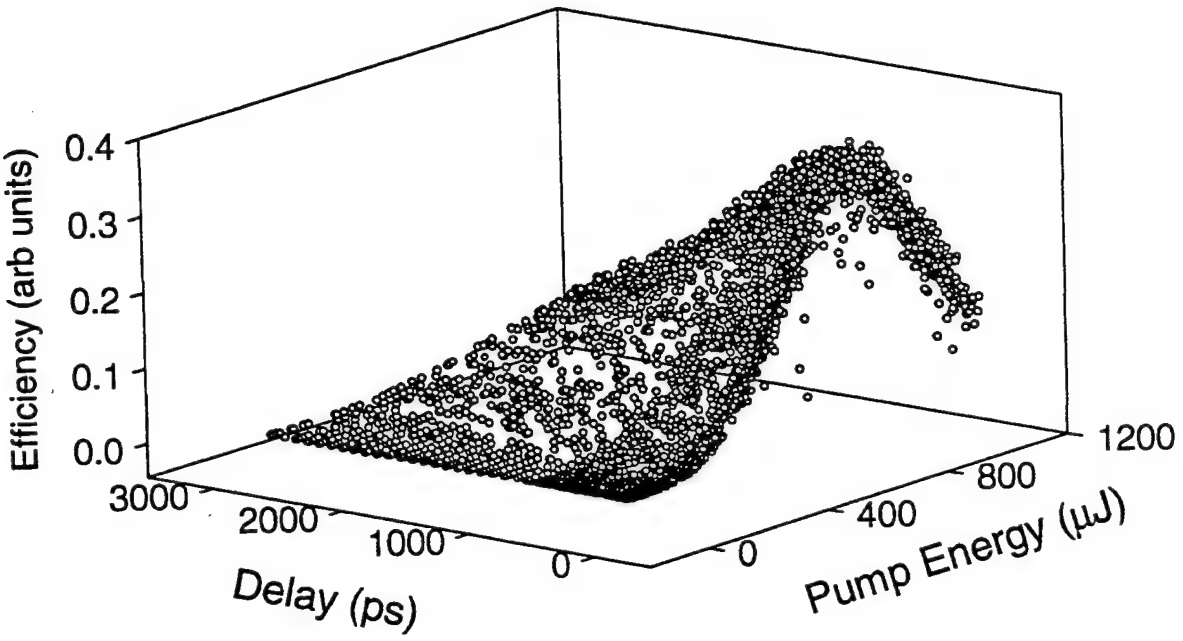

Figure 4: Scattering efficiency of the probe beam as a function of the pump beam energy and probe beam delay.

where $\triangle n$ and $\triangle \alpha$ are related to the free electrons through σ_r and σ, respectively. Any time dependence of the scattering enters the equation through the time dependence of the free carriers. This is determined by the diffusion equation[10]:

$$\frac{\partial N}{\partial t} = -\frac{N}{\tau(N)} + \nabla(D(N)\nabla N) \tag{8}$$

where, in general, the lifetime, τ, and the diffusion coefficient, D, are carrier concentration dependent. For the case of excitation through two photon absorption, we expect that the carrier concentration be small enough to ignore these higher order terms. However, for the sake of completeness, these terms were included.

Figure 4 shows the scattering efficiency of the probe beam as a function of the delay and the pump beam energy for CdTe. There are two interesting time regimes to be considered, (i) delay=0 and (ii) delay > 0. In the first case, we see that the scattering efficiency increases with

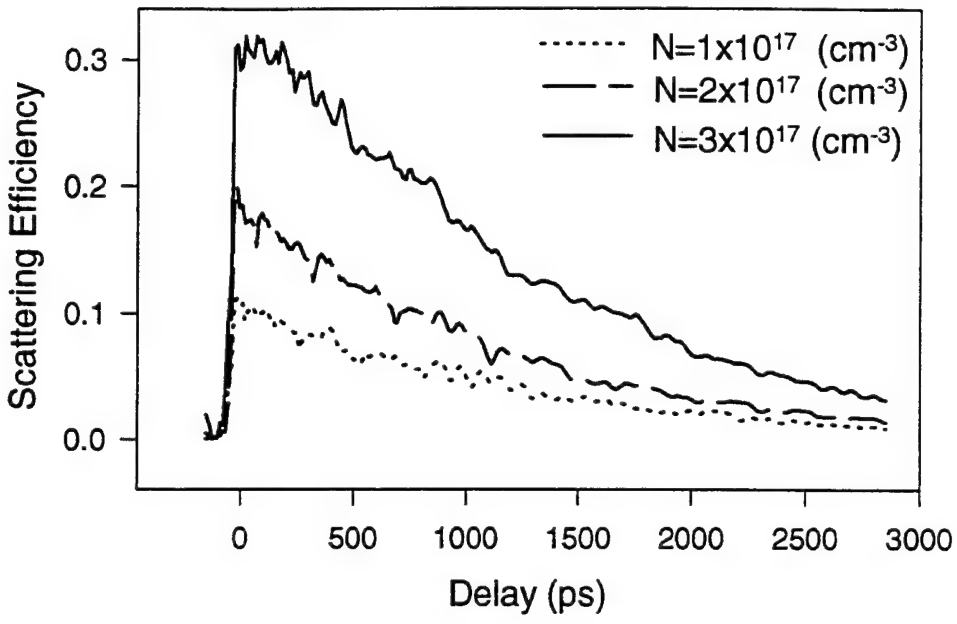

Figure 5: Scattering efficiency of the probe beam as a function of the delay for a number of pump generated carrier concentrations.

the pump beam energy followed by saturation and a subsequent decrease in the scattered signal. This behavior is typical for scattering from a phase grating (first term in Eq. 7). In a highly degenerate semiconductor, however, the contributions from the absorption grating (second term in Eq. 7) can be significant. Furthermore, these contributions may oppose those due to a pure phase grating.[10] To elucidate the significance of the absorption grating, using the results of the preceding section, carrier concentrations in the peaks of the grating were determined for this geometry. These calculations predicted carrier concentrations of $0 - 4 \times 10^{17}$ cm^{-3} in these regions. At these levels any contribution from the absorption grating can be neglected. A fit to the zero delay efficiency confirmed this result as well as yielding a value of 2.6 for the magnitude of σ_r, in excellent agreement with the value found earlier.

Figure 5 is a plot of the time dependence of the scattering efficiency for a number of pump generated carrier concentrations. From Eq. 8, an exponential decay of the grating is expected with the decay time, τ_g, dictated by the recombination lifetime of the carriers and the ambipolar diffusion coefficient[10] . Substitution of this result into Eq. 7 predicts a time dependence for the scattering efficiency of the form $\eta(t) \sim \sin^2(a \exp(-t/\tau_g))$. For small values of a, this reduces to the familiar exponential decay. This is in accordance with the observed time behavior presented in Fig. 5.

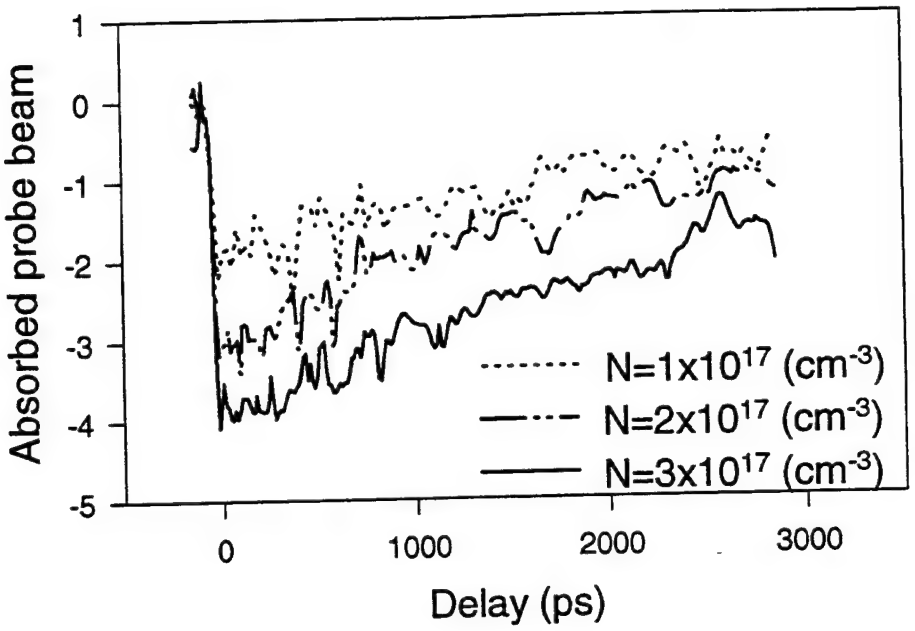

Figure 6: Loss in the probe beam energy vs delay for different carrier concentrations.

It is possible to determine the recombination lifetime of the carriers from the time dependence of the total probe beam energy emerging from the sample. From Eq. 7 we see that attenuation of the probe beam can occur by (i) scattering in the Bragg direction and (ii) absorption by the carriers. The latter will be present for the scattered beam also, and is insensitive to the spatial nature of the carrier concentration. Furthermore, this absorption persists throughout the duration that the electrons are in the conduction band. Therefore, by monitoring the total energy of the post sample probe beam, scattered + transmitted, as a function of time, it is possible to determine the carrier lifetime. Figure 6 shows the total probe energy after the sample vs. time for different carrier concentrations. The time dependence of the signal has no saturation effects, which further emphasizes that the saturation observed in the FWM scattering efficiency was not caused by a saturation in the generated free carriers. This graph was used to determine the lifetime of the electrons in the band. It was found that for the concentrations reached the decay, τ, was a constant.

4 SUMMARY

Table I is a summary of the measured parameters for each samples. There are a few points of interest. First, the two photon absorption, β, and the nonlinear refraction, σ_τ, coefficients

Table 1

Material	Thickness (mm)	$\beta(cm/GW)$	$\sigma(10^{-18}cm^2)$	$\sigma_{ro}(10^{-21}cm^3)$	$\tau(ns)$
CdSe	0.695	35	5	-2.7	4.4
$Cd_{0.9}Mn_{0.1}Se$	0.695	20	5	-1.5	7.0
$Cd_{0.8}Mn_{0.2}Se$	0.695	15	5	-2.0	12.0
$Cd_{0.7}Mn_{0.3}Se$:In	0.695	10	5	-1.1	2.2
$Cd_{0.6}Mn_{0.4}Se$	0.695	2.5	5	-0.6	71.4
CdTe	0.802	20	20	-2.5	4.8
$Cd_{0.9}Mn_{0.1}Te$	0.980	15	13	-2.5	*
$Cd_{0.6}Mn_{0.4}Te$	2.46	6.5	5	-0.75	*

* Signal insufficient for accurate determination

decrease with an increase in the Mn concentration. This is to be expected, since addition of Mn will result in an increase in the bandgap of the DMS and these coefficients are inversely proportional to the bandgap. Secondly, the free carrier absorption cross section remained constant for $Cd_{1-x}Mn_xSe$ but decreased for $Cd_{1-x}Mn_xTe$. The origin of this is not known but it may be related to the strain present in $Cd_{1-x}Mn_xTe$ due to addition of Mn. Finally, the recombination lifetime of $Cd_{1-x}Mn_xSe$ increased with the Mn concentration with the exception of $x = 0.30$ value, which may be due to presence of In in these samples. Furthermore, from the fits it was concluded that for the carrier concentrations achieved ($\sim 10^{17}\ cm^{-3}$), the concentration dependence of the recombination lifetime plays an insignificant role in the recombination process.

5 ACKNOWLEDGEMENTS

This work was supported by the Army Research Office (at Oklahoma State) and by National Science Foundation MRG program (at Notre Dame). The authors would like to thank Dr. P. Becla for providing some of the CdMnTe samples.

* Department of Physics, Universidad Autonoma Metropolitana, Mexico City, Mexico.

**Optical Sciences Center, University of Arizona, Tucson, AZ 85721.

6 REFERENCES

[1] J.K. Furdyna, "Diluted magnetic semiconductors", *J. Appl. Phys.*, **64**, R29-R64, 1988.

[2] See for example, *Semiconductors and Semimetals*, R.K. Willardson and A.C. Beer, Treatise Editors; J.K. Furdyna and J. Kossut, Volume Editors, (Academic, Boston, 1988), vol. **25**.

[3] E.W. Van Stryland, H. Vanherzeele, M.A. Woodall, M.J. Soileau, A.L. Smirl, S. Guha and T.F. Boggess, "Two photon absorption, nonlinear refraction, and optical limiting in semiconductors", *Optical Engineering*, **24**, 613-623, 1985.

[4] M. Sheik-Bahae, D.C. Hutchings, D.J. Hagan and E.W. Van Stryland, "Dispersion of Bound Electronic Refraction in Solids", *IEEE J. Quantum Electron*, **27**, 1296-1309, 1991.

[5] D. Weaire, B.S. Wherrett, D.A.B. Miller, and S.D. Smith, "Effect of low-power nonlinear refraction on laser beam propagation in InSb", *Opt. Lett.*, **4**, 331-333, 1974.

[6] M. Born and E. Wolf, *Principles of Optics*, (Pergamon Press, Oxford, 1980).

[7] W. Zawadzki, in *Handbook on Semiconductors, vol 1: Band Theory and Transport Properties*, T.S. Moss and W. Paul, Editors, (North Holland, Amsterdam, 1980).

[8] K.W. Boer, *Survey of Semiconductor Physics*, Van Nostrand Reinhold, New York, 1990.

[9] H.J. Eichler, P. Gunter and D.W. Pohl, *Laser-Induced Dynamic Gratings*, (Springer-Verlag, New York, 1986).

[10] H.J. Eichler, F. Massmann,"Diffraction efficiency and decay times of free-carriers gratings in silicon", *J. Appl. Phys.*, **53**, 3237-3242, 1982.

PHYSICAL REVIEW B VOLUME 50, NUMBER 23 15 DECEMBER 1994-I

Femtosecond four-wave-mixing studies of exciton localization and exciton-exciton interaction in $ZnSe/Zn_xCd_{1-x}Se$ quantum wells

A. J. Fischer, D. S. Kim,* J. Hays, W. Shan, and J. J. Song
Center for Laser Research and Department of Physics, Oklahoma State University, Stillwater, Oklahoma 74078

D. B. Eason, J. Ren, and J. F. Schetzina
Department of Physics, North Carolina State University, Raleigh, North Carolina 27695

H. Luo and J. K. Furdyna
Department of Physics, University of Notre Dame, Notre Dame, Indiana 46556
(Received 16 August 1994)

Femtosecond degenerate four-wave-mixing experiments are performed in the two-beam self-diffracted geometry in two inhomogeneously broadened $ZnSe/Zn_xCd_{1-x}Se$ multiple-quantum-well samples at the excitonic resonances at 10 K. A large change in the dephasing time across the linewidth of one sample is observed, whereas it is nearly constant in the other, implying a different degree of localization in these two samples. Exciton-exciton interaction rates are determined across the linewidth, and it is shown that the exciton-exciton interaction rate is much less for excitons that are strongly localized compared to those that are extended.

When the excitonic resonance of a quantum well (QW) is optically excited with an ultrafast laser pulse, the excitons in the material rapidly begin to lose their phase coherence. This phase coherence is lost due to scattering with phonons, free carriers, impurities, or other excitons. Using coherent transient four-wave mixing (FWM), interaction rates, such as exciton-acoustic phonon or exciton exciton, can be determined by measuring the dephasing time under appropriate conditions. This dephasing time can be long for an exciton with a wave function that is confined to some spatial region, whereas an exciton with an extended wave function tends to dephase more rapidly.[1] Many experimental techniques are sensitive to exciton localization including resonant Raleigh scattering,[2] wave mixing,[3,4] and spectral hole burning.[3,5]

In semiconductor QW's, well width fluctuations can lead to inhomogeneous broadening of the excitonic transition.[6] By using chemical lattice imaging, this type of well width fluctuation has been observed in $GaAs/Al_xGa_{1-x}As$ QW's.[7] Depending on the dimension of the well width fluctuation relative to the exciton diameter or intrinsic coherence length, excitons on the low-energy side of the transition can be affected by the potential well created by the well width fluctuations.[1-4,8,9] One mechanism for the dephasing of localized excitons is by phonon-assisted migration. During this process an exciton loses its phase coherence by absorbing or emitting an acoustic phonon while hopping to another localization site.[10] Exciton interaction rates can also be affected by exciton localization. For example, exciton-exciton scattering may be reduced for localized excitons.

The multiple-quantum-well (MQW) samples used in this study were grown by molecular-beam epitaxy (MBE) to have six 50-Å layers of $Zn_{0.88}Cd_{0.12}Se$ as the well material and ZnSe for the barrier. The first sample (sample *A*) has a first heavy-hole linewidth of about 6-meV full width at half maximum (FWHM) near zero delay as determined by spectrally resolved FWM and linear absorption data. The second sample (sample *B*) has a somewhat larger FWM linewidth of about 10 meV near zero delay. Although the samples were grown to have similar parameters, the heavy-hole excitonic transitions in these samples differ in energy by about 45 meV. This energy difference is probably due to a slight difference in well widths and Cd concentrations between the two samples. The large linewidths of these samples as well as the relatively long decay times of FWM indicate that the heavy-hole excitonic transitions are predominantly inhomogeneously broadened.

In this paper, we have used the second harmonic of a self-mode-locked Ti:sapphire laser (100 fs) to perform fs FWM experiments in the two-beam, self-diffraction geometry in $Zn_xCd_{1-x}Se$ MQW samples near the excitonic resonances.[11,12] The time-integrated (TI) diffracted signal, in the direction $2\mathbf{k}_2$-$\mathbf{k}_1$, was measured as a function of delay T between the two pulses. Figure 1(a) shows a schematic representation of the experimental setup. A 0.6-m triple spectrometer was used to spectrally resolve the FWM signal.

Figure 1(b) shows typical TI and spectrally integrated measurements of the diffracted intensity as a function of delay for the two different samples. For an inhomogeneously broadened transition, the homogeneous linewidth is given by $\Gamma_{hom}=2\hbar/T_2$, where the dephasing time T_2 is four times the decay constant measured by FWM.[13] These two samples have similar dephasing times, but the line shape of the TI-FWM signal for each sample is very different. Sample *A* has a monoexponential decay with a decay time at 10 K of about 500 fs. This sample has only one well-defined decay time which indicates that the homogeneous linewidth is constant across the inhomo-

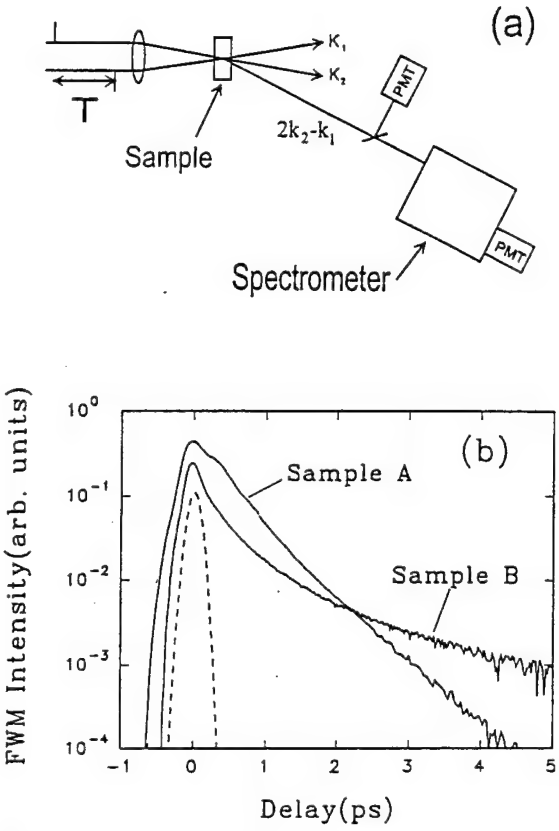

FIG. 1. (a) Schematics for the experimental setup; PMT denotes a photomultiplier tube. (b) FWM data shown for samples A and B at 10 K and $\approx 10^{12}$ cm^{-2}, along with the cross-correlation of the pulse shape (broken lines), obtained by up-converting the second harmonic with the primary infrared beam, generating a third harmonic.

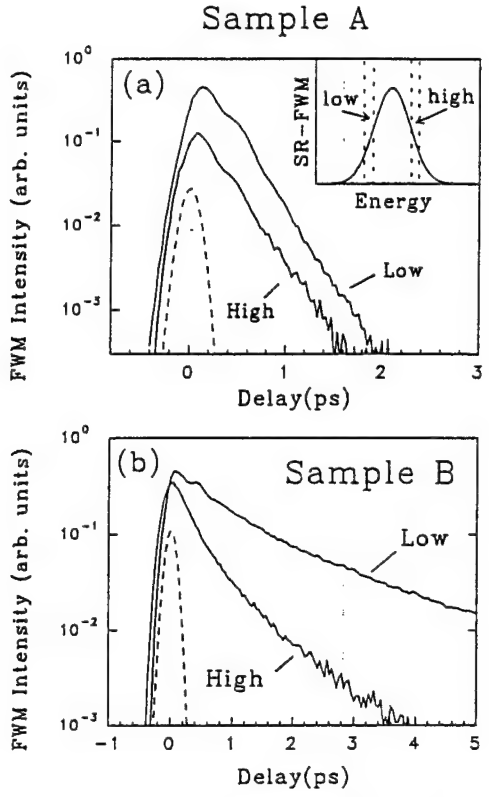

FIG. 2. (a) SR-FWM data for sample A at 10 K and $\approx 10^{12}$ cm^{-2} for energies above and below line center, as described in the inset. (b) SR-FWM data are shown for sample B for energies above (4 meV) and below (4 meV) the line center under similar conditions. Cross-correlated pulse shape is shown as broken lines.

geneous linewidth. Sample B, on the other hand, consists of many decay times and cannot be fit to a single exponential, suggesting that the excitonic transition is broadened in a more complicated manner. The data for sample B can be explained by assuming that the homogeneous linewidth is changing across the inhomogeneous linewidth. This interpretation is consistent with localization due to potential fluctuations from well width variations.

To further investigate the differences in these samples, the dephasing time of the excitons was also studied for various points across the inhomogeneous linewidth. For this study the exit slit of the spectrometer was used to select a bin of energy on the inhomogeneous linewidth. For our experimental apparatus, an energy bin size of 1 meV was required to give an acceptable signal-to-noise ratio. Typical data for each sample are shown in Figs. 2(a) and 2(b). Sample A shows very little change in the dephasing time as a function of energy. Sample B, on the other hand, shows a dramatic change in the decay rate for data above and below the exciton line center. Excitons on the high-energy side have a decay time of about 200 fs, whereas excitons on the low-energy side dephase with a characteristic time of 1 ps. Figures 3(a) and 3(b) show the decay rate plotted along with spectrally

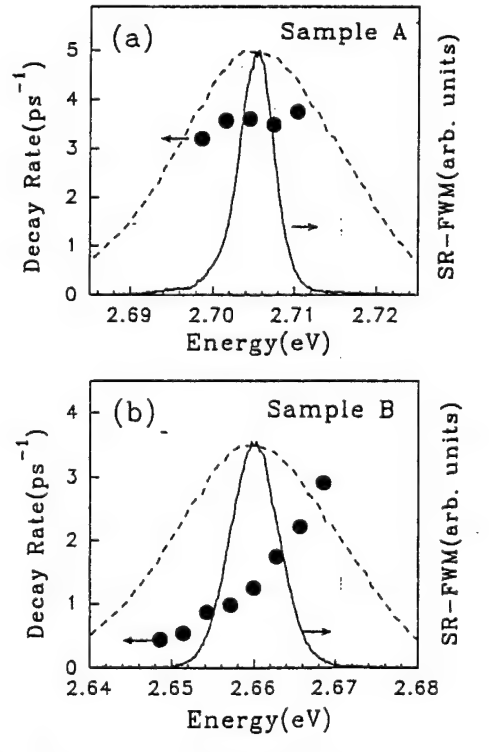

FIG. 3. Decay rate (1/decay time) for samples (a) A and (b) B plotted as a function of energy along with the SR-FWM line shapes at $T=0$. Broken lines denote spectral shapes of the exciting laser pulses.

resolved (SR)-FWM data for each sample. Although the large linewidth of sample A (6 meV) and the decay constant of ≈ 500 fs indicate that it is inhomogeneously broadened with a homogeneous linewidth of about 0.6 meV, very little change in the dephasing time was observed as a function of energy. On the other hand, for sample B, there exists nearly a factor of 10 change across the linewidth, implying that the excitons on the low-energy side are more localized.

A direct comparison of data from these samples is difficult, since the samples were grown at different times, on different MBE machines, and with different sample substrates (sample A on ZnSe; sample B on GaAs). One possible explanation for the difference is that one sample has much larger regions where the well width is constant. Sample B, with its larger linewidth and inherent substrate-induced strain, may have potential islands that are small enough in area in the plane of the well to more effectively localize excitons. Sample A, on the other hand, may have islands that are larger in spatial extent and hence localize the excitons to a lesser degree. However, as mentioned above, the large differences between the samples makes a comparison difficult. Next, exciton-exciton interaction for these samples is discussed.

In order to study exciton-exciton interaction, the exciton density must be estimated for a given laser power. One large source of error in estimating the exciton density results from inaccurate determination of the FWM focal spot size. In order to accurately determine our spot size, we placed a sensitive charge coupled device (CCD) detector designed for beam analysis in the focal plane of our lens where the beams overlap. A three-dimensional (3D) plot of the beam profile at this position is shown in Fig. 4(a). The spot diameter for these experiments at FWHM was 60 μm with $1/e^2$ of the energy within a 100-μm diameter. Our beam spot was slightly elliptical with a FWHM semimajor axis of 65 μm and a FWHM semiminor axis of 55 μm. With this accurate information on the photon density, the exciton density was estimated from linear absorption data.

Finally, the dephasing time for both samples was studied as a function of exciton density. As the exciton density increases, the excitons begin to dephase more rapidly due to collisions with each other. Since the binding energy for excitons in these samples is around 35 meV (Ref. 14) and the laser bandwidth is only 25 meV, the scattering due to free carriers is very small. Figure 4(b) shows the homogeneous linewidth as a function exciton density for both samples. Since sample A has a constant decay rate across the linewidth, we were able to use the spectrally integrated data in this density dependent measurement. However, for sample B, we measured the decay rate as a function of density above and below the exciton line center. Exciton-exciton interaction rates are determined by fitting the data using a least-squares fit to a linear density dependence given by[15]

$$\Gamma(N_{ex})=\Gamma_0+\alpha N_{ex} ,$$

where Γ_0 represents any residual phase coherence which decays via scattering mechanisms other than exciton-exciton scattering. For sample A, the exciton-exciton interaction rate α is 0.63 meV/10^{12} cm^{-2}. This value is in good agreement with values obtained by Hellmann *et al.* for CdTe/$Cd_{1-x}Mn_xTe$ MQW's.[16] For sample B, the exciton-exciton interaction rates are 0.93 and 0.11 meV/10^{12} cm^{-2} for energies above and below line center, respectively. It is clear from this fit, that for sample B, there is almost an order of magnitude difference in the interaction rates above and below the line center. These data show that excitons localized on the low-energy side interact much less than the more extended excitons on the high-energy side. Excitons that are more extended are expected to interact more strongly with each other. This is simply because extended excitons exist in a larger spatial region and, therefore, can interact more.

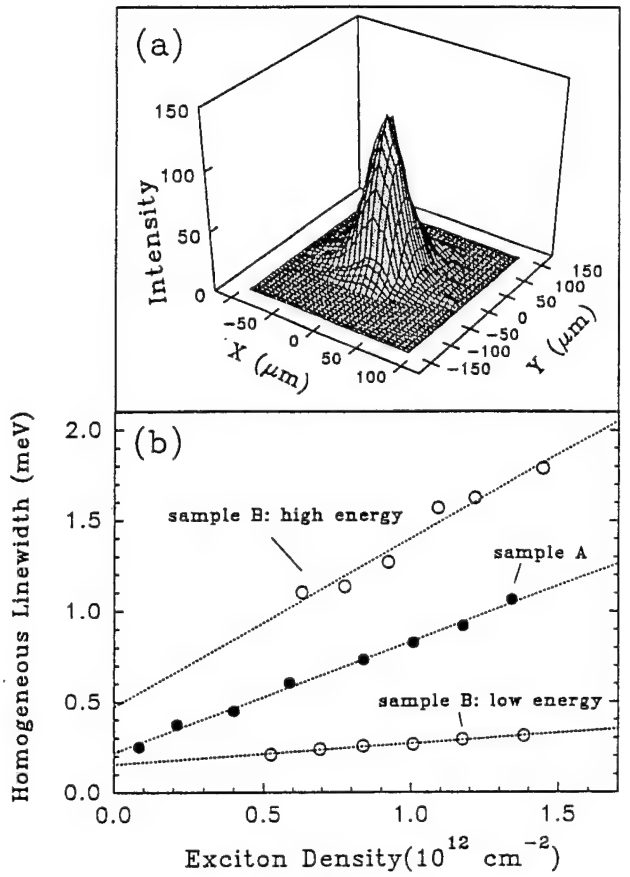

FIG. 4. (a) A 3D graph of the transverse beam profile at the region of overlap of the two beams obtained using a sensitive CCD camera. (b) Decay rate plotted as a function of exciton density for sample A (closed circles) using spectrally integrated FWM, and for sample B (open circles) using SR-FWM at 4 meV above and below the line center.

In conclusion, we have studied the dephasing times of two $Zn_xCd_{1-x}Se$/ZnSe MQW samples for various points across the inhomogeneous linewidth. Although both samples are inhomogeneously broadened, for one sample we observe a large change in dephasing time across the linewidth, while for the other sample, little change is observed. One explanation for this difference is offered in terms of exciton localization at potential fluctuations.

That is, for one sample the size of the islands in the plane of the well may be different than the other sample, resulting in a different degree of exciton localization. Exciton-exciton interaction rates are also accurately determined for these $Zn_xCd_{1-x}Se/ZnSe$ QW's. A difference in the exciton-exciton interaction rate above and below the line center is observed in one sample, indicating that localized excitons interact less strongly than extended excitons.

The work at Oklahoma State University was supported by ONR, ARPA, and OCAST. The work at University of Notre Dame was supported by NSF/MRG.

---

*Present address: Department of Physics, Seoul National University, Seoul 151, Korea.

[1]L. Schultheis, A. Honold, J. Kuhl, and K. Köhler, Phys. Rev. B **34**, 9027 (1986).

[2]J. Hegarty, M. D. Sturge, C. Weisbuch, A. C. Gossard, and W. Wiegmann, Phys. Rev. Lett. **49**, 930 (1982).

[3]J. Hegarty and M. D. Sturge, J. Opt. Soc. Am. B **2**, 1143 (1985).

[4]H. Wang and D. G. Steel, Appl. Phys. A **53**, 514 (1991).

[5]J. Hegarty and L. Goldner, Phys. Rev. B **30**, 7246 (1984).

[6]C. Weisbuch, R. Dingle, A. C. Gossard, and W. Weigmann, Solid State Commun. **38**, 709 (1981).

[7]A. Ourmazd, D. W. Taylor, and J. Cunningham, Phys. Rev. Lett. **62**, 933 (1989).

[8]S. T. Cundiff, H. Wang, and D. G. Steel, Phys. Rev. B **46**, 7248 (1992).

[9]M. D. Webb, S. T. Cundiff, and D. G. Steel, Phys. Rev. B **43**, 12 658 (1991).

[10]T. Takagahara, Phys. Rev. B **32**, 7013 (1985).

[11]Fischer *et al.*, Phys. Rev. Lett. **73**, 2368 (1994).

[12]Kim *et al.*, Appl. Phys. Lett. **65**, 1534 (1994).

[13]T. Yajima and Y. Taira, J. Phys. Soc. Jpn. **47**, 160 (1980).

[14]J. Hays and J. J. Song (unpublished).

[15]L. Shultheis, J. Kuhl, and A. Honold, Phys. Rev. Lett. **57**, 1635 (1986).

[16]R. Hellmann *et al.*, Phys. Rev. B **48**, 2847 (1993).

Femtosecond Coherent Spectroscopy of Bulk ZnSe and ZnCdSe/ZnSe Quantum Wells

A. J. Fischer, D. S. Kim,* J. Hays, W. Shan, and J. J. Song
Center for Laser Research and Department of Physics, Oklahoma State University, Stillwater, Oklahoma 74078

D. B. Eason, J. Ren, and J. F. Schetzina
Department of Physics, North Carolina State University, Raleigh, North Carolina 27695

H. Luo and J. K. Furdyna
Department of Physics, University of Notre Dame, Notre Dame, Indiana 46556

Z. Q. Zhu and T. Yao
Department of Electrical Engineering, Hiroshima University, Higash-Hiroshima, 724, Japan

J. F. Klem
Sandia National Laboratories, Albuquerque, New Mexico 87185

W. Schäfer
Hochstleistungsrechenzentrum Forschungszentrum, Jülich, W-5170 Jülich, Germany
(Received 26 April 1994)

Femtosecond two beam, self-diffraction experiments are performed in ZnSe and ZnCdSe/ZnSe quantum wells. Degenerate wave mixing signals from the third to the thirteenth order are easily visible to the naked eye, implying that nonlinear effects in this system may already be in the nonperturbative regime. Spectrally resolved data indicate that the nonlinearities originate entirely from the excitonic resonance. In addition, the existence of four-wave mixing signals in bulk ZnSe at negative time delay suggests that exciton-exciton interaction plays an important role. Exciton-phonon interaction rates are deduced as a function of temperature in ZnSe and ZnCdSe/ZnSe quantum wells.

PACS numbers: 78.47.+p, 42.50.Md, 42.65.−k, 78.30.Fs

It has been many years since strong nonlinearities in II-VI compounds were first recognized and studied, both theoretically and experimentally [1–5]. Recently, linear and nonlinear optical properties of excitons in II-VI compounds and their quantum wells (QW's) have attracted renewed attention [6–15], in part because of the development of blue-green lasers using wide band gap II-VI materials such as ZnSe and ZnCdSe QW's [16,17]. Another exciting development of recent years has been the increasing use of picosecond and femtosecond transient nonlinear spectroscopies in bulk semiconductors and QW's. In wide gap II-VI compound semiconductors, a large third order nonlinearity was reported in ZnSe using picosecond polarization spectroscopy [6], whereas femtosecond Faraday rotation has been used to investigate dephasing and spin relaxation in ZnSe-based magnetic QW's [7]. In CdTe, CdSe, and their QW's, four-wave mixing (FWM) has been used to investigate exciton-acoustic phonon and exciton-exciton interactions, as well as hot exciton relaxation [8–11].

Transient FWM has been extensively used to study interactions among many elementary excitations in III-V compounds such as GaAs and GaAs/AlGaAs QW's [18–21], while the origin of the optical nonlinearity itself has also been widely investigated [22–31]. It is now well established that the coherent exciton-exciton interactions and biexcitonic effects [22–29] play major roles in nonlinearities of GaAs QW's.

In this Letter, we have used the second harmonic of a self-mode-locked Ti:sapphire laser (100 fs, 76 MHz) to perform degenerate femtosecond two beam (with wave vectors $\mathbf{k}_1$ and $\mathbf{k}_2$), self-diffraction experiments in a ZnSe epilayer and ZnCdSe multiple quantum well (MQW) samples near excitonic resonances. The time-integrated (TI) diffracted signals were measured as a function of delay T between the two pulses. In a thin ZnCdSe/ZnSe sample (total ZnCdSe thickness is 300 Å), the diffracted signals are very strong and *easily visible to the naked eye all the way up to the thirteenth order signal.* This sample was molecular-beam epitaxy technique (MBE) grown on a ZnSe substrate (homoepitaxial) so as to perform transmission experiments without removing the substrate. By spectrally resolving (SR) the diffracted signals, we found that the FWM as well as higher order signals are completely dominated by the excitonic resonances in both ZnSe and ZnCdSe MQW's. In ZnSe, the existence of the FWM signal at negative time delays indicates that the *coherent exciton-exciton interaction* [1–5,30] plays an important role in nonlinearities. Furthermore, exciton-phonon interaction rates in bulk ZnSe and bulklike ZnCdSe MQW's are accurately determined using FWM.

Figure 1(a) shows diffracted signals observed from a $6 \times (Zn_{0.88}Cd_{0.12}Se/ZnSe$, 50 Å/250 Å) MQW sample grown on ZnSe (homoepitaxial) at $T = 200$ fs. For comparison, we show the third and fifth order signals from a GaAs MQW sample whose total well thickness is *10 times*

 0031-9007/94/73(17)/2368(4)$06.00

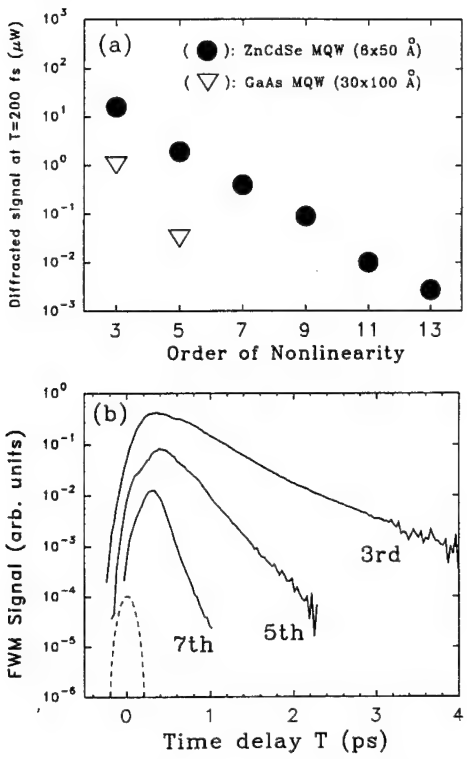

FIG. 1. (a) Average power (μW) of the diffracted signals at $T = 200$ fs and 10 K plotted against the order of nonlinearity for a 6 × ($Zn_{0.88}Cd_{0.12}Se$/ZnSe, 50 Å/250 Å) MQW grown on ZnSe (●), and for a GaAs MQW with 30 × (GaAs/$Al_{0.3}Ga_{0.7}As$, 100 Å/100 Å) (▽). The blue pulse shape (broken lines) is obtained by cross correlating the second harmonic with the primary infrared beam. The 100 fs pulses with an average power of 10 mW per beam are tuned to the HH resonance of the ZnCdSe MQW (2.71 eV) or to that of the GaAs MQW (1.56 eV). (b) Semilogarithmic plot of diffracted signals for the ZnCdSe MQW as a function of T. The experimental conditions are nearly identical to those of (a). The third, fifth, and seventh order signals are shown.

larger (3000 Å). This GaAs MQW was chosen since the absorption coefficient of GaAs is roughly 10 times less than that of ZnSe around the band edge [13], and also because T_2 is comparable to that of the ZnCdSe MQW. Therefore, the total number of photoexcited excitons in these two MQW's is expected to be comparable. The data were taken at 10 K with the exciting photon energy tuned near the heavy-hole (HH) excitonic resonance of each sample (1.56 and 2.71 eV for the GaAs and ZnCdSe MQW's, respectively) and with the average power of each beam at 10 mW. The diffracted signals from the ZnCdSe MQW decreases very slowly as the order of nonlinearity increases; the signal decreases only by a factor of ≈5 as we go to the next higher order. In contrast, *the signals from the GaAs MQW are much weaker and decay faster as the order increases so that only up to the fifth order signal is observed.*

The strong diffracted signals in this wide gap II-VI MQW are consistent with the elegant bond charge model [3–5] which predicts higher nonlinearities as the material becomes more polar. Furthermore, the stronger oscillator strength relative to GaAs QW's is also likely to lead to the large high order nonlinearities observed. Since the relative strength of the diffracted signal originating from coherent exciton-exciton interaction scales with $VT_2/\hbar$ [22–25] (V is the average interaction potential), it is expected that the larger binding energy of wide band gap II-VI compared with GaAs-based materials is also an important factor. Clearly, more detailed studies are needed to compare the nonlinearities of GaAs- and ZnSe-based QW's, while from an experimental point of view, nonlinear signals of ZnCdSe QW's are much stronger and easier to find than those of GaAs QW's, especially as the order of nonlinearity increases.

The striking results shown in Fig. 1(a) may imply that at this modest power density, nonlinear optics of the ZnCdSe MQW are already in the *nonperturbative regime,* while GaAs MQW can be treated by a more conventional perturbation approach. Theoretical investigation of our results in the ZnCdSe MQW using exact, nonperturbative semiconductor Bloch equations is currently in progress [31].

In Fig. 1(b), the third, fifth, and seventh order wave mixing signals from the same sample observed in the phase-matched directions of $2\mathbf{k}_2 - \mathbf{k}_1$, $3\mathbf{k}_2 - 2\mathbf{k}_1$, and $4\mathbf{k}_2 - 3\mathbf{k}_1$ are plotted as a function of T. The laser is tuned to the HH exciton resonance at 10 K. The fifth order signal decays faster than the third order FWM signal, and the seventh order signal, in turn, decreases even faster as a function of T. The reason for this faster decrease in the higher order diffracted signal as a function of T is that the diffraction of higher order signals involves additional multiplications of polarizations, resulting in faster decay [32]. More detailed theoretical studies on the high order diffracted signals are in progress [31].

The broad femtosecond pulses with the full width at half maximum (FWHM) of ≈25 meV used in our experiments can excite both the excitons and the free carriers, especially in ZnSe where the excitonic binding energy is ≈20 meV [14]. To determine the relative contributions of excitons and free carriers to the nonlinearities, we have investigated the spectral behaviors of the diffracted signals in both the ZnCdSe MQW and ZnSe sample. In Fig. 2, spectrally resolved signals at $T = 200$ fs for the third, fifth, and seventh order are plotted for both the ZnCdSe MQW and a ZnSe epilayer grown on GaAs (solid lines), along with the exciting laser spectra (broken lines). Sharp excitonic resonances dominate in all spectra shown here. No substantial free carrier contribution is observed. From these observations, we conclude that the excitonic contribution completely dominates FWM as well as higher order signals. The same phenomenon has been observed in GaAs QW's and was explained by much faster dephasing of free carriers relative to excitons [21].

Another interesting subject that has been widely investigated in III-V materials is whether or not the coherent exciton-exciton interaction plays an important role in nonlinearities of these systems. Existence of strong negative time delay signals can be an indication of this interac-

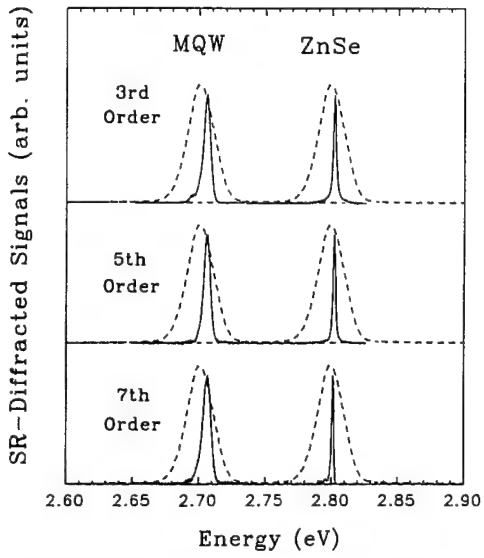

FIG. 2. SR-diffracted signals of the third, fifth, and seventh order for the 6 × ($Zn_{0.88}Cd_{0.12}Se$/ZnSe, 50 Å/250 Å) MQW and for a ZnSe epilayer. Experimental conditions are nearly identical to those of Figs. 1(a) and 1(b).

tion effect [1–4,30]. However, generally large inhomogeneous broadening in these II-VI samples, compared with GaAs QW's, makes it very difficult to observe negative time delay signals.

In Fig. 3(a), FWM signals of ZnSe are plotted at several temperatures. In this case, the relatively small linewidth (2.3 meV obtained from the SR FWM shown in Fig. 2) makes the observation of negative time delay signals possible; at low temperatures, there exist negative time delay signals far away from the pulse overlap region. Ideally, in homogeneously broadened excitons where the coherent exciton-exciton interaction plays an important role, there would be a factor of 2 difference in time constants: it would be $T_2/2$ for the positive time delay and $T_2/4$ for the negative time delay [1–4,30]. It is clear from Figs. 3(a) and 3(b) that the negative time delay signal indeed exists. Therefore, we can conclude that the coherent exciton-exciton interaction does play a role in FWM in bulk ZnSe. Whether or not coherent exciton-exciton interaction is the dominant contribution in bulk ZnSe, as it is in GaAs QW's [5], cannot be answered at this point because of relatively large exciton linewidth and inhomogeneous broadening (≈2 meV) in this epilayer in comparison to high quality GaAs or GaAs QW's (1 meV or less). In the ZnCdSe MQW, negative time delay signals were not observable due to even larger inhomogeneous broadening (≈6 meV measured by absorption and FWM). Nevertheless, the relative contribution from the coherent exciton-exciton interaction to FWM generally scales with the binding energies, and therefore, it is likely that coherent exciton-exciton interaction plays a major role in ZnCdSe MQW's.

We now discuss exciton-phonon interactions in bulk ZnSe and bulklike ZnCdSe, where only a lower limit

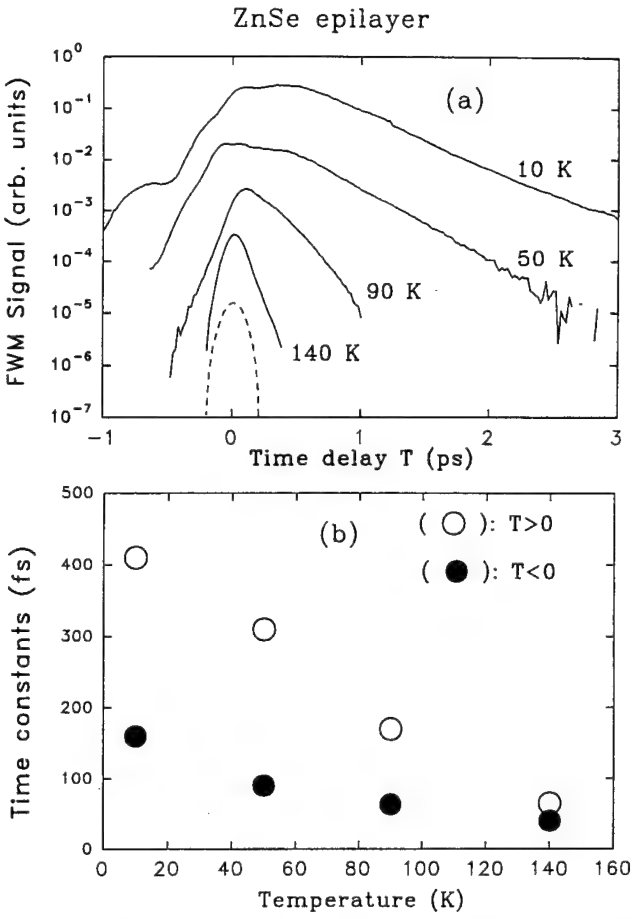

FIG. 3. (a) FWM signals near HH excitonic resonances at 10, 50, 90, and 140 K for the ZnSe epilayer, along with cross correlation of the pulse shape (broken lines) obtained by mixing the blue second harmonic with the primary infrared beam, generating the third harmonic. Negative time delay signals are clearly visible. (b) Time constants for negative (filled circles) and positive time delays (empty circles) at 10, 50, 90, and 140 K.

on the exciton-LO phonon interaction strength is available for bulk ZnSe in the literature [14]. In Fig. 4, the decay rates of TI FWM in the reflection geometry [33] are plotted as a function of temperature for bulk ZnSe (□), along with those of two QW samples: 3 × ($Zn_{0.88}Cd_{0.12}Se$/ZnSe, 300 Å/300 Å) grown on GaAs (▽) and a ZnSe/$Zn_{0.88}Cd_{0.12}Se$/ZnSe (500 Å) single QW grown on GaAs (○). Decay rates of all three samples show essentially identical behaviors with temperature. Two temperature ranges can be clearly seen: at low temperatures (< 70 K), the rate is roughly linear with T_L, whereas at T_L > 100 K, the slope is much larger, indicating that below 100 K, acoustic phonon-exciton interaction dominates dephasing, whereas at higher temperatures, the contribution by optical phonons becomes important.

Considering the large well widths of the two QW samples compared to the exciton radius, it is not surprising that they exhibit bulklike behavior in exciton-phonon interactions. Since both QW samples and the bulk ZnSe sample have nearly identical decay rates as a function

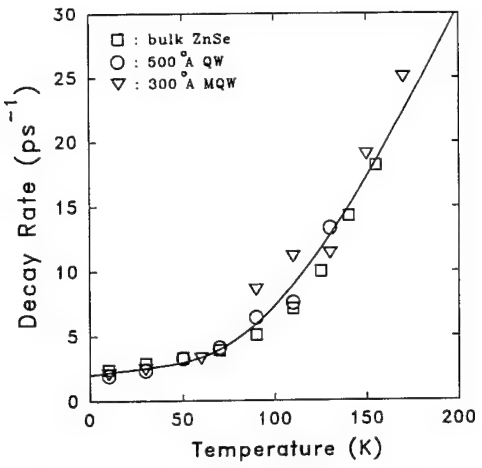

FIG. 4. The decay rates of FWM for a 3 × ($Zn_{0.88}Cd_{0.12}Se$/ZnSe, 300 Å/300 Å) MQW grown on GaAs (▽), a single ZnSe/$Zn_{0.88}Cd_{0.12}Se$/ZnSe (500 Å) single quantum well (○) grown on GaAs, and the ZnSe epilayer grown on GaAs (□). The fit corresponds to $\gamma = 11$ μeV/K, and $\Gamma_{LO} = 81$ meV (see text).

of temperature, we try to fit the decay rates of these three samples using a least squares fit with the following phenomenological equation [34]: decay rate $1/\tau = A + BT_L + C/\{\exp E_{LO}/k_BT_L) - 1\}$, where E_{LO} is the optical phonon energy and k_B is the Boltzmann constant. The constant A represents the contribution at $T_L = 0$, from impurities or interface roughnesses. BT_L is the contribution due to acoustic phonons, whereas the last term is the contribution from optical phonons. The best fit, represented by a solid line, is obtained with $A = 2.05 \pm 0.05$ ps^{-1}, $B = 0.017 \pm 0.003$ ps^{-1}/K, and $C = 127 \pm 13$ ps^{-1}. These values can be compared with much smaller values for a GaAs MQW of Ref. [21]: $B = 0.007$ ps^{-1}/K and $C = 21$ ps^{-1}. The large B and C values indicate that exciton-phonon interactions, especially the exciton-LO phonon interaction, are much stronger in ZnSe and ZnCdSe QW's than in GaAs quantum wells.

While A is simply an average of the decay rates of the three samples at $T_L = 0$, and therefore, contains little information, B and C can be used to obtain the phonon contributions Γ_{ph} to the homogeneous linewidth of excitons assuming $\Gamma_{ph} = \gamma T_L + \Gamma_{LO}/\{\exp(E_{LO}/k_BT_L) - 1\}$. The values for γ and Γ_{LO} are, from B and C, respectively, $\gamma = 11$ μeV/K and $\Gamma_{LO} = 81$ meV. In deriving these values, it is assumed that excitons are homogeneously broadened. This is a very good assumption at high temperatures and, therefore, Γ_{LO} is accurately determined this way. However, at low temperatures, these samples are only partially homogeneously broadened. Therefore, γ can be smaller than 11 μeV, as much as by a factor of 2. It should be noted that this factor of 2 and small errors in γ do not affect the value of Γ_{LO} since the decay rates at high temperature are almost entirely due to exciton-LO phonon interaction. $\Gamma_{LO} = 81$ meV is in agreement with those of wide MQW's and the lower limit to Γ_{LO} given for ZnSe (> 60 meV) in Ref. [14], whereas γ is very close to the value obtained for CdTe-based QW's using FWM [8].

In conclusion, we found very strong nonlinear signals, up to the thirteenth order (or 14-wave mixing), in femtosecond two-beam, self-diffraction experiments in ZnSe and ZnCdSe QW's. Nonlinear signals of higher order, as well as the FWM signal, are completely dominated by excitonic resonances, and the FWM signal in the negative time delays in ZnSe indicates that coherent exciton-exciton interaction plays an important role. The exciton-acoustic phonon and exciton-LO phonon interaction rates were determined for bulk ZnSe and two bulklike ZnCdSe QW samples.

This work was supported by ONR, ARPA, and OCAST. The work at University of Notre Dame was supported by NSF/MRG.

*Present address: Department of Physics, Seoul National University, Seoul 151, Korea.

[1] R. C. Miller *et al.*, Phys. Rev. Lett. **11**, 146 (1963).
[2] R. A. Soref and H. W. Moos, J. Appl. Phys. **35**, 2152 (1964).
[3] F. W. Scholl and C. L. Tang, Phys. Rev. B **8**, 4607 (1973).
[4] C. L. Tang and Chr. Flytzanis, Phys. Rev. B **4**, 2520 (1971).
[5] B. F. Levine, Phys. Rev. B **7**, 2600 (1973).
[6] T. Saiki *et al.*, Appl. Phys. Lett. **60**, 192 (1992).
[7] J. Baumberg *et al.*, Phys. Rev. Lett. **72**, 717 (1994).
[8] R. Hellmann *et al.*, Phys. Rev. B **48**, 2847 (1993).
[9] R. P. Stanley *et al.*, Phys. Rev. Lett. **67**, 128 (1991).
[10] H. Schwab *et al.*, Phys. Rev. B **44**, 3999 (1991).
[11] G. Noll *et al.*, Phys. Rev. Lett. **64**, 792 (1990).
[12] N. T. Pelekanos *et al.*, Appl. Phys. Lett. **61**, 3154 (1992).
[13] S. Adachi and T. Taguchi, Phys. Rev. B **43**, 9569 (1991).
[14] N. T. Pelekanos *et al.*, Phys. Rev. B **45**, 6037 (1992).
[15] P. C. Becker *et al.*, Phys. Rev. Lett. **68**, 1876 (1992).
[16] M. A. Hasse *et al.*, Appl. Phys. Lett. **59**, 1272 (1991).
[17] H. Jeon *et al.*, Appl. Phys. Lett. **59**, 3619 (1991).
[18] L. Schultheis *et al.*, Phys. Rev. Lett. **57**, 1635 (1986); *ibid*, 1797 (1986).
[19] J. Kuhl *et al.*, Adv. Solid State Phys. **29**, 157 (1990).
[20] D. S. Kim *et al.*, Phys. Rev. Lett. **68**, 2838 (1992).
[21] D. S. Kim *et al.*, Phys. Rev. Lett. **68**, 1006 (1992).
[22] K. Leo *et al.*, Phys. Rev. Lett. **65**, 1340 (1990).
[23] K. Leo *et al.*, Phys. Rev. B **44**, 5726 (1991).
[24] M. Wegener *et al.*, Phys. Rev. A **42**, 5675 (1990).
[25] D. S. Kim *et al.*, Phys. Rev. Lett. **69**, 2725 (1992).
[26] S. Weiss *et al.*, Phys. Rev. Lett. **69**, 2685 (1992).
[27] B. F. Feuerbacher *et al.*, Phys. Rev. B **43**, 2439 (1991).
[28] S. Bar-Ad and I. Bar-Joseph, Phys. Rev. Lett. **66**, 2491 (1991).
[29] R. Raj *et al.*, Solid State Commun. **81**, 51 (1992).
[30] C. Stafford *et al.*, Phys. Rev. B **41**, 10 000 (1990).
[31] W. Shäfer *et al.* (unpublished).
[32] T. Yajima and Y. Taira, J. Phys. Soc. Jpn. **47**, 1620 (1979).
[33] A. Honold *et al.*, Appl. Phys. Lett. **52**, 2105 (1988).
[34] J. Lee *et al.*, Phys. Rev. B **33**, 5512 (1986).

Femtosecond wave mixing experiments in ZnCdSe/ZnSe quantum wells

D. S. Kim,[a] A. J. Fischer, J. Hays, W. Shan, and J. J. Song
Center for Laser Research and Department of Physics, Oklahoma State University, Stillwater, Oklahoma 74078

D. B. Eason, J. Ren, and J. F. Schetzina
Department of Physics, North Carolina State University, Raleigh, North Carolina 27695

(Received 17 May 1994; accepted for publication 18 July 1994)

Extreme high order nonlinear diffracted signals are found in ZnCdSe/ZnSe quantum wells in two beam, self-diffraction geometry. Diffracted signals of all observed orders are shown to originate predominantly from excitonic resonances. Using four-wave mixing, an indication of hole-longitudinal optical phonon scattering between the heavy and the light hole states is found, and exciton-phonon interaction is studied.

In the last few years, picosecond and femtosecond nonlinear spectroscopy of bulk semiconductors and quantum wells (QWs) near band-gap regions have attracted much attention. Most of these studies were focused on III-V materials such as GaAs or GaAs/AlGaAs quantum wells, whose band gaps are in the near infrared region. In wide gap II-VI compound semiconductors, a large third order nonlinearity was reported in ZnSe using picosecond polarization spectroscopy,[1] whereas femtosecond Faraday rotation has been used to investigate dephasing and spin relaxation in ZnSe-based magnetic QW's.[2] In CdTe, CdSe, and their QWs, four-wave mixing (FWM) has been used to investigate exciton-acoustic phonon and exciton-exciton interactions, as well as hot exciton relaxation.[3–6]

In this letter, we have used the second harmonic of a self-mode-locked Ti:sapphire laser (100 fs, 76 Mhz) to perform degenerate femtosecond two beam (with wave vectors $\mathbf{k}_1$ and $\mathbf{k}_2$), self-diffraction experiments [Fig. 1(a)] near the excitonic resonance at low temperature. The sample was a ZnCdSe multiple quantum well (MQW) sample grown on ZnSe. Since ZnCdSe has a lower band gap than ZnSe, transmission experiments are easily performed on the ZnCdSe MQW without etching. The time-integrated (TI) diffracted signals were measured as a function of delay T between the two pulses. In the MQW sample, the diffracted signals are very strong and *easily visible to the naked eye all the way up to the 13th order (fourteen-wave mixing) signal, even though the total well thickness is only 300 Å*. By studying the total diffracted signals as a function of the laser photon energy, we have found that diffracted signals of all observed orders are completely dominated by the excitonic resonances.

Figure 1(b) shows a photograph of the diffracted signals at $T=200$ fs from a 6($Zn_{0.88}Cd_{0.12}Se$/ZnSe, 50 Å/250 Å) MQW sample, together with the two attenuated incident beams at $\mathbf{k}_1$ and $\mathbf{k}_2$. The picture was taken with the exciting photon energy tuned near the heavy-hole (HH) excitonic resonance of the MQW (2.71 eV) at 10 K with the average power of each beam of 10 mW and the focal spot of ≈100 μm. The third, fifth, seventh, ninth, and eleventh order signals in the phase matching directions of $\approx 3\mathbf{k}_2-2\mathbf{k}_1$, $\approx 4\mathbf{k}_2-3\mathbf{k}_1$, $\approx 5\mathbf{k}_2-4\mathbf{k}_1$, and $\approx 6\mathbf{k}_2-5\mathbf{k}_1$ are clearly visible. The 13th order signal, while clearly visible to the naked eye, is weakly visible in Fig. 1(b) in the direction of $\approx 7\mathbf{k}_2-6\mathbf{k}_1$. The observation of strong nonlinear diffracted signals up to the 13th order is in stark contrast with GaAs MQWs where diffracted signals only up to the fifth order has been observed.[7] Considering the fact that our MQW sample is optically thin, even higher order signals are very likely to be observed in thicker MQW samples.

The broad femtosecond pulses with the full width at half-maximum (FWHM) of ≈25 meV used in our experiments can excite both the excitons and the free carriers. To determine the relative contributions of excitons and free carriers to the nonlinearities, we have measured the FWM signal as a function of the center laser photon energy. In Fig. 2, FWM signals at $T=200$ fs are plotted as a function of the

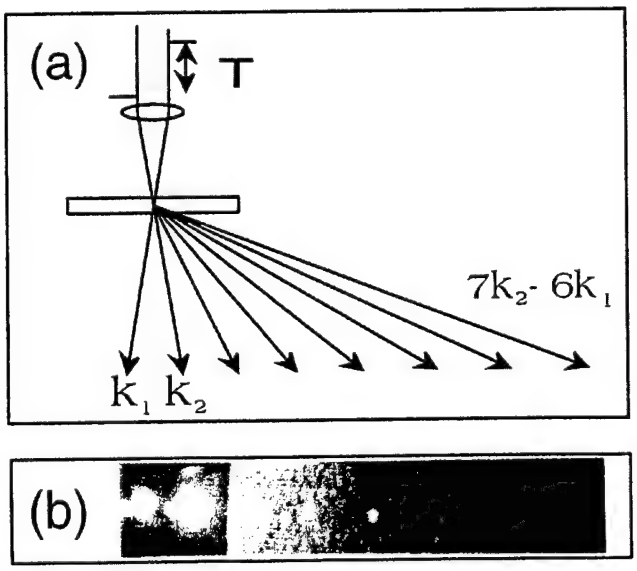

FIG. 1. (a) Schematic representation of the wave mixing experiment showing diffracted signals in the directions $2\mathbf{k}_2-\mathbf{k}_1$, $3\mathbf{k}_2-2\mathbf{k}_1$, up to $7\mathbf{k}_2-6\mathbf{k}_1$. (b) Photograph of the wave mixing signal showing, from left to right, two attenuated pump beams, third order spot, fifth order spot, up to thirteenth order spot barely visible at the right edge. The laser photon energy is centered at the HH exciton at 10 K, with power of each beam at 10 mW focused into ≈100 μm spot.

[a]Present address: Department of Physics, Seoul National University, Seoul 151, Korea.

 0003-6951/94/65(12)/1534/3/$6.00

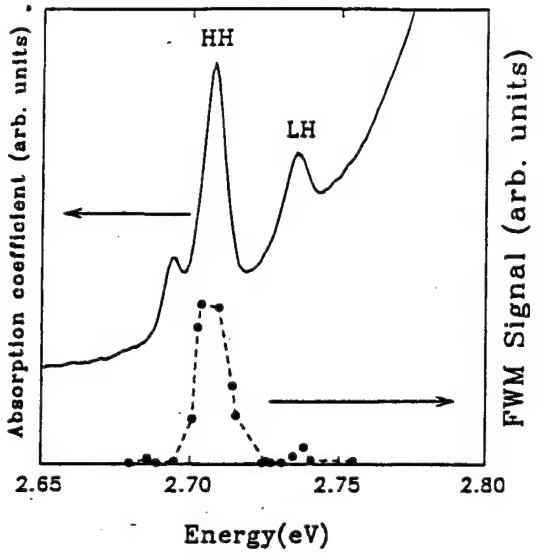

FIG. 2. FWM signal at $T=200$ fs as a function of the center laser energy for a 6($Zn_{0.88}Cd_{0.12}Se$/ZnSe, 50 Å/250 Å) MQW sample. The top curve shows the absorption spectrum for the MQW.

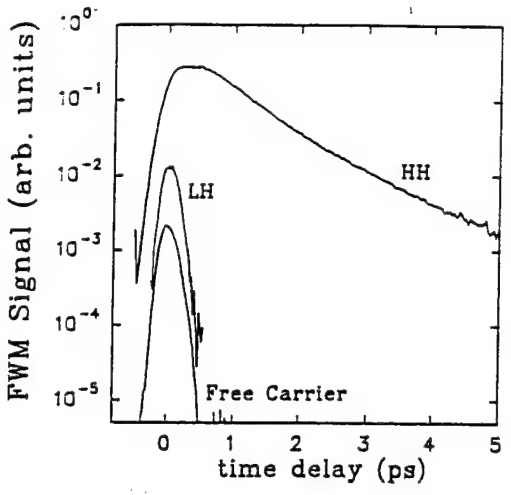

FIG. 3. TI-FWM when the laser is centered at the HH exciton (top), LH exciton (middle), or at the free carrier continuum ~40 meV above the HH exciton.

laser photon energy for the MQW sample, together with the absorption spectrum. The weaker peak in the absorption spectrum at the lower energy side of the HH is thought to be due to a well width fluctuation. This is supported by luminescence measurements and band structure calculations.[8] A strong resonance centered at the HH exciton is visible together with a much weaker one at the light-hole (LH) excitonic resonance. The FWM signal at the free carrier continuum is two orders of magnitude weaker than the main peak. From these observations, we conclude that the excitonic contribution completely dominates FWM in ZnCdSe MQW. Higher order signals display similar behavior, indicating that excitons dominate nonlinear diffracted signals of all orders.

The same resonance phenomenon has been observed in FWM signal from GaAs QWs and was explained by much faster dephasing of free carriers relative to excitons.[9] This interpretation is confirmed by FWM experiments on the MQW sample when the laser is tuned to the HH resonance, LH resonance, or roughly at the edge of the free carrier continuum. Figure 3 shows TI-FWM signal as a function of T when the laser is tuned to the HH exciton (top), LH exciton (middle), or at the free carrier continuum (bottom). A much slower (by more than a factor of 10) decay of TI-FWM at the HH resonance relative to those of LH resonance or free carrier continuum is observed. Therefore, we conclude that at 10 K, there exists at least a factor of 10 difference between dephasing times of HH excitons and those of LH excitons or free carriers. By comparing the decay constant of TI-FWM at the HH resonance and the absorption width, we can readily conclude that the HH exciton is inhomogeneously broadened at 10 K. Since in an inhomogeneously broadened system, the decay constant of TI-FWM is equal to $T_2/4$,[10] T_2 for the HH exciton in Fig. 3 is ~4 ps. Those of the LH exciton or the free carrier continuum are deduced to be less than ~300 fs. It is interesting to note that the dephasing time of LH exciton is so much shorter than that of HH exciton. The near resonance of the separation between the HH and the LH excitons, and the LO phonon energy, is a likely cause for this short dephasing time for the LH excitons. Further investigation is needed on the subject of exciton-LO phonon scattering between the HH and the LH states.

One important subject that has been widely investigated in III-V materials is the role of the coherent exciton-exciton interaction in nonlinearities of these systems. Existence of strong negative time delay signals can be an indication of this interaction effect.[11–15] However, generally large inhomogeneous broadening in our II-VI MQW sample (≈6 meV), compared with those of high quality GaAs QWs (<1 meV), makes it very difficult to observe negative time delay signals regardless of whether coherent exciton-exciton interaction plays a major role or not.

We now discuss exciton-phonon interactions in this sample. In Fig. 4, the decay rates of TI-FWM signals are plotted as a function of temperature. Two temperature ranges can be clearly seen: at low temperatures (<70 K), the rate is roughly linear with T_L, whereas at $T_L>100$ K, the slope is much larger. We fit the decay rates using a least-square fit with the following equation:[16] decay rate $1/\tau=A+BT_L+C/\{\exp(E_{LO}/k_bT_L)-1\}$, where E_{LO} is the optical phonon energy and k_b is the Boltzmann constant. BT_L is the contribution due to acoustic phonons, whereas the last term is the contribution from optical phonons. The best fit, represented by a solid line, can be used to obtain the phonon contributions to the homogeneous line width of excitons Γ_{ph} assuming $\Gamma_{ph}=\Gamma T_L+\Gamma_{LO}/\{\exp(E_{LO}/k_bT_L)-1\}$. The values thus obtained for γ and Γ_{LO} are $\gamma=8.3$ μeV/K and $\Gamma_{LO}=81$ meV. In deriving these values, it is assumed that excitons are inhomogeneously broadened at low temperatures, while they are homogeneously broadened at high temperatures. The values γ and Γ_{LO} are in agreement with those of Refs. 3 and 17.

In conclusion, we found extremely strong nonlinear signals, up to 13th order, in femtosecond two beam, self-

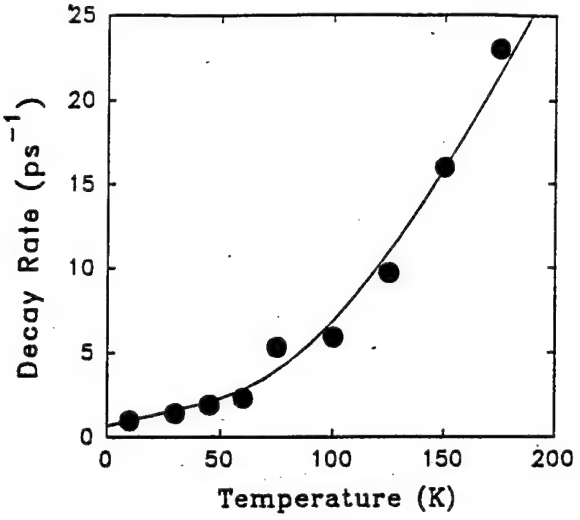

FIG. 4. Decay constants of TI-FWM of HH exciton plotted against lattice temperature. The fit corresponds to acoustic phonon-exciton coupling constant γ=8.3 μeV/K, and exciton-optical phonon coupling constant Γ_{LO}=81 meV.

diffraction experiments on a ZnCdSe MQW sample. Diffracted signals of all observed orders are completely dominated by excitonic resonances, and the dephasing time of LH excitons are much shorter than those of HH excitons, possibly due to hole-LO phonon scattering between the HH and LH states. The exciton-acoustic and exciton-optical phonon interactions were studied using FWM and were found to be much stronger than those of GaAs quantum wells.

This work was supported by ONR, ARPA, and OCAST.

[1] T. Saiki, K. Takeuchi, M. Kuwata-Gonokami, T. Mitsuyu, and K. Ohkawa, Appl. Phys. Lett. **60**, 192 (1992).
[2] J. Baumberg, D. D. Awschalom, N. Samarth, H. Luo, and J. K. Furdyna, Phys. Rev. Lett. **72**, 717 (1994).
[3] R. Hellman, M. Koch, J. Feldmann, S. T. Cundiff, and E. O. Göbel, D. R. Yakovlev, A. Waag, and G. Landwehr, Phys. Rev. B **48**, 2847 (1993).
[4] R. P. Stanley, J. Hegarty, R. Fischer, J. Feldmann, E. O. Göbel, R. D. Feldman, and R. F. Austin, Phys. Rev. Lett. **67**, 128 (1991).
[5] H. Schwab, V. G. Lyssenko, and J. M. Hvam, Phys. Rev. B **44**, 3999 (1991).
[6] G. Noll, U. Siegner, S. G. Shevel, and E. O. Göbel, Phys. Rev. Lett. **64**, 792 (1990).
[7] S. Wu, X.-C. Zhang, and R. L. Fork, Appl. Phys. Lett. **61**, 919 (1992).
[8] S. J. Hwang and J. Hays (unpublished).
[9] D. S. Kim, J. Shah, J. E. Cunningham, T. C. Damen, W. Schäfer, M. Hartmann, and S. Schmitt-Rink, Phys. Rev. Lett. **68**, 1006 (1992).
[10] T. Yajima and Y. Taira, J. Phys. Soc. Jpn. **47**, 1620 (1979).
[11] C. Stafford, S. Schmitt-Rink, and W. Schäfer, Phys. Rev. B **41**, 10000 (1990).
[12] K. Leo, M. Wegener, J. Shah, D. S. Chemla, E. O. Göbel, T. C. Damen, S. Schmitt-Rink, and W. Schäfer, Phys. Rev. Lett. **65**, 1340 (1990).
[13] K. Leo, E. O. Göbel, T. C. Damen, J. Shah, S. Schmitt-Rink, W. Schäfer, J. F. Muller, K. Köhler, and P. Ganser, Phys. Rev. B **44**, 5726 (1991).
[14] M. Wegener, D. S. Chemla, S. Schmitt-Rink, and W. Schäfer, Phys. Rev. A **42**, 5675 (1990).
[15] D. S. Kim, J. Shah, T. C. Damen, W. Schäfer, F. Jahnke, and S. Schmitt-Rink, Phys. Rev. Lett. **69**, 2725 (1992).
[16] J. Lee, E. Koteles, and M. O. Vassell, Phys. Rev. B **33**, 5512 (1986).
[17] L. Schultheis, J. Kuhl, A. Honold, and C. W. Tu, , Phys. Rev. Lett. **57**, 1635 (1986); **57**, 1797 (1986).

Room temperature blue lasing of ZnS_xSe_{1-x} alloys by photopumping

X. H. Yang, J. Hays, W. Shan,[a] and J. J. Song
Center for Laser Research and Department of Physics, Oklahoma State University, Stillwater, Oklahoma 74078-0444

E. Cantwell and J. Aldridge
Eagle Picher Research Laboratories, Miami, Oklahoma 74354

(Received 7 October 1991; accepted for publication 5 December 1991)

Photopumped lasing of $ZnS_{0.05}Se_{0.95}$ alloys grown by seeded physical vapor-phase transport technique is observed at room temperature for the first time. This is achieved with the excitation photon energy tuned close to the band gap. The longitudinal lasing modes are well resolved. This work demonstrates that ZnS_xSe_{1-x} alloys can be used as an alternative to ZnSe in blue light-emitting device fabrications.

Recently, great efforts have been devoted to the development of blue light-emitting lasers and light-emitting diodes (LEDs) from ZnSe-based materials because of their potential applications in optical recording, display, and undersea communications.[1] The fabrication of high efficiency LEDs requires high quality *p-n* junctions. Much progress has been made recently in *p*-type doping, *p-n* junction LEDs, and laser diodes.[2–4] However, high quality room temperature *p-n* junction ZnSe laser diodes are not yet available. As a result, photopumping and electron beam pumping are extensively used as a convenient means to check various sample structures for their suitability for current injection lasing.[5–9] Recently, room temperature photopumped lasing has been observed in both ZnSe bulk[10,11] and epilayers,[12] as well as ZnSe-$ZnS_{0.06}Se_{0.94}$ double heterostructures (DH)[13] using an excitation photon energy very close to the band-gap energy. One of the problems associated with the epilayers grown on a GaAs substrate is the lattice mismatch between the ZnSe epilayer and the GaAs substrate. This can cause the presence of misfit dislocations when the epilayer is thicker than the critical thickness of $\sim$1500 Å, which would adversely affect both device performance and operation lifetime.[14] As a result, the epilayer samples should be restricted to a layer thickness of less than 1500 Å, but for photopumped lasing studies, the penetration depth of the light is usually larger than 1500 Å, especially in the case of the near-band-gap pumping. Thus, the active gain volume for ZnSe grown on GaAs is limited by the critical length, resulting in a high lasing threshold.[12] In order to improve the electronic and optical confinement, a DH structure was used in Ref. 13. However, since the total band-gap energy difference between ZnSe and $ZnS_{0.06}Se_{0.94}$ is only $\sim$36 meV and most of this difference is taken up in the valence-band offset, the electron confinement is very poor (this is true, in general, for any ZnSe-ZnS_xSe_{1-x} system, $0<x<1$).[13]Also, the optical confinement is very poor due to the small index of refraction difference in this system (less than 1%). New sample structures with different combinations of binary and ternary systems are needed to optimize the lasing properties.

While various superlattice structures have been lased with some successes,[14–20] there have not been many photopumped lasing studies on the ZnS_xSe_{1-x} alloys. Along with ZnSe, other properties of ZnS_xSe_{1-x} alloys have been extensively studied.[21–24] Due to the lattice match between ZnS_xSe_{1-x} (with $x\sim5\%$–6%) and GaAs, the photoluminescence (PL) efficiency from lattice matched ZnS_xSe_{1-x} samples is at least one order of magnitude larger than that from ZnSe films,[22,25] indicating the high quality of the sample with less nonradiative recombination due to the misfit dislocations. Thus, ZnS_xSe_{1-x} can be an alternative in blue optoelectronic applications.

In this letter, we report the first observation of room temperature photopumped lasing in bulk $ZnS_{0.05}Se_{0.95}$ alloy samples. The alloys were grown by the seeded physical vapor phase technique (SPVT). This new crystal growth technique can provide high quality samples.[11] Strong blue lasing was obtained at room temperature by tuning the pumping photon energy very close to the band gap. The lasing emission peaked at 464 nm, which is about 35 meV higher in energy compared to our previous result of ZnSe.[11] The threshold pumping power for lasing was found to be as low as 96 kW/cm^2. Also, the longitudinal cavity modes can be observed in the emission spectra.

$ZnS_{0.05}Se_{0.95}$ single crystals with (111) orientation were mechanically polished and then chemically etched with 0.5% bromine/methanol for 5 min to reduce surface roughness. Laser cavities 300–400 μm wide were cleaved, using the natural facets as reflective mirrors. The thickness of all samples was 100 μm. The samples were excited from the top and the lasing output from one of the cleaved facets was directed to a distant spectrometer with and/or without a collection lens. The basic lasing characteristics of these two experimental arrangements, such as the differential quantum efficiency, lasing threshold power density, are the same except that the signal levels are higher with the collection lens. This implies that in this experimental configuration the influence from the scattered spontaneous emission is negligible with a collection lens. As a result, the data presented in the following are taken with a collection lens because of the higher sensitivity. The excitation source and

[a]On leave from National Laboratory for Infrared Physics, Shanghai Institute of Technical Physics, Chinese Academy of Sciences, Shanghai, 200083, Peoples Republic of China.

 0003-6951/92/080926-03$03.00

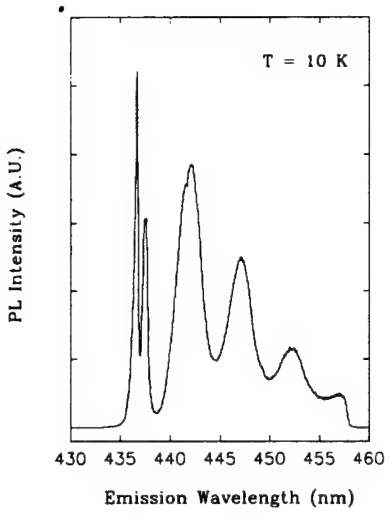

FIG. 1. Continuous wave photoluminescence spectrum of $ZnSe_{1-x}S_x$, with $x = 0.05$. The excitation source is a HeCd laser operating at 325 nm. The sharp high energy peaks at 436.63 and 437.50 nm are identified as neutral donor and neutral acceptor bound excitons.

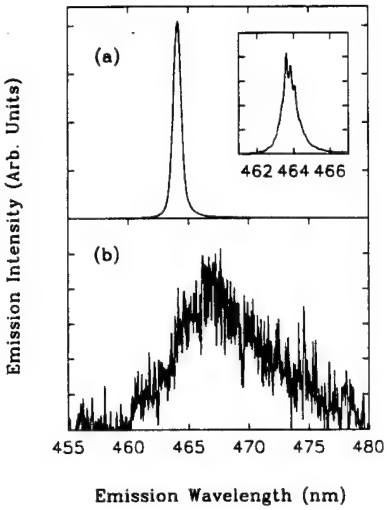

FIG. 2. Typical emission spectra from a $ZnS_{0.05}Se_{0.95}$ sample with a cavity length of 399 μm pumped at 459 nm with pump power densities of (a) $1.4I_{th}$ and (b) $0.76I_{th}$. The threshold pump power density I_{th} was determined to be 350 kW/cm^2. The inset shows the longitudinal modes.

detection systems used in this study are described in Ref. 11.

The sulphur concentration was determined by x-ray rocking curves and room temperature optical absorption measurements. For optical absorption measurements, a linear interpolation was used to determine the x value from the change in the band gap. The x-ray measurements yield an x value of 5.17% and the optical absorption yields a value of 5%–6%. An example of the low temperature (10 K) photoluminescence emission spectra taken using a continuous wave (cw) HeCd laser at 325 nm as the excitation source is shown in Fig. 1. The sharp, high energy peaks at 436.63 and 437.50 nm are identified as neutral donor and neutral acceptor bound excitons, respectively.

The emission spectra taken with a 10 ns pulsed laser, below and above the estimated threshold pumping power density, are plotted in Fig. 2 for a sample with the cavity length 399 μm with the excitation wavelength at 459 nm. The spontaneous emission has a broad spectral feature located around 467 nm, as shown in Fig. 2(b). A sharp peak appears at 464 nm, as shown in Fig. 2(a), with an increase of the pumping power density. This peak has a full width at half-maximum (FWHM) of 5 meV. This spectra narrowing is a clear indication of lasing. Under close examination, the longitudinal mode structures due to the reflection from the cleaved facets of the sample and the dispersion of the index of refraction of ZnS_xSe_{1-x} are resolvable, as shown in the inset of Fig. 2.

Figure 3 demonstrates the well-defined lasing threshold observed at two different excitation wavelengths for the sample with a cavity length of 399 μm. The onset of lasing action was evidenced by the spectral narrowing, as well as the steep rise of the emission intensity-versus-pumping intensity curve. The threshold powers are found to be 350 kW/cm^2 for a pump wavelength of 459 nm and 96 kW/cm^2 for a wavelength of 455 nm. These values are one order of magnitude higher than the photopumped lasing threshold for bulk ZnSe in our previous report.[11] However, they are still comparable to those reported for an antiguiding ZnSe epilayer structure[12] and DH structures.[13] The threshold could be reduced when the ZnS_xSe_{1-x} alloy sample quality is further improved or a ZnS_xSe_{1-x} epilayer grown on the lattice-matched GaAs substrate is used.

The effect of excitation photon wavelength λ_p on the lasing characteristics was also observed. There are several noteworthy results. The first is the dependence of the lasing threshold pump power density on λ_p, as illustrated in Fig. 3. We attempted lasing the sample with $\lambda_p = 433$ nm and shorter, i.e., with an excitation energy much higher than the ZnS_xSe_{1-x} band gap. Only the spontaneous emission similar to Fig. 2(b) can be observed under pumping power densities equal to or higher than the threshold power densities needed to lase when pumping at 459 nm. This may be due to the competition of the nonradiative recombinations

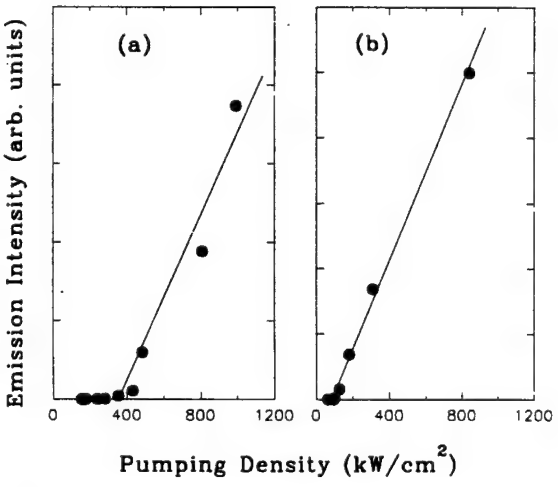

FIG. 3. Emission output vs optical pumping power densities for the sample used in Fig. 2 pumped at 459 nm (a), 455 nm (b). The vertical axis is linear in intensity.

near the surface with the stimulated recombination; with the excitation photon energy tuned far above the band gap, the penetration depth of the light was very short due to the large absorption coefficient of the alloy sample and the scattering losses due to many body effects.[26] As a result, the photoexcited carriers are concentrated near the surface, where the surface-related recombination centers may compete strongly with the stimulated emission process. This results in a high-lasing threshold which makes it difficult to observe lasing. On the other hand, if λ_p is tuned very close to the band gap, the light-penetration depth increases and this extends the excitation volume into the bulk of the sample, where there are much less surface-related defects, resulting in a much reduced lasing threshold. This is supported by the observation of lasing when λ_p is tuned into the range between 460 and 455 nm. When λ_p is tuned from 460 to 455 nm, the lasing threshold decreases monotonically from 450 to 96 kW/cm^2. This may be due to some resonant pumping effect although the exact origin is not known at this point.

The shift of the emission peak with λ_p is also observed. The peak shifts from 464.5 to 462.6 nm when λ_p is tuned from 460 to 455 nm while keeping the excitation power density fixed. This shift was also observed in ZnSe bulk[27] and epilayers.[12] This implies that the lasing is not likely to occur via some extrinsic recombination channels such as native impurity bound excitons, shallow donor or acceptor levels, since their energy levels should be independent of the excitation photon energy. The lasing is most likely of intrinsic origin. The full understanding of this shift requires further study of the lasing mechanisms.

In summary, we have observed photopumped blue lasing at room temperature for $ZnS_{0.05}Se_{0.95}$ alloy samples using a near-band-gap pumping photon energy. Our results demonstrate the feasibility of using lattice-matched ZnS_xSe_{1-x} as an active light-emitting region in place of ZnSe in most applications where the device is grown on GaAs substrate. For example, a DHs can be grown on a GaAs substrate using the $ZnS_{0.05}Se_{0.95}$ as an active region. The barrier layers can use ZnS_ySe_{1-y} with y greater than 5%. In this situation, the active layer can be grown coherently for a large layer thickness as long as the barrier layer is grown below its critical thickness. This DHs can, therefore, have a large gain volume as well as reduced strain-induced defects. Also, a buffer layer of a superlattice structure ZnS_xSe_{1-x}/ZnSe with low x values, e.g., $x = 0.1$, of equal well and barrier thickness can be inserted on top of GaAs substrate to smooth the subsequent growth, since the average lattice constant of this buffer layer is lattice-matched to the GaAs substrate.[18,19] The emitting light wavelength can be tuned further into the blue by varying the ZnS_xSe_{1-x} alloy concentration.

This work was supported by DARPA, ONR, and OCAST.

[1] R. A. Reynolds, J. Vac. Sci. Technol. A **7**, 269 (1989).
[2] M. A. Haase, J. Qiu, J. M. Depuydt, and H. Chang, Appl. Phys. Lett. **59**, 1272 (1991).
[3] H. Cheng, J. M. Depuydt, J. E. Potts, and T. L. Smith, Appl. Phys. Lett. **52**, 147 (1988).
[4] R. M. Park, M. B. Troffer, C. M. Rouleau, J. M. Depuydt, and M. A. Haase, Appl. Phys. Lett. **57**, 2127 (1990).
[5] S. Colak, J. Khurgin, W. Seemungal, and A. Hebling, J. Appl. Phys. **62**, 2633 (1987).
[6] D. A. Cammack, R. J. Dalby, H. J. Cornelissen, and J. Khurgin, J. Appl. Phys. **62**, 3071 (1987).
[7] J. E. Potts, T. L. Smith, and H. Cheng, Appl. Phys. Lett. **50**, 7 (1987).
[8] I. Suemune, H. Masato, K. Nakanishi, K. Yamada, Y. Kan, and M. Yamanishi, J. Cryst. Growth **101**, 754 (1990).
[9] R. B. Bylsma, W. M. Becker, T. C. Bonsett, L. A. Kolodziejski, R. L. Gunshor, M. Yamanishi, and S. Datta, Appl. Phys. Lett. **47**, 1039 (1985).
[10] C. A. Zmudzinski, Y. Guan, and P. S. Zory, IEEE Photon. Technol. Lett. **2**, 94 (1990).
[11] X. H. Yang, J. Hays, W. Shan, J. J. Song, E. Cantwell, and J. Aldridge, Appl. Phys. Lett. **59**, 1681 (1991).
[12] Y. Guan, C. A. Zmudzinski, P. S. Zory, and R. M. Park, IEEE Photon. Technol. Lett. **3**, 685 (1991).
[13] G. Sun, K. Shahzad, J. M. Gaines, and J. B. Khurgin, Appl. Phys. Lett. **59**, 310 (1991).
[14] I. Suemune, K. Yamada, H. Masato, Y. Kan, and M. Yamanishi, Appl. Phys. Lett. **54**, 981 (1989).
[15] A. M. Glass, and K. Tai, Appl. Phys. Lett. **53**, 834 (1988).
[16] H. Jeon, J. Ding, A. V. Nurmikko, H. Luo, N. Samarth, J. K. Furdyna, W. A. Bonner, and R. E. Nahory, Appl. Phys. Lett. **57**, 2413 (1990).
[17] H. Jeon, J. Ding, A. V. Nurmikko, H. Luo, N. Samarth, and J. Furdyna, Appl. Phys. Lett. **59**, 1293 (1991).
[18] K. Nakanishi, I. Suemune, Y. Fujii, Y. Kuroda, and M. Yamanishi, Jpn. J. Appl. Phys. **30**, L1399 (1991).
[19] K. Nakanishi, I. Suemune, Y. Fujii, Y. Kuroda, and M. Yamanishi, Appl. Phys. Lett. **59**, 1401 (1991).
[20] Y. Kawakami, S. Yamaguchi, Y. Wu, K. Ichino, S. Fujita, and S. Fujita, Jpn. J. Appl. Phys. **30**, L605 (1991).
[21] J. Saraie, N. Matsumura, M. Tsubokura, K. Miyagawa, and N. Nakamura, Jpn. J. Appl. Phys. **28**, L108 (1989).
[22] H. M. Yates, J. O. Williams, Appl. Phys. Lett. **51**, 809 (1987).
[23] I. Suemune, K. Yamada, H. Masato, T. Kanda, Y. Kan, and M. Yamanishi, Jpn. J. Appl. Phys. **27**, L2195 (1988).
[24] P. R. Newbury, K. Shahzad, J. Petruzzello, and D. A. Cammack, J. Appl. Phys. **66**, 4950 (1989).
[25] K. Yamada, I. Suemune, T. Kanda, H. Masato, Y. Kan, and M. Yamanishi, *Extended Abstract of 1988 International Conference on Solid State Devices and Materials* (Business Center for Academic Societies, Tokyo, 1988), p. 403.
[26] I. M. Catalano, A. Cingolani, M. Ferrara, and M. Lugara, Solid State Commun. **27**, 1331 (1978).
[27] X. H. Yang, W. Shan, J. J. Song, E. Cantwell, and J. Aldridge (unpublished results).

Bound exciton luminescence in ZnSe under hydrostatic pressure

W. Shan,[a] J. M. Hays, X. H. Yang, and J. J. Song
Department of Physics and University Center for Laser Research, Oklahoma State University, Stillwater, Oklahoma 74078

E. Cantwell and J. Aldridge
Eagle Picher Research Laboratories, Miami, Oklahoma 74354

(Received 30 September 1991; accepted for publication 25 November 1991)

We report pressure-dependent photoluminescence (PL) measurements on ZnSe single crystals grown by the seeded physical vapor phase transport technique. Two kinds of ZnSe samples, the as-grown and Zn-extracted single crystals were used in this study. The I_1^d line is the predominant spectral feature for the as-grown samples and shifts with pressure at a rate of 7.3 meV/kbar. The I_3 emission dominates the PL spectra of the Zn-extracted samples and has a pressure coefficient of 6.6 meV/kbar, which is inconsistent with the assumption of the I_3 line originating from the recombination of the excitons bound to ionized donors.

ZnSe is one of the most widely studied semiconductor materials since its wide band gap ($\approx$2.7 eV at room temperature) gives the promise of fabricating optoelectronic devices such as diode lasers operating at blue color range. Extensive optical measurements have been performed on ZnSe since Dean and Merz's first measurement on the pair spectra and edge emission of ZnSe in 1969.[1] It has been found that the low-temperature luminescence spectra observed from nominally undoped ZnSe crystals were usually quite complicated, characterized by the emission lines from bound excitons denoted by I_1, I_2, and I_3 in the near-band-gap region.[2–11] The I_2 lines have been well identified as originating from the recombination of excitons bound to neutral shallow donors with a luminescence peak at approximately 2.797 eV. The I_1 lines have been considered as emission from excitons bound to acceptors, for instance the notable I_1^d line located at about 2.780 eV has been attributed to the recombination of excitons bound to deep acceptors such as Zn vacancies or substitutional impurities (e.g., Cu_{Zn}), and the I_3 line was proposed to be associated with the recombination of excitons bound to the ionized donors due to the peak position a little lower than I_2 in energy.[2,3] However, there has been some contradictory experimental evidence recently, in particular, regarding the proposed physical origin of the I_3 emission line.[8,12,13] Judging from the donor-concentration dependence of the intensity ratio between the I_2 and I_3 emission lines, Isshiki *et al.* argued that the recombination of the excitons bound to ionized donors responsible for the I_3 emission line is not reliable.[8] Apparently more detailed experimental and theoretical work is needed to fully understand the physical origins of those bound excitons. This is of particular importance in the development of blue lasers. To give more insights to the problem of the bound excitons in ZnSe, we report in this letter a first photoluminescence study of the bound excitons in ZnSe under pressure at low temperature. The ZnSe crystals were grown by the seeded physical vapor phase transport technique (SPVT). The low-temperature photoluminescence spectra of the SPVT samples consisted of a few strong bound-exciton emission lines such as I_1, I_2, I_3, and I_1^d with its phonon replica lying in the near-band-gap region. However, the donor-acceptor pair recombination spectral signatures[1,2] could be scarcely observed from the SPVT ZnSe samples. The change of the I_1^d emission line in energy with pressure is shown to follow the ZnSe band gap.[14,15] The change of the I_3 line with pressure, however, is found to be about 10% lower than the pressure dependence of the band gap, which is not consistent with the proposal that the radiative recombination of excitons bound to ionized donors is responsible for the I_3 emission.[2,3]

Two kinds of ZnSe samples, as-grown and Zn-extracted ZnSe bulk material were studied in this work. They were nominally undoped SPVT single crystals. The Zn-extracted treatment was performed by dipping SPVT ZnSe crystals into molten Zn at 850 °C for 96 h. For pressure measurement the samples were mechanically polished and chemically etched to give final sample thicknesses around 50 μm, then were cut into about 200 μm^2 in size and loaded into a diamond anvil pressure cell. The pressure apparatus was attached to the cold finger of a closed cycle refrigerator and cooled down to 10 K for photoluminescence (PL) measurement. Photoluminescence was excited by the 325 nm line of a HeCd laser with 10 mW power. The emission signals were measured by a Spex 0.6 m triple-grating spectrometer in conjunction with an optical multichannel analyzer and data acquisition system.

Photoluminescence spectra of the as-grown SPVT ZnSe samples measured at different selected pressures are shown in Fig. 1. The spectra are dominated by the strong, sharp I_1^d bound-exciton recombination line and its LO phonon replica. The peak position of the I_1^d line at atmospheric pressure was measured to be 2.7803 eV and shifts to higher energy with applied pressure. The small resolvable peak at higher energy side of I_1^d is due to I_1 emission. However its pressure dependence could not be reliably obtained due to the poor signal to noise ratio. The PL spectra of the Zn-extracted SPVT ZnSe samples are very different from the

[a]On leave from the National Laboratory for Infrared Physics, Shanghai Institute of Technical Physics, Chinese Academy of Sciences, Shanghai, 200083, People's Republic of China.

 0003-6951/92/060736-03$03.00

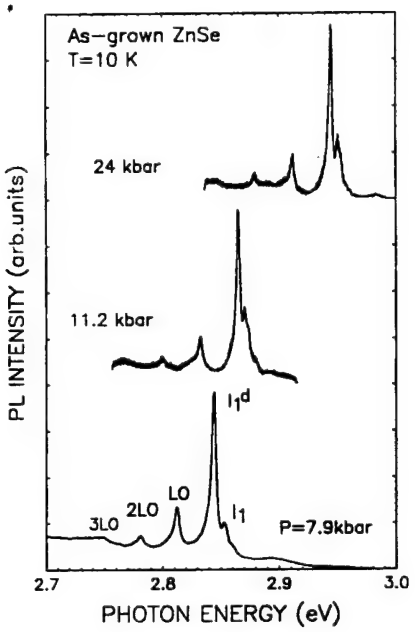

FIG. 1. PL spectra of the as-grown ZnSe samples at selected pressures. The small peak at higher energy bound of I_1^d is assigned to I_1.

spectra of as-grown samples as shown in Fig. 2. After Zn-extracted treatment, the noteworthy spectral changes at atmospheric pressure are that the emission intensity of I_1^d line decreases a great deal and the I_3 line (2.7941 eV) rather than the I_2 or the free-exciton line has the strongest emission intensity. Meanwhile a new emission peak appears at 2.7702 eV marked by an X in Fig. 2. A phonon replica of this new peak is also observable. The intensity of this emission line relative to that of the I_3 line decreases very rapidly as pressure increases and the spectral line be-

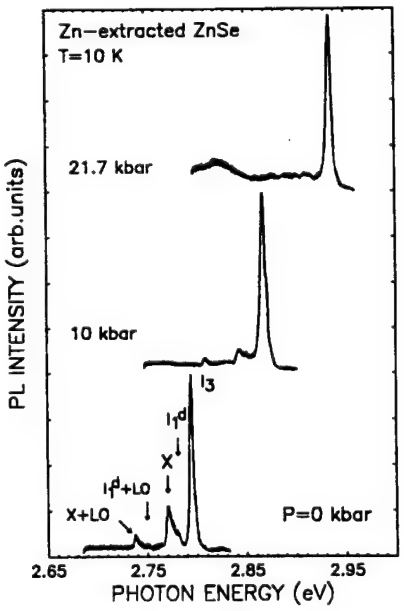

FIG. 2. PL spectra of the Zn-extracted samples at different pressures. The intensity of the emission line labeled by X decreases with pressure very rapidly and disappeared after $P \gtrsim 20$ kbar.

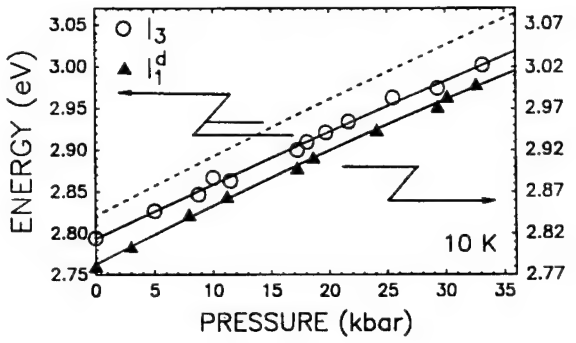

FIG. 3. The variations of the energy positions for the I_1^d and I_3 lines as a function of pressure. The solid lines drawn through the experimental points represent the least-squares fits. The pressure dependence of the ZnSe band gap is plotted (dashed line) as well for comparison.

comes unresolvable above 20 kbar. This spectral feature was previously viewed as an LO phonon replica of the emission of free excitons in ZnSe.[16] However, there has been strong argument over this identification.[10] This is an issue requiring further study. The strong emission of I_1^d in the as-grown samples is most likely to be related to a large number of Zn vacancies or/and substitutional impurities such as Cu_{Zn}.[5,17] The reduction of the concentrations of those acceptorlike deep centers by Zn-extracted treatment resulted in a drastic decrease of I_1^d luminescence intensity.

Figure 3 shows the variations of the energy positions of the I_3 and I_1^d emission lines in conjunction with the ZnSe band gap as a function of pressure. As is clear from the figure, the I_3 line shows a smaller slope of pressure dependence compared to I_1^d. The pressure coefficients of the I_3 and I_1^d lines derived from the equation

$$E(P) = E(0) + \alpha P + \beta P^2 \qquad (1)$$

are listed in Table I. Here $\alpha = dE/dP$ and $\beta = d^2E/dP^2$. The linear and quadratic pressure coefficients of the ZnSe band gap reported by the literature[14,15] are also listed for comparison. The pressure coefficient for the ZnSe band gap in the SPVT samples should not be expected to differ significantly from the reported values. Table I shows that the pressure dependence of the I_1^d emission line observed in as-grown samples is the same as that of the fundamental band gap of ZnSe. This is in agreement with the assumption that it results from the recombination of excitons bound to neutral acceptors,[2] because the effect of hydrostatic pressure on acceptor energy levels is negligible.

TABLE I. Observed energy positions and pressure coefficients of the I_1^d, I_3 lines and the ZnSe band gap.

	$E(0)$ (eV)	dE/dP (meV/kbar)	d^2E/dP^2 (10^{-2} meV/kbar^2)
I_1^d	2.7803	7.3(4)	−2.3(5)
I_3	2.7941	6.6(5)	−1.0(7)
E_g(ZnSe)	2.821[a]	7.2(2)[b] 7.4;7.5[c]	−1.5

[a]Reference 10.
[b]Reference 14.
[c]Reference 15.

It should be noted that the pressure coefficient of I_3 is only 6.6 meV/kbar, about 10% smaller than that of the ZnSe band gap. Application of pressure increases the binding energy of a shallow exciton arising from an increase of electron effective mass and a decrease in dielectric constant as the band gap increases.[18–20] The pressure-induced increase in exciton binding in ZnSe has been estimated to vary the pressure coefficient of I_3 by less than 1% in numerical value. Therefore the effect of pressure on the binding energy is not likely to produce a significant difference between the pressure coefficient of I_3 and that of the ZnSe band gap. The pressure dependence of the I_3 line is expected to be ZnSe-like ($dE/dP = 7.3$ meV/kbar) if it originates from the recombination of the excitons bound to ionized donors described on the basis of the effective mass approximation. The recombination line associated with the radiative decay of an exciton bound to a neutral or ionized donor should shift with the host semiconductor band gap under hydrostatic pressure at almost the same rate,[18,21] since the bound electron stays in the conduction valley orbit Γ_1-like donor state and the excitonic hole bound in the Coulomb field retains the Γ_{15} symmetry of the valence band edge. However, the effect of pressure on the I_3 emission line obtained in this work ($dE/dP = 6.6$ meV/kbar) shows an inconsistency with the ionized-donor-bound exciton model. Isshiki and co-workers have reported the similar observation of the emission intensity of I_3 line larger than that of I_2 line from Zn-dip treatment samples.[8] By changing the intensity and photon energy of the excitation light to measure the donor-concentration dependence of the intensity ratio between the I_2 and I_3 emission lines, they concluded that the assumption of the I_3 line is the radiative recombination of excitons bound to ionized donors[2] is not reliable. Detailed Zeeman effect measurement results are unfortunately not available at present to give a decisive identification of the origin responsible for the I_3 emission in ZnSe. It seems that I_3 might result from the radiative recombination of the excitons bound to donorlike deep centers rather than ionized shallow donors according to our results. This is because the pressure dependence of an energy level of a deep center is mainly determined by the composition of its wavefunction and the pressure coefficient of a deep donor will be determined mainly by the pressure dependence of the average conduction band energy.[22]

In conclusion, pressure-dependent photoluminescence measurements have been performed at 10 K on the as-grown and Zn-extracted SPVT ZnSe single crystals for the first time. Our results showed that I_1^d is the predominant emission line for the as-grown samples and the effect of pressure on I_1^d is in agreement with the proposed physical origin that the radiative recombination of excitons bound to deep acceptors responsible for the emission. The I_3 emission dominated the PL spectra of Zn-extracted samples and the effect of pressure on it showed a significant difference from the pressure dependence of the ZnSe band gap. This is not consistent with what has been assumed, i.e., the I_3 emission originated from the radiative decay of the excitons bound to ionized shallow donors in ZnSe and suggests that the I_3 emission might result from donorlike deep center bound excitons in ZnSe.

This work was supported by ONR, DARPA, and OCAST.

[1] P. J. Dean and J. L. Merz, Phys. Rev. **178**, 1310 (1969).
[2] J. L. Merz, H. Kukimoto, K. Nassau, and J. W. Shiever, Phys. Rev. B **6**, 545 (1972).
[3] J. L. Merz, K. Nassau, and J. W. Shiever, Phys. Rev. B **8**, 1444 (1973).
[4] R. N. Bhargava, J. Cryst. Growth **59**, 15 (1982).
[5] S. M. Huang, Y. Nozue, and K. Igaki, Jpn. J. Appl. Phys. **22**, L420 (1983).
[6] V. I. Sokolov, T. P. Surkova, M. V. Chukichev, and Vu Zoan M'en, Sov. Phys. Solid State **26**, 2215 (1984).
[7] T. Steiner, M. L. W. Thewalt, and R. N. Bhargava, Solid State Commun. **56**, 933 (1985).
[8] M. Isshiki, T. Kyotani, K. Masumoto, W. Uchida, and S. Suto, Phys. Rev. B **36**, 2568 (1987).
[9] K. Akimoto, T. Miyajima, and Y. Mori, Phys. Rev. B **39**, 3138 (1989).
[10] K. Shahzad, D. J. Olego, and D. A. Cammack, Phys. Rev. B **39**, 13016 (1989).
[11] P. J. Dean and D. C. Herbert, Phys. Rev. B **23**, 4888 (1981).
[12] T. Ohyama, E. Otsuka, T. Yoshida, M. Isshiki, and K. Igaki, in *Proceedings of the 17th International Conference on the Physics of Semiconductors*, edited by J. Chadi and W. A. Harrison (Springer, New York, 1985), p. 1313.
[13] M. Isshiki, T. Tomizono, Y. Yoshida, and K. Igaki, Jpn. J. Inst. Metals **48**, 1176 (1984).
[14] S. Ves, K. Strossner, N. E. Christensen, C. K. Kim, and M. Cardona, Solid State Commun. **56**, 479 (1985).
[15] Landolt-Bornstein, New Series, Group III, Vol. 22a, edited by O. Madelung (Springer, Berlin, 1988), p. 178, and references therein.
[16] N. Shibata, A. Ohki, S. Zembutsu, and A. Katsui, Jpn. J. Appl. Phys. **27**, L441 (1988).
[17] D. J. Robbins, P. J. Dean, P. E. Simmonds, and H. Tews, in *Deep Centers in Semiconductors*, edited by S. T. Pantelides (Gordon and Breach, New York, 1986), Chap. 11.
[18] D. J. Wolford and J. A. Bradley, Solid State Commun. **53**, 1069 (1985).
[19] L. G. Shantharama, A. R. Adams, C. N. Ahmad, and R. J. Nicholas, J. Phys. C **17**, 4429 (1984).
[20] G. A. Samara, Phys. Rev. B **27**, 3494 (1983).
[21] B. Gil, M. Baj, J. Camassel, H. Mathieu, C. Benoit a la Guillaume, N. Mestres, and J. Pascual, Phys. Rev. B **29**, 3398 (1984).
[22] J. Chadi and K. J. Chang, Phys. Rev. Lett. **61**, 873 (1988).

Semicond. Sci. Technol. 7 (1992) 1407–1415. Printed in the UK

Optical investigations of ZnSe crystals grown by the seeded vapour phase transport technique

J M Hays†, W Shan†§, X H Yang†, J J Song† and E Cantwell‡

†Department of Physics and University Center for Laser Research, Oklahoma State University, Stillwater, OK 74078, USA
‡Eagle-Picher Research Laboratories, Miami, OK 74354, USA

Received 7 May 1992, accepted for publication 15 June 1992

Abstract. The optical properties of ZnSe bulk crystals grown by the seeded physical vapour phase transport technique (SPVT) were studied by low-temperature photoluminescence and room-temperature stimulated emission measurements. Large strain-free ZnSe single crystals with a diameter as large as 5 cm have been grown uniformly, without twinning by the SPVT technique. A variety of ZnSe samples, the as-grown and post-growth treated as well as intentionally doped crystals, were prepared in this study. Low-temperature photoluminescence measurements showed that near band edge I_1^d line and its LO phonon replicas dominated the spectra, and that donor–acceptor pair emission signatures were absent for SPVT as-grown samples; the intensity of the I_1^d line decreased considerably and the I_3 line became predominant after Zn extraction treatment. The pressure dependence on the bound exciton emission lines suggested that the I_3 line might originate from excitons bound to a donor-like deep centre rather than to ionized shallow donors. The room-temperature optically pumped stimulated emission and blue lasing from the as-grown samples demonstrated that SPVT ZnSe single crystals have the quality sufficient to develop low-threshold, high-power output blue lasers.

1. Introduction

In recent years the II–VI compound semiconductors have attracted much attention for their technological importance appropriate for optoelectronic devices such as semiconductor diode lasers and light-emitting diodes (LEDs) [1, 2]. ZnSe is one of the most extensively studied II–VI materials due to its zinc blende structure with a band gap of ~2.7 eV at room temperature which gives the promise of fabricating diode lasers and LEDs operating at blue colour range [3–10]. To achieve the ultimate goal of a current injection diode laser it is necessary to grow both n-type and p-type conducting ZnSe materials for the preparation of p–n junctions. There have been some very recent reports on the exciting achievements of blue LEDs from ZnSe-based single quantum-well structures on GaAs substrates under pulsed current injection at relatively low temperatures [11–13]. However, the built-in biaxial strain resulting from the lattice mismatch and the different thermal expansion coefficients of ZnSe and GaAs, as well as the chemical-valence mismatch which induces the formation of a vacancy-rich Ga_2Se_3 layer at GaAs/ZnSe interfaces [14], can severely influence the device performance and shorten the device operating lifetime. Therefore, the successful commercial fabrication of reliable CW blue laser diodes and LEDs operating at room temperature with long operating lifetimes still relies on the preparation of heavy p- or n-type doped ZnSe and ZnSe-based materials or the growth of homoepitaxial layers of ZnSe on ZnSe substrates.

Recently, a new technique called seeded physical vapour phase transport (SPVT) has been developed to grow high-quality large ZnSe samples [14]. Using this technique one can grow strain-free relatively high-purity ZnSe crystals of 5 cm in diameter. It opens up new possibilities of mass producing blue photonic devices combining II–VI materials with III–V technology. In this paper we report a study on the optical properties of ZnSe bulk crystals grown by the SPVT technique. Samples used in this investigation included undoped as-grown and post-growth treated (Zn-extraction and Se-enrichment treatments) as well as intentionally (Ga, Cl, N) doped crystals. Photoluminescence (PL) measurements were performed to evaluate qualitatively the purity of nominally undoped ZnSe samples and to characterize the intentionally doped samples by monitoring the notable near band gap bound-exciton (BE) I_1^d, I_2, I_3 emission lines and donor–acceptor pair (DAP) emission band at lower energies. The pressure dependence on the bound exciton

§On leave from Shanghai Institute of Technical Physics, Chinese Academy of Sciences, Shanghai, 200083, People's Republic of China.

0268-1242/92/111407+09 $07.50

emissions was measured to examine their proposed physical origins. The properties of stimulated emission and lasing were studied at room temperature under near resonant pumping with the excitation photon energy very close to the fundamental band gap of ZnSe. The experimental results showed that the SPVT-grown ZnSe single crystals have sufficient quality to develop optoelectronic devices such as blue laser diodes and LEDs.

2. Experimental procedure

2.1. Crystal growth and sample preparation

The seeded physical vapour phase transport growth technique can generally provide large size, uniformly strain-free ZnSe single crystals with diameters up to 5 cm without twinning for optical studies and optoelectronic device applications. Basically, the vapour phase growth technique takes advantage of the fact that II–VI compounds have significant elemental vapour pressures well below their melting point. As a result, crystal growth can take place when a source of the compound is heated until the vapour pressures are significant and a temperature gradient is established such that transport of elemental vapours takes place to a cooler region in a growth ampoule where they are deposited. The recently developed seeded technique allows single crystals to be formed from the onset of crystal growth by placing a seed crystal in the cooler region. Special procedures have been taken to outgas the volatile impurities prior to onset of crystal growth and to stop crystal growth before all of the source material is exhausted so that less volatile impurities will tend to remain in source rather than transport to the growing crystals. Another unique aspect of the crystal growth technique is that the growing crystal is initially seeded at the full diameter of the final crystal. Material is therefore not wasted in increasing the diameter from a small seed to a larger growing crystal and extraneous seeding from the ampoule walls during diameter enlargement is eliminated. In addition, there is no inherent limit to the diameter of the growing crystal. The currently achieved ZnSe crystal size (5 cm in diameter) is limited by the type of furnace available.

In attempts to dope shallow impurities such as Cl, Ga, and N in ZnSe, crystal growth runs were conducted using doped ZnSe charges with different elements. ZnSe powder synthesised from high-purity Zn(99.9999%) and Se(99.9995%) was mixed with an appropriate amount of zinc chloride and melted in a pressure furnace to produce poly-ZnSe containing 200 ppm Cl. This was then mixed 10:1 with ZnSe to obtain the 20 ppm Cl doped ZnSe charge for SPVT growth. The Ga-doped ZnSe charges containing 1, 10, 50, and 100 ppm Ga for SPVT growth were prepared in a manner similar to that used in Cl-doped ZnSe growth. The Cl-doped SPVT growth resulted in single crystals. However, using the same method to grow Ga-doped ZnSe yielded polycrystalline material. Also, the colour of the as-grown Ga-doped ZnSe has a reddish cast instead of the normal pale yellow cast of undoped ZnSe. The N-doped ZnSe crystals were grown in N_2 atmosphere with standard ZnSe charges.

Two post-growth treatments, Zn extraction and Se enrichment, were carried out on nominally undoped as-grown SPVT ZnSe crystals. The Zn-extraction treatment was performed by submersion of ZnSe crystals into molten Zn at 850 °C for 96 h. The Se-enrichment treatment was achieved by annealing ZnSe wafers in selenium vapour produced in a closed quartz tube placed in a three-zone furnace. The Se metal is heated in one zone to 700 °C while the temperature of the ZnSe wafers is held at 930 °C in another zone. The treatment time is 68 h. All samples used for photoluminescence measurements were mechanically polished and then chemically etched with 0.5% bromine/methanol for 5 min to reduce the surface roughness.

2.2. Experimental details

The PL spectra were measured at 10 K using a Spex 1000M monochromator with a photomultiplier tube (PMT) or an optical multichannel analyser (OMA) followed by a data acquisition system. Photoluminescence was excited by the 325 nm line of a 10 mW HeCd laser. For pressure measurements the final sample thicknesses were further reduced to around 50 μm, then cut into about 200 μm^2 in size and loaded into a diamond anvil cell. The pressure apparatus was attached to a cold finger of a closed cycle refrigerator and cooled down to 10 K for PL measurement. For optically pumped stimulated emission and lasing measurements, (111)-oriented ZnSe samples were carefully prepared to ensure the perfection of sample edge facets. A frequency-doubled pulsed Nd:YAG laser (532 nm) with a pulse width of 10 ns and repetition rate of 10 Hz was used to pump a dye laser as a primary optical pumping source. A frequency tracking doubler was used to double the near-infrared photon energy of the dye laser. The emission signal was measured from the edge of the ZnSe sample in a side pumping geometry by the OMA connected to a Spex 0.6 m triple-grating spectrometer.

3. Photoluminescence measurements

Extensive photoluminescence (PL) measurements have been performed on ZnSe since the first measurement by Dean and Merz on the pair spectra and edge emission of ZnSe in 1969 [3]. It has been found that the low-temperature luminescence spectra observed from nominally undoped ZnSe crystals were usually quite complicated, characterized by the emission lines from bound excitons denoted by I_1, I_2, and I_3 in the near band gap region [4–8, 15–18]. The I_2 lines have been clearly identified as originating from the recombination of excitons bound to neutral shallow donors with a luminescence peak at approximately 2.797 eV. The I_1 lines have been considered as emission from excitons bound to acceptors. For instance the notable I_1^q line located at about 2.780 eV has been attributed to the recombination of excitons bound to deep acceptors such as Zn vacancies

or substitutional impurities (e.g. Cu_{Zn}), and the I_3 line was proposed to be associated with the recombination of excitons bound to the ionized donors due to the peak position slightly lower than I_2 in energy [4, 5]. In this section we present the PL measurement data taken from various SPVT grown ZnSe samples. In general, the low-temperature PL spectra of nominally undoped SPVT samples consist of a few strong bound exciton emission lines such as I_2, I_3, and I_1^d with its phonon replicas lying in the near band gap region. The donor–acceptor pair recombination spectral signatures could be hardly observed from those samples. However, the PL spectra from the intentionally doped SPVT samples are characterized by relatively weak near band gap bound-exciton emissions along with a broad emission band in the lower energy region.

Figure 1 shows a typical PL spectrum measured on as-grown SPVT ZnSe crystals. The spectrum was characterized by the strong sharp I_1^d emission line with peak position at 2.7803 eV and its LO phonon replicas. The donor–acceptor pair (DAP) recombination spectral signatures [3, 4] were not observed from the as-grown samples. The DAP emission band is usually a very strong feature of melt-grown specimens. The PL spectra of post-growth treated ZnSe samples are very different from those of as-grown samples, as shown in figures 2(*a*) and (*b*) for Zn-extraction and Se-enrichment treatments respectively. After Zn-extraction treatment, the noteworthy spectral changes are that the emission intensity of the I_1^d line decreases a great deal and the I_3 line (2.7941 eV), rather than the I_2 or the free-exciton line, has the strongest emission intensity. Meanwhile a new emission peak appears at 2.7702 eV marked by X in figure 2(*a*). A phonon replica of this new peak is also observable. This spectral feature was previously identified as a LO phonon replica of the emission of free excitons in ZnSe with the

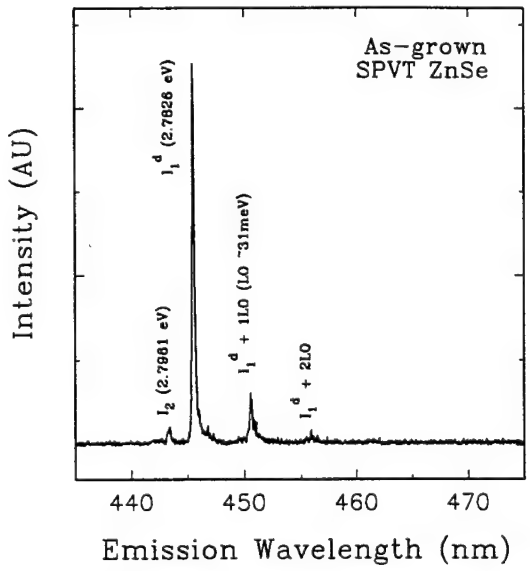

Figure 1. A typical PL spectrum taken from as-grown ZnSe samples at 10 K. The strong I_1^d emission line and its LO phonon replicas are dominant and no DAP emission spectral feature is observable.

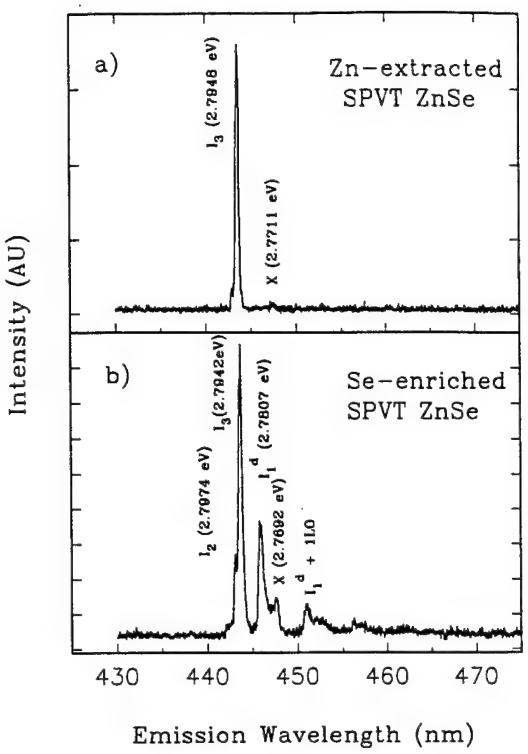

Figure 2. PL spectra of (*a*) Zn-extracted and (*b*) Se-enriched ZnSe samples. Zn-extraction treatment removes the I_1^d emission and I_3 becomes the dominant feature. Se-enrichment treatment results in a great increase of the I_3 and I_2 emission intensities.

acoustic phonon scattering of the I_1^d peak contributing [4, 19]. However, there has been strong argument over this identification [8]. In this study, no correlation between the emission intensity of I_1^d and the emission at 2.7702 eV is seen, which is contrary to the identification of acoustic phonon scattering of I_1^d. The strong emission of I_1^d in the as-grown samples is most likely to be related to a large number of Zn vacancies or/and substitutional impurities such as Cu_{Zn} [14, 15, 20]. The drastic decrease of the I_1^d luminescence intensity indicates that the Zn-extraction treatment can reduce the concentrations of those acceptor-like deep centres. Haynes' rule applied to the observed I_2 peak yields donor ionization energies of 25.5 meV, which is consistent with the effective mass approximation [2, 4]. The PL spectra from the samples which have undergone Se-enrichment treatment show that the I_2, I_3 emission lines become pronounced features along with I_1^d. The incremental changes of the emission intensities of I_2 and I_3 are apparently related to an increase in the concentration of isolated donors or/and donor-like centres caused by the Se-enrichment treatment. This suggests that the vacancies on Se sites which are donor-like native defects can be excluded as contributing significantly to I_2 and I_3 emissions.

Figures 3 and 4 show PL spectra from SPVT-grown Cl-doped and N-doped ZnSe respectively. The spectrum for the Cl-doped sample is basically very similar to that from the as-grown samples shown in figure 1 in that I_1^d and its LO phonon replicas are the primarily prominent spectral features. The intensities of I_2 and I_3 changed very little

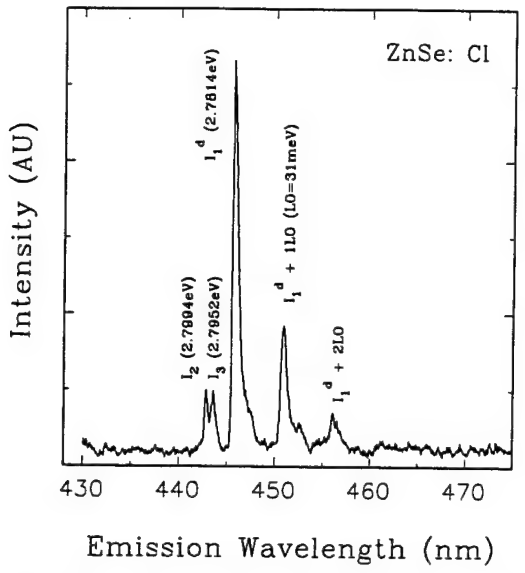

Figure 3. The PL spectrum from Cl-doped ZnSe samples. There is little difference from that of as-grown samples. The donor-related I_2 and I_3 BE emissions are very weak, which indicates very little change in donor concentration.

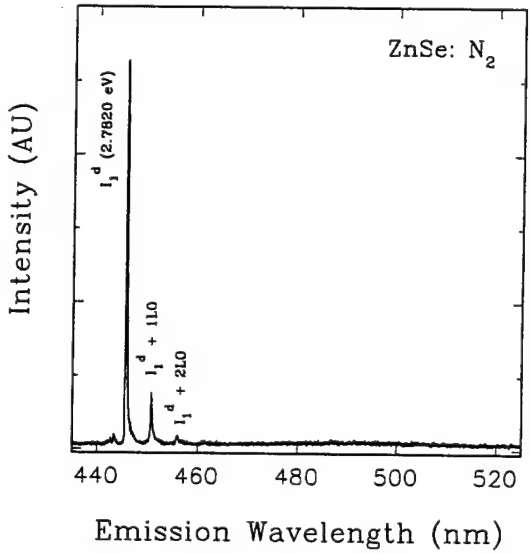

Figure 4. The PL spectrum from N-doped SPVT-grown ZnSe. No I_1 emission feature could be resolved from the spectrum. The spectrum is expected to exhibit I_1 emission if nitrogen is properly incorporated into ZnSe crystal as a shallow impurity. The broad emission band peaks at about 490 nm and I_1^d emission indicate that nitrogen is not incorporated into the ZnSe.

compared with those observed from the as-grown samples. This indicates that there is no change in the donor concentration resulting from the SPVT *in situ* Cl-doping process. The PL spectrum of SPVT-grown N-doped ZnSe does not exhibit the radiative recombination of shallow neutral acceptor bound exciton I_1 emission signature, which is expected to appear if nitrogen is properly incorporated into ZnSe crystal as shallow impurity. The I_1^d emission line remains the strongest structure. However, its signal intensity is much weaker than those of nominally undoped as-grown samples and varies from sample to sample. Apparently, nitrogen was not properly incorporated into ZnSe as shallow acceptor impurities by merely growing ZnSe at nitrogen atmosphere. These results suggest that the current method of intentionally doping during the SPVT growing process cannot properly incorporate dopant impurities into ZnSe such as to introduce shallow levels into the near band gap region.

The PL results measured from the SPVT- grown Ga-doped ZnSe samples show a very strong, broad emission band with peak position around 650 nm and no resolvable lines. The near band gap bound-exciton emissions from the samples are relatively weak. Shown in figure 5(*a*) and (*b*) are typical spectra taken from the samples with 50 ppm and 100 ppm Ga respectively (prepared prior to SPVT growth). The inset shows the details of the near band gap emission features. The feature with energy position at 2.7943 eV in the 50 ppm sample emission is attributed to I_3 emission. In the 100 ppm sample emission just below I_1^d is seen. This emission is tentatively attributed to deep acceptor bound excitons. The process of incorporation of Ga dopant into ZnSe by SPVT growth introduces a large number of defects into ZnSe crystals and results in heavy overdoping. In turn, it radically disturbs the crystallization of ZnSe. As a result, only polycrystalline material was yielded. The strong, broad emission band observed from PL spectra is believed to be related to the mid-gap deep levels resulting from those defects.

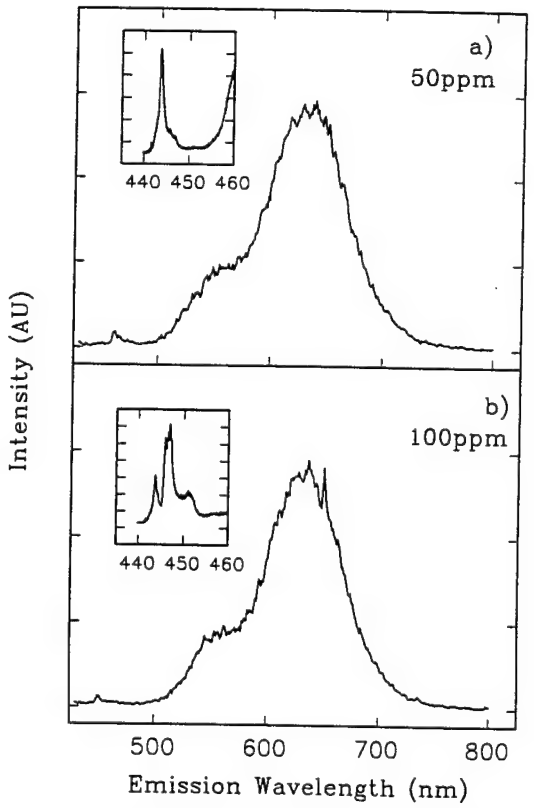

Figure 5. PL spectra taken from ZnSe samples with (*a*) 50 ppm and (*b*) 100 ppm Ga (prepared prior to SPVT growth). The insets show the details of the near band gap emission features.

4. Pressure dependence of bound-exciton emissions

Recently, there has been some experimental evidence which contradicts the proposed physical origin of the I_3 emission line as the radiative recombination from excitons bound to ionized donors [6, 21, 22]. To give more insight into the problem of bound excitons in ZnSe, we examine the effect of pressure on the bound-exciton emissions using low-temperature PL measurements in this section.

Three kinds of ZnSe sample, as-grown, Zn-extracted and Se-enriched SPVT ZnSe single crystals were studied under hydrostatic pressure in this work. Shown in figure 6 are PL spectra of the Se-enriched SPVT ZnSe samples at different pressures. As clearly shown in the figure, the I_1^d and I_3 bound-exciton emission lines shift to higher energies with applied pressure at different rates. The I_1^d line merges with the I_3 line at pressures around 25–30 kbar. As the pressure was increased beyond this range, the lines could be observed separately, again with I_1^d lying on the higher energy side. Figure 7 shows the variations of the energy positions of the I_3 and I_1^d emission lines measured from as-grown and Zn-extracted samples respectively, in conjunction with the ZnSe band gap as a function of pressure. As is clear from the figure, the I_3 line shows a smaller slope of pressure dependence than does

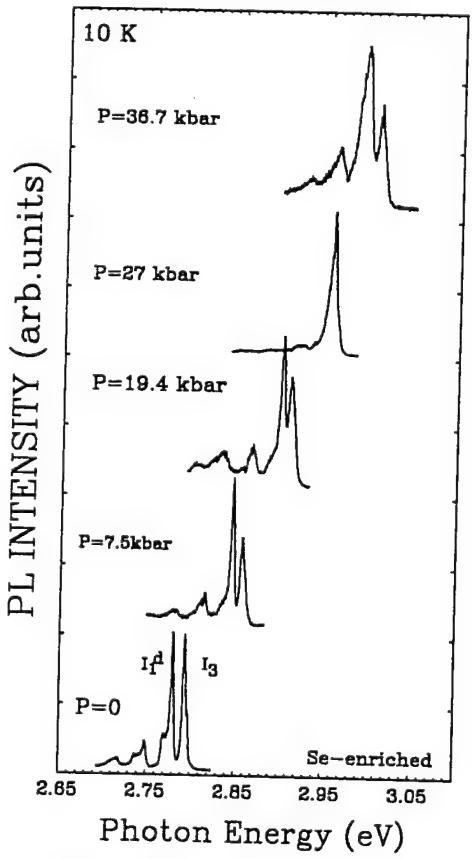

Figure 6. PL spectra of Se-enriched ZnSe samples at different pressures. The I_1^d line exhibits a higher pressure coefficient than I_3 and the two lines merge at around 27 kbar.

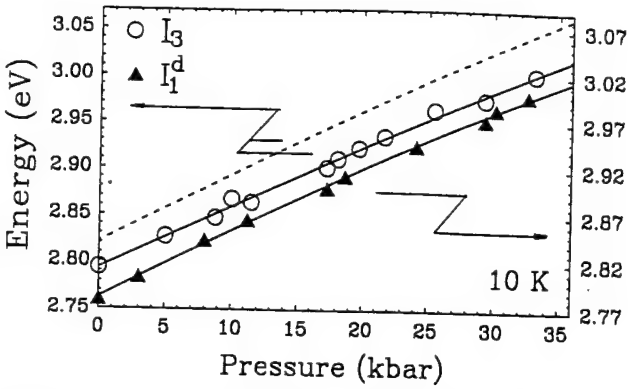

Figure 7. The variations of the energy positions for the I_1^d and I_3 lines as a function of pressure. The full lines drawn through the experimental points represent the least-squares fits. The pressure dependence of the ZnSe band gap is also plotted (broken line) for comparison.

I_1^d. The pressure coefficients of the I_3 and I_1^d lines derived from the equation

$$E(P) = E(0) + \alpha P + \beta P^2 \qquad (1)$$

are listed in table 1. Here $\alpha = dE/dP$ and $\beta = d^2E/dP^2$. The linear and quadratic pressure coefficients of the ZnSe band gap reported in the literature [23, 24] are also listed for comparison. The pressure coefficient for the ZnSe band gap in the SPVT samples should not be expected to differ significantly from the reported values.

Table 1 shows that the pressure dependence of the I_1^d emission line observed in as-grown samples is the same as that of the fundamental band gap of ZnSe. This is in agreement with the assumption that it results from the recombination of excitons bound to deep neutral acceptors [3, 4]. The effect of hydrostatic pressure on acceptor energy levels is negligible because their wavefunctions are mainly derived from the valence bands. However, the pressure coefficient of I_3 is only 6.6 meV kbar^{-1}, about 10% smaller than that of the ZnSe band gap. This phenomenon is quite different from what is expected, as the origin of the I_3 emission is considered to be a radiative recombination of excitons bound to ionized shallow donors. The pressure dependence of the I_3 line is expected to be ZnSe-like ($dE/dP = 7.3$ meV kbar^{-1}) if it originates from the recombination of excitons bound to ionized donors described on the basis of the effective mass approximation. The recombination line associated with the radiative decay of an exciton bound to a neutral or ionized donor should shift with the host semiconduc-

Table 1. Observed energy positions and pressure coefficients of the I_1^d, I_3 lines and the ZnSe band gap. Square parentheses indicate references.

	$E(0)$ (eV)	dE/dP (meV kbar^{-1})	d^2E/dP^2 (10^{-2} meV kbar^{-2})
I_1^d	2.7803	7.3(4)	−2.3(5)
I_3	2.7941	6.6(5)	−1.0(7)
E_g(ZnSe)	2.821 [8]	7.2(2) [23] 7.4; 7.5 [24]	−1.5

tor band gap under hydrostatic pressure at almost the same rate [25, 26], since the bound electron stays in the conduction valley orbit Γ_1-like donor state and the excitonic hole bound in the Coulomb field retains the Γ_{15} symmetry of the valence band edge.

It is known that application of pressure increases the binding energy of a shallow exciton arising from an increase of electron effective mass and a decrease in the dielectric constant as the band gap increases [25, 27, 28]. The pressure-induced increase in exciton binding in ZnSe has been estimated to vary the pressure coefficient of I_3 by less than 1% in numerical value. Therefore, the effect of pressure on the binding energy cannot account for the significant 10% difference between the pressure coefficient of I_3 and that of the ZnSe band gap. The binding energy of a neutral donor in ZnSe can be estimated using an effective mass approximation larger than 25 meV [4, 18]. This means that at low temperature a large proportion of donors are not thermally ionized. Photoneutralization of ionized donors could also take place under continuous photoexcitation due to the large cross section for capture of free electrons by Coulomb interaction. Isshiki and co-workers have reported a similar observation of the emission intensity of I_3 line larger than that of I_2 line from Zn-dip treated samples [6]. By changing the intensity and photon energy of the excitation light to measure the donor concentration dependence of the intensity ratio between the I_2 and I_3 emission lines, they concluded that the assumption of the I_3 line as the radiative recombination of excitons bound to ionized donors [2] is not reliable. It seems that I_3 might result from the radiative recombination of excitons bound to donor-like deep centres rather than ionized shallow donors according to our results. This is because the pressure dependence of an energy level of a deep centre is mainly determined by the composition of its wavefunction and the pressure coefficient of a deep donor will be determined mainly by the pressure dependence of the average conduction band energy [29].

5. Optically pumped stimulated emission and lasing

Room-temperature stimulated emission spectra of a 5 × 5 mm^2 SPVT ZnSe sample with 0.8 mm thickness taken with a pumping wavelength of 460 nm (2.695 eV) at three different excitation power densities are shown in figure 8. Under low-excitation intensity conditions the spectrum is characterized by a very broad emission band located around ~2.61 eV, which is presumably related to the emissions from impurities introduced into the sample during the crystal growing process. With increasing excitation power densities, a second emission band peaked at 2.639 eV appears as shown in figure 8(*a*). The intensity of this emission band increases superlinearly and becomes predominant and much sharpened as seen in figures 8(*b*) and (*c*). The full width at half maximum (FWHM) of the spectral feature narrows down to about 12 meV. A time-resolved photoluminescence measurement was performed to trace the temporal profiles of the

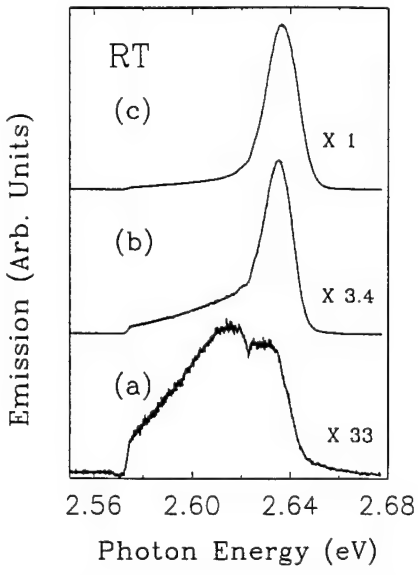

Figure 8. Stimulated emission spectra of SPVT ZnSe samples at room temperature taken with pumping wavelength of 460 nm under different excitation power densities. (*a*) Power density 16 kW cm^{-2}, the peak at higher energy position corresponding to the stimulated emission band; (*b*) power density 21 kW cm^{-2}; (*c*) power density 26 kW cm^{-2}.

excitation pulse, the photoluminescence under low-excitation power density (lower energy emission band) and that under high-excitation power density (the stimulated emission band). The results are shown in figure 9. It is evident that the higher energy emission band observed under high-excitation power has a temporally narrowed profile, which is the typical time-resolved trace of stimulated emission.

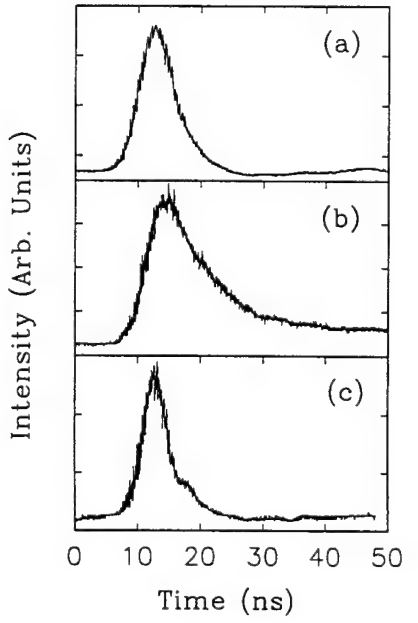

Figure 9. Comparison of temporal profiles of the excitation pulse (upper trace), spontaneous emission (centre trace) and stimulated emission (lower trace) at room temperature. The zero point of time is arbitrary.

In order to achieve room-temperature optically pumped lasing from SPVT ZnSe crystals, small bar-like samples were carefully prepared by mechanically polishing, chemically etching and manually cleaving. The sample bars were attached to a sample mount to allow the cleaved faces of the bar be positioned horizontally so as to form a resonant cavity and to allow the pump face to be illuminated from the top. Under the condition of high-excitation power densities with the pumping beam wavelength tuned close to the room-temperature band gap of ZnSe, extremely strong output of the laser emission from the ZnSe bar-like sample was achieved and the laser light was found to be polarized along the direction of the bar. Blue laser emission from the ZnSe samples could be observed by the naked eye. Figure 10 shows typical laser emission spectra taken from two ZnSe samples with resonator lengths 0.376 mm and 0.302 mm, pumped at 460 nm wavelength with about 10–11 kW cm^{-2} pumping power density. The spectra are characterized by sharp narrow lineshapes consisting of a few spectrally spaced fringes. For example, the overall FWHM of the total laser emission band of the sample with resonator length 0.376 mm is 10 meV under an excitation power density of 10.5 kW cm^{-2}. The spectrally resolvable fringes correspond to the cavity modes resulting from the reflection from the cleaved facets of the sample and the dispersion of the index of refraction for ZnSe. There is considerable dispersion in the index of refraction near the band edge [30] which influences the distribution of allowed modes oscillating in the Fabry–Pérot resonant cavity formed by mirror-like cleaved sample faces.

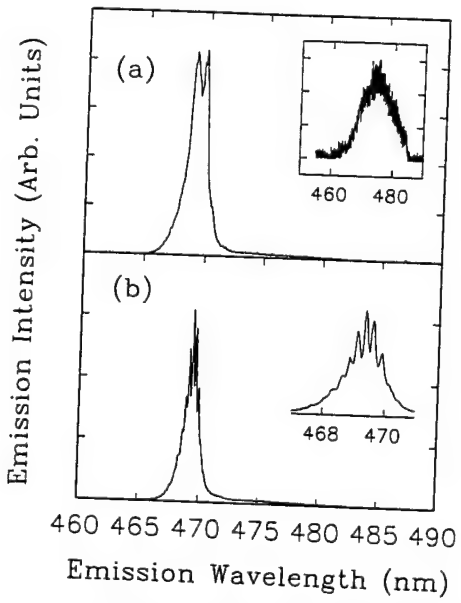

Figure 10. Typical lasing spectra taken from two ZnSe samples pumped at 460 nm wavelength. Fabry–Pérot interference fringes are easily observable. (*a*) The resonant cavity length of the sample is 0.376 mm, pumping power density 10.5 kW cm^{-2}. The inset shows the line shape of the spontaneous emission band obtained at low-excitation power density. (*b*) The resonant cavity length is 0.302 mm, pumping power density 11.0 kW cm^{-2}. The inset shows the detailed laser mode spacings.

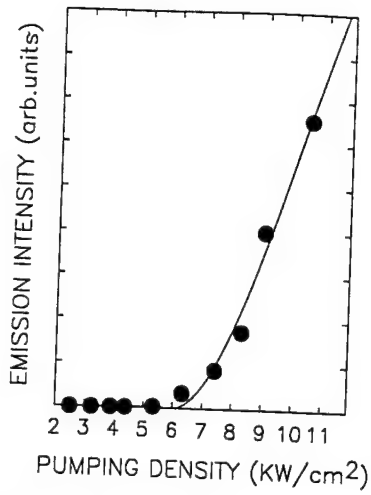

Figure 11. Emission output against optical pumping power densities for the ZnSe sample with a resonator length of 0.376 mm (sample C-3), showing a linear rise at low-excitation densities and a superlinear rise beyond 7 kW cm^{-2} at the pumping wavelength of 460 nm.

The onset of the steeply rising slope of the emission intensity plotted against pumping power densities in figure 11 is defined as the threshold for lasing. The lasing threshold pump power at room temperature was determined to be 7 kW cm^{-2} which is a surprisingly low value. This value is approximately two orders of magnitude less than that reported by Zmudzinski *et al* [31] using a high-reflection-coated ZnSe laser resonator. The lasing threshold can be severely affected by parameters dependent on both the pumping beam and the sample. The main influence of pumping-beam dependent parameters on the threshold in this work is from the excitation photon energy as far as the experimental set-up is concerned. When the photopumping wavelength is tuned to be very close to the ZnSe band gap, the sample can be efficiently pumped due to the enhancement of the carrier generation rate as observed in this work. A more important influence on the lasing threshold is from the sample itself. This can be classified into two groups: one is associated with its bulk material properties, such as impurities, crystallinity, and defects; the second is related to laser cavity length, the quality of cleaved edge facets of the sample (which formed the oscillation cavity in our case here), and the sample surface quality. It is known that the surface condition of II–VI compound semiconductor samples can greatly affect the efficiency of radiative recombinations, and that poor surface quality causes surface recombination losses [32, 33]. It is evident from our experimental results that ZnSe samples have a high degree of uniformity and that the cleaved edges of the samples have a fairly high efficiency of reflection, so that the surface recombination losses, which compete with the radiative recombination emission, are sufficiently reduced. Furthermore, there have been some new developments on blue-green LEDs and laser diodes from current injection ZnSe-based material quantum well structures [11–13] and the techniques of making heavily n- and p-doped ZnSe materials [19–23]. This means that the

practical, convenient and useful p–n junction structure of ZnSe may be fabricated and that a low-threshold high-power current injection ZnSe laser could be developed to operate in the blue range in the near future.

Another interesting result is that the stimulated emission peak energy is dependent upon the excitation photon wavelength. The energy position of the stimulated emission peak varied from 2.647 eV to 2.639 eV with the excitation photon wavelength change from 455 nm to 460 nm while keeping the excitation power density constant as shown in figure 12. The blue shift of the stimulated emission peak implies that the energy levels involved in the stimulating recombination processes vary as the excitation photon energy changes.

So far, the detailed mechanism of stimulated recombination in highly excited II–VI wide band gap compounds such as ZnSe, CdSe, ZnO is still not clear. A large variety of models have been proposed. The free-exciton–free-exciton (FE–FE) scattering and free-exciton–electron (FE–e) scattering have been among the most frequently discussed alternatives [34–38]. In such interactions one exciton is scattered into a lower energy photon-like polariton state, when a photon can be emitted from the crystal. By conservation of energy and momentum the recoiling particle is scattered into a higher energy state, making a considerable range of the polariton branch accessible. These photons will be amplified if the scattering process can be stimulated. Another possible mechanism for stimulated emission might involve the contribution from free exciton–phonon or electron–phonon interactions, particularly at room temperature. The LO phonon ($\approx$31 meV) assisted annihilation of free excitons could be one of the radiative recombination processes. But this process should not be the dominant process responsible for stimulated emission in the present study since it is not consistent with the emission peak energy being dependent on excitation wavelength. It seems that our experimental results of the excitation-wavelength-dependent stimulated emission line favour the FE–FE scattering and/or FE–e scattering models which are intrinsic recombination processes by taking into account the dispersion of the lower polariton branch in k space. However, this is an issue requiring further detailed study.

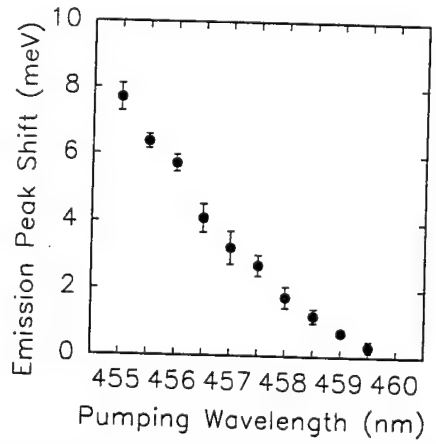

Figure 12. The dependence of the stimulated emission peak energy on the pumping wavelength. The stimulated emission peak blue shifts about 8 meV with the pumping wavelength change from 460 nm to 455 nm.

6. Conclusions

Large-size strain-free ZnSe single crystals have been successfully grown by the newly developed seeded physical vapour phase transport technique. Low-temperature photoluminescence measurements were used to examine the qualities of undoped as-grown and post growth treated ZnSe samples and to characterize the intentionally doped samples by studying the near band gap bound-exciton emission lines and donor–acceptor pair emission band. It has been found that a Zn-extraction treatment can drastically reduce the density of deep acceptors in SPVT-grown ZnSe crystals, resulting in a strong suppression of the I_1^d emission. The PL results from Ga-, Cl- and N-doped ZnSe samples indicate that the dopants were not properly incorporated into ZnSe crystals as shallow impurities by *in situ* doping during SPVT growth process. The pressure dependence of bound-exciton emissions has also been studied at low temperature using a diamond anvil cell. The pressure effect on different bound-exciton emission lines suggests that the I_3 line might originate from excitons bound to donor-like deep centres instead of ionized shallow donors due to the significant difference between the pressure coefficients of the I_3 line and ZnSe band gap. Finally, optically pumped stimulated emission and lasing studies have been conducted at room temperature. Strong blue lasing was achieved under near resonant pumping with the excitation photon energy very close to the fundamental band gap of ZnSe with a pumping density as low as 7 kW cm^{-2}. The experimental results demonstrate that SPVT ZnSe single crystals have sufficient quality to develop optoelectronic devices such as blue diode lasers and LEDs.

Acknowledgments

This work was supported by DARPA, ONR and OCAST.

References

[1] Reynolds R A 1989 *J. Vac. Sci. Technol.* A **7** 269
[2] Bhargava R N 1988 *J. Cryst. Growth* **86** 873
[3] Dean P J and Merz J L 1969 *Phys. Rev.* **178** 1310
[4] Merz J L, Kukimoto H, Nassau K and Shiever J W 1972 *Phys. Rev.* B **6** 545
[5] Merz J L, Nassau K and Shiever J W 1973 *Phys. Rev.* B **8** 1444
[6] Isshiki M, Kyotani T, Masumoto K, Uchida W and Suto S 1987 *Phys. Rev.* B **36** 2568
[7] Akimoto K, Miyajima T and Mori Y 1989 *Phys. Rev.* B **39** 3138
[8] Shahzad K, Olego D J and Cammack D A 1989 *Phys. Rev.* B **39** 13016
[9] Chadi D J 1991 *Appl. Phys. Lett.* **59** 3589

[10] Shan W, Hays J M, Yang X H, Song J J, Cantwell E and Aldridge J 1992 *Appl. Phys. Lett.* **60** 736
[11] Haase M A, Qiu J, DePuydt J M and Cheng H 1991 *Appl. Phys. Lett.* **59** 1272
[12] Jeon H, Ding J, Patterson W, Nurmikko A V, Xie W, Grillo D C, Kobayashi M and Gunshor R L 1991 *Appl. Phys. Lett.* **59** 3619
[13] Jeon H, Ding J, Nurmikko A V, Xie W, Kobayashi M and Gunshor R L 1992 *Appl. Phys. Lett.* **60** 892
[14] Cantwell G, Harsch W C, Cotal H L, Markey B G, McKeever S W S and Thomas J E 1992 *J. Appl. Phys.* **71** 2931
[15] Huang S M, Nozue Y and Igaki K 1983 *Japan. J. Appl. Phys.* **22** L420
[16] Sokolov V I, Surkova T P, Chukichev M V and Zoan M'en Vu 1984 *Sov. Phys. Solid State Phys.* **26** 2215
[17] Steiner T, Thewalt M L W and Bhargava R N 1985 *Solid State Commun.* **56** 933
[18] Dean P J and Herbert D C 1981 *Phys. Rev.* B **23** 4888
[19] Shibata N, Ohki A, Zembutsu S and Katsui A 1988 *Japan. J. Appl. Phys.* **27** L441
[20] Robbins D J, Dean P J, Simmonds P E and Tews H 1986 *Deep Centers in Semiconductors* ed S T Pantelides (New York: Gordon and Breach) ch 11
[21] Ohyama T, Otsuka E, Yoshida T, Isshiki M and Igaki K 1985 *Proc. 17th Int. Conf. on the Physics of Semiconductors* ed J Chadi and W A Harrison (New York: Springer) p 1313
[22] Isshiki M, Tomizono T, Yoshida Y and Igaki K 1984 *Japan. J. Inst. Met.* **48** 1176
[23] Ves S, Strossner K, Christensen N E, Kim C K and Cardona M 1985 *Solid State Commun.* **56** 479
[24] *Landolt-Börnstein, New Series, Group III* 1988 **22a** ed O Madelung (Berlin: Springer) p 178 and references therein
[25] Wolford D J and Bradley J A 1985 *Solid State Commun.* **53** 1069
[26] Gil B, Baj M, Camassel J, Mathieu H, Benoit à la Guillaume C, Mestres N and Pascual J 1984 *Phys. Rev.* B **29** 3398
[27] Shantharama L G, Adams A R, Ahmad C N and Nicholas R J 1984 *J. Phys. C: Solid State Phys.* **17** 4429
[28] Samara G A 1983 *Phys. Rev.* B **27** 3494
[29] Chadi J and Chang K J 1988 *Phys. Rev. Lett.* **61** 873
[30] Adachi S and Taguchi T 1991 *Phys. Rev.* B **43** 9569 and references therein
[31] Zmudzinski C A, Guan Y and Zory P S 1990 *IEEE Photon. Technol. Lett.* **2** 94
[32] Pankove J I 1971 *Optical Processes in Semiconductors* (New York: Dover) ch 7
[33] Cotal H L, Lewandowski A C, Markey B G, McKeever S W S, Cantwell E and Aldridge J 1990 *J. Appl. Phys.* **67** 975
[34] Benoit à la Guillaume C, Debever J M and Salvan F 1969 *Phys. Rev.* **177** 567
[35] Moriya T and Kushida T 1976 *J. Phys. Soc. Japan* **40** 1668, 1676
[36] Magde D and Mahr H 1970 *Phys. Rev. Lett.* **24** 890; 1970 *Phys. Rev.* B **2** 4098
[37] Mahr H 1975 *Excitons at High Density* eds H Haken and S Nikitine (New York: Springer) p 265
[38] Newbury P R, Shahzad K and Cammack D A 1991 *Appl. Phys. Lett.* **58** 1065

Two-photon pumped blue lasing in bulk ZnSe and ZnSSe

X. H. Yang, J. M. Hays, W. Shan,[a] and J. J. Song
Center for Laser Research and Department of Physics, Oklahoma State University, Stillwater, Oklahoma 74078

E. Cantwell
Eagle Picher Research Laboratories, Miami, Oklahoma 74354

(Received 5 October 1992; accepted for publication 14 December 1992)

We have studied laser action of ZnSe and $ZnS_{0.05}Se_{0.95}$ samples grown by seeded physical vapor phase transport (SPVT) technique in the near resonant two-photon absorption regime. The two-photon pumped lasing was observed using a tunable near-infrared nanosecond laser (830–890 nm). Blue lasing could be observed up to 200 K and the two-photon pumped lasing threshold was measured to be ~ 7 MW/cm^2 at 10 K. This work demonstrates the applicability of using near-infrared diode lasers as pumping sources to excite the ZnSe-based materials. By comparing the energy position of two-photon pumped lasing with that of the one-photon pumped lasing and examining the red shift of the energy position, we suggest that the free-exciton free-exciton scattering and resultant band filling are the dominant processes involved in the lasing action of ZnSe and ZnSSe alloy crystals at low temperature.

Compact coherent sources with low cost and high efficiency operating in the blue and green regions of the visible spectrum are required for a broad range of applications, including compact displays, data storage and biomedical diagnostics, ZnSe and ZnSe-based materials give promise in the development of such sources as blue-green diode lasers and therefore have been extensively studied.[1–12] The lasing characteristics in these materials have been studied both by optical and electron beam pumping.[2,3,8–12] In general, the optical excitation was achieved in the one-photon absorption regime by using excitation photon energies above the band gap of ZnSe. The blue lasing from ZnSe and ZnSSe bulk samples have been previously obtained by using the one photon pumping (OPP) method.[2,3,8,9,12] In this letter, we report new experimental results on the study of low-temperature laser action of ZnSe and $ZnS_{0.05}Se_{0.95}$ bulk samples in the near resonant two-photon absorption regime by using the two photon pumping (TPP) method. By using a tunable near-infrared nanosecond laser (830–890 nm), the two-photon pumped blue lasing could be observed up to 200 K and the lasing threshold was measured to be ~ 7 MW/cm^2. This observation of infrared-pumped visible laser action in ZnSe and ZnSSe single crystals indicates the applicability of using near-infrared GaAs-based III-V semiconductor compound diode lasers as a pumping source to excite the ZnSe-based materials for blue laser.

Samples used in this study were ZnSe and $ZnS_{0.05}Se_{0.95}$ single crystals. Samples were prepared to be barlike with cavity length of ~ 300–500 μm and mounted to a cold finger of a closed recycle refrigerator. The natural facets acted as reflective mirrors. The detailed description of sample growth and preparation has been discussed in our previous reports.[8,9] The difference of the current experimental setup and the single photon pumping case described in Refs. 8 and 9 is in the use of a near-infrared dye laser as the optical pumping source, rather than the use of a frequency tracking doubler to double the near-infrared laser beam for excitation.

The laser emission generated by TPP in both ZnSe and $ZnS_{0.05}Se_{0.95}$ samples is very strong. The blue light emitted from samples is visible to the naked eye at ambient room illumination. The emission spectra from a ZnSe sample with a cavity length of 430 μm measured at 10 K are shown in Fig. 1(a). The excitation wavelength is 850 nm. From the figure one can see that the spontaneous emission from the sample has a few relatively broad peaks. Under high excitation conditions the dominant emission spectral feature is a narrow peak at ~ 446.4 nm whereas the other features present in the spontaneous emission spectrum are suppressed. The longitudinal cavity mode structures are also resolvable in the laser emission spectrum. The threshold of the excitation power for lasing was measured to be ~ 7 MW/cm^2. The emission spectra taken from $ZnS_{0.05}Se_{0.95}$ samples are similar to those from ZnSe samples and are shown in Fig. 1(b). Due to the alloying effect the laser emission peak shifts to ~ 438 nm in $ZnS_{0.05}Se_{0.95}$ samples. Figure 2 shows the emission intensity versus pumping power density for the ZnSe sample. A functional form of x^n with $n=5.2$ can be derived from the curve above the lasing threshold for the ZnSe sample. This power characteristic, together with the spectral narrowing, are manifestations of laser action resulting from TPP.[13] Similar results were observed for ZnSSe samples. A functional form of x^6 could be obtained before the onset of saturation of the laser emission in this sample.

The laser action could be observed up to 200 K for both ZnSe and ZnSSe samples. In Fig. 3 we show the experimentally measured energy position of lasing peaks as a function of temperature. The solid line in the figure is the temperature dependence of energy position of free exciton in ZnSe.[14] Typical spectra of the lasing output are shown in the inset of the figure. The lasing threshold power density increases by a factor of about three when the temperature

[a]On leave from National Laboratory for Infrared Physics, Shanghai Institute of Technical Physics, Chinese Academy of Sciences, Shanghai, 200083, People's Republic of China.

 0003-6951/93/101071-03$06.00

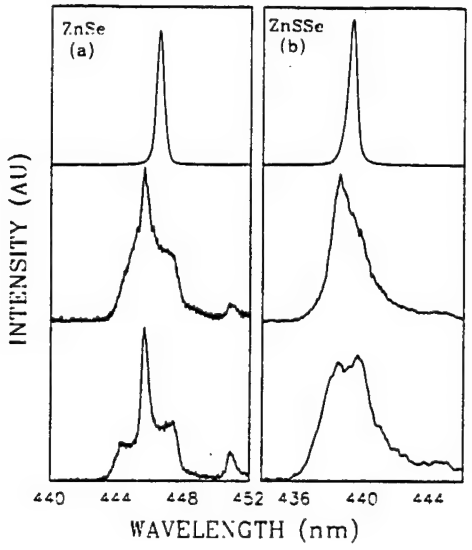

FIG. 1. Typical emission spectra from ZnSe (a) and $ZnS_{0.05}Se_{0.95}$ (b) at 10 K with the excitation wavelength at 850 nm under different excitation densities. Lower spectra: (a) 2.3 MW/cm^2, (b) 8 MW/cm^2; middle: (a) 5 MW/cm^2, (b) 13 MW/cm^2; upper: (a) 16 MW/cm^2, (b) 21 MW/cm^2.

changes from 10 to 200 K. The linewidth is broadened by a factor less than two (from ~4.9 to 7.3 meV in full width at half maximum) and the longitudinal modes could be also observed even at 200 K. While tuning the pumping wavelength from 830 to 867 nm, the laser action could be observed at 10 K from all the samples used in this study. When the pumping wavelength is longer than 867 nm, the laser action quenches regardless of the pumping power density used. Compared to the OPP situation, where the laser action could be observed with pumping wavelengths as long as 442 nm, it appears that the two-photon pumped lasing process requires a higher effective excitation energy (twice of the pumping photon energy). One of the reasons responsible for this difference has been suggested to be due to the fact that the two-photon absorption coefficient changes much more drastically with incident laser wavelength than the one-photon absorption coefficient for semi-

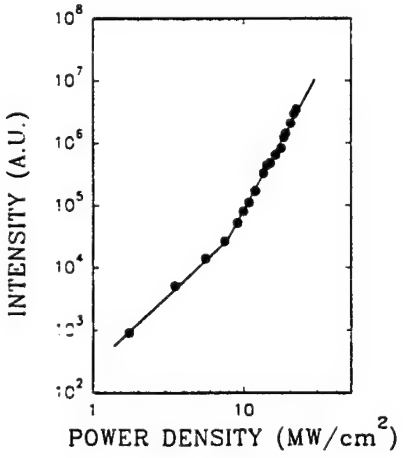

FIG. 2. The lasing emission intensity dependence of the ZnSe sample with 420 μm cavity length on the pumping power density at 10 K. The solid line through the data points is a guide for the eye.

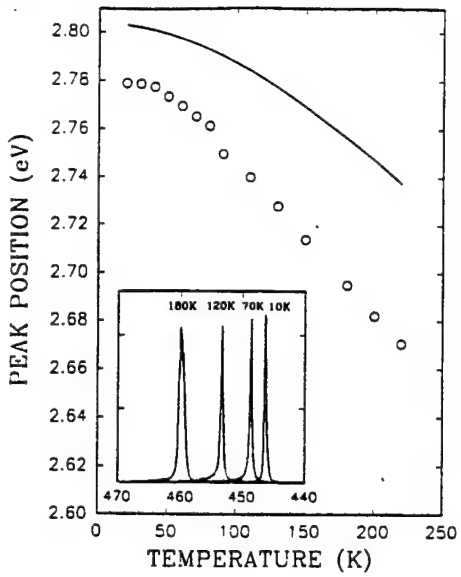

FIG. 3. Variation of the measured lasing energy position with temperature. The solid line in the figure is the temperature dependence of energy position of free exciton in ZnSe. The inset shows lasing spectra of a ZnSe sample at different temperatures.

conductor materials.[13,15] The difference between TPP and OPP methods is that in the TPP case a much larger excitation volume can be efficiently achieved. The influence of sample surface related defects could be therefore greatly reduced. In addition, different transition selection rules are involved in two-photon pumping, compared with one photon pumping. TPP can induce optical transitions between levels having the same parity, which are forbidden under OPP condition. As a result, TPP is complimentary to OPP in studying the laser action and its physical origins. We have also found that the TPP lasing peak position at threshold pump powers for ZnSe samples is approximately the same as those of our previous OPP experimental results.[16] Nearly the same lasing peak positions of TPP and OPP suggests that the TPP lasing process might be of the same physical origin as OPP lasing processes.

In wide band-gap II-VI compound semiconductor materials excitons are known to play important roles in lasing processes.[3] The LO-phonon assisted free exciton (FE) recombination, i.e., a FE-phonon scattering process, was proposed to be the dominant lasing mechanism under two photon pumping.[13,17] However as shown in Fig. 3, the laser transition shifts to lower energy with increasing temperature more rapidly than the FE energy. This shift cannot be explained with recourse to the FE-phonon scattering process. The sample heating effect can be also excluded. The low average excitation intensity of the near-infrared dye laser with a pulse of 10 ns and a repetition rate of 10 Hz and small two-photon absorption coefficients of ZnSe and ZnSSe at the near-band-gap region are not likely to cause significant heating on the samples. By monitoring the peak position of the LO-phonon assisted deep acceptor bound exciton line in ZnSe as a function of excitation intensity, we found that it is independent of the excitation intensity. Another alternative is a free-exciton free-exciton (FE–FE) scattering process. In such a scattering process, one exciton

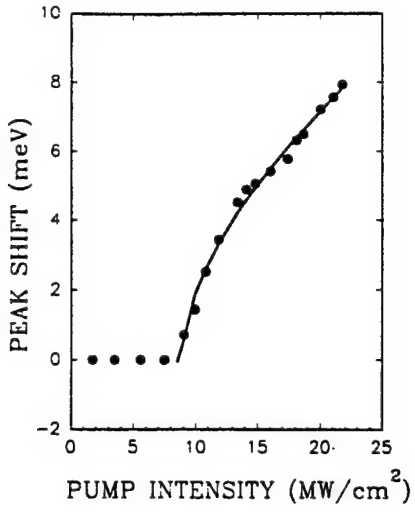

FIG. 4. The lasing peak energy shift of a ZnSe sample vs pump intensities. The solid line is a theoretical fit to the experimental data.

is scattered into a lower energy photonlike part of polariton dispersion curve then annihilated to emit a photon while the recoiling exciton is scattered into a higher energy state, which could be the continuum of free electron and hole states. In the case of high excitation, a high density of free carriers could be created resulting in the occurrence of the band filling effect. When the FE–FE interaction process takes place, the free carriers created must obtain sufficient kinetic energy from the exciton in order to reach the higher lying unfilled states in the bands. Consequently, the exciton scattered into the photonlike branch of polariton will lose more energy. A red shift of the lasing transition is therefore expected to occur with increasing carrier densities originating from the excitation power density increase. Such a red shift with the pump intensity was indeed observed in this work as shown in Fig. 4. The solid line in the figure is a fit of the lasing peak energy shift ΔE as a function of TPP density using the equation

$$\Delta E = a(I_p - I_{p0})^N + b. \quad (1)$$

Here a and b are fitting parameters and I_{p0} is TPP lasing threshold. Recently, Newbury *et al.* have studied one-photon pumped stimulated emission in ZnSe epilayers[18] and suggested that, by energy conservation, the red shift of the lasing peak (ΔE) should equal the kinetic energies of the recoiling electron and hole obtained due to FE–FE scattering with the assumption of that all carriers relax down to the bottom of their respective bands. Therefore the total energy required to reach the lowest unfilled states of free-carrier continuum is proportional to two thirds power of the generated free carrier concentration.[18] On the other hand, the free-electron (hole) concentration is proportional to the square root of the free-carrier generation rate for the FE–FE scattering process[18] and in the two-photon absorption regime the generation rate is proportional to the square of the pumping intensity.[19] This means that the free-carrier (either electron and/or hole) concentration is a linear function of the two-photon pumping density. Therefore, theoretical estimation gives $N=2/3$ in Eq. (1). By using fitting parameters $a=2.02$ and $b=0.58$, along with the measured $I_{p0}=7$ MW/cm^2, the best fit gives $N=0.64$. This value is close to the value of 2/3 derived from the theoretical estimation based on the FE–FE scattering process. Hence our results suggest that the FE–FE scattering dominates the low-temperature lasing process in ZnSe and ZnSSe alloy crystals.

In summary, we have studied the laser action of SPVT ZnSe and $ZnS_{0.05}Se_{0.95}$ alloy crystals in the two photon absorption regime. The infrared pumped visible lasing has been observed in both ZnSe and ZnSSe alloy samples up to 200 K by tuning the pumping light wavelength in the range of 830–890 nm. These experimental results indicate the possibility of using near-infrared GaAs based III-V compound diode lasers as excitation sources to pump ZnSe based II-VI materials for blue lasing. Based on the peak energy position and the red shift of the lasing line above threshold, the dominant physical mechanism of lasing is attributed to the free-exciton scattering and resultant band filling processes.

This work was supported by ONR, DARPA, and OCAST.

[1] G. Sun, K. Shahzad, J. M. Gaines, and J. B. Khurgin, Appl. Phys. Lett. **59**, 310 (1991).
[2] C. A. Zmudzinski, Y. Guan, and P. S. Zory, IEEE Photon. Technol. Lett. **2**, 94 (1990).
[3] H. Jeon, J. Ding, A. V. Nurmikko, H. Luo, N. Samarth, and J. Furdyna, Appl. Phys. Lett. **59**, 1293 (1991).
[4] K. Nakanishi, I. Suemune, Y. Fujii, Y. Kuroda, and M. Yamanishi, Appl. Phys. Lett. **59**, 1401 (1991).
[5] M. A. Haase, J. Qiu, J. M. Depuydt, and H. Cheng, Appl. Phys. Lett. **59**, 1271 (1991).
[6] H. Jeon, J. Ding, A. V. Nurmikko, W. Xie, D. C. Grillo, M. Kobayashi, R. L. Gunshor, G. C. Hua, and N. Otsuka, Appl. Phys. Lett. **60**, 2045 (1992).
[7] T. Ishihara, G. Brunthaler, W. Walecki, M. Hagerott, A. V. Nurmikko, N. Samarth, H. Luo, and J. Furdyna, Appl. Phys. Lett. **60**, 2460 (1992).
[8] X. H. Yang, J. Hays, W. Shan, J. J. Song, E. Cantwell, and J. Aldridge, Appl. Phys. Lett. **59**, 1681 (1991).
[9] X. H. Yang, J. Hays, W. Shan, J. J. Song, E. Cantwell, and J. Aldridge, Appl. Phys. Lett. **60**, 926 (1992).
[10] S. Colak, R. N. Bhargava, B. J. Fitzpatrick, and A. Sicignano, J. Lumin. **31&32**, 430 (1984).
[11] H. Jeon, J. Ding, A. V. Nurmikko, H. Luo, N. Samarth, J. K. Furdyna, W. A. Bonner, and R. E. Nahory, Appl. Phys. Lett. **57**, 2413 (1990).
[12] M. A. Haase, J. Qiu, J. M. DePuydt, and H. Cheng, Appl. Phys. Lett. **59**, 1272 (1991).
[13] V. P. Gribkovskii, V. A. Zaporozhchenko, V. A. Ivanov, A. V. Kachinskii, V. V. Parashchuk, and G. P. Yablonskii, Sov. J. Quantum Electron. **9**, 1305 (1980).
[14] M. H. Weiler, Solid State Commun. **39**, 937 (1981).
[15] C. R. Pidgeon, B. S. Wherrett, A. M. Johnston, J. Dempsey, and A. Miller, Phys. Rev. Lett. **42**, 1785 (1979).
[16] X. H. Yang, J. J. Song, E. Cantwell, and J. Aldridge, Phys. Status Solidi **127**, A K79 (1991).
[17] I. M. Catalano, A. Cingolani, M. Ferrara, and M. Lugara, Solid State Commun. **43**, 371 (1982).
[18] P. R. Newbury, K. Shahzad, and D. A. Cammack, Appl. Phys. Lett. **58**, 1065 (1991).
[19] C. Klingshirn and H. Haug, Phys. Rep. **70**, 315 (1981).

Optical properties of highly strained CdSe/ZnSe quantum wells

W. Shan,[a] S. J. Hwang, J. M. Hays, and J. J. Song
Department of Physics and Center for Laser Research, Oklahoma State University, Stillwater, Oklahoma 74078

Z. Q. Zhu and T. Yao
Department of Electrical Engineering, Hiroshima University, Higashi-Hiroshima 724, Japan

(Received 5 May 1993; accepted for publication 13 July 1993)

We present a study of the optical properties of highly strained CdSe/ZnSe quantum well system. A variety of CdSe/ZnSe samples containing single quantum well or multiple quantum wells grown by molecular beam epitaxy has been studied by using low-temperature photoluminescence (PL), photoluminescence excitation, and photoreflectance measurements. The strong PL signals associated with excitonic emissions from the samples show that the CdSe/ZnSe heterostructure system is promising in the development of laser diodes and light-emitting diodes operating in the blue-green range. Linewidth narrowing of PL spectra with decreasing well width is observed and attributed to alloy formation at the interface due to lateral interdiffusion. The PL signal intensities and the pressure coefficients of interband transitions are also found to depend on the well width, which can be explained in terms of strain relaxation induced misfit dislocations and the critical thickness in the heterostructure system. Our results suggest that the critical thickness for a CdSe layer coherently grown on ZnSe is less than four monolayers.

I. INTRODUCTION

Wide band gap II-VI compound semiconductor multilayer heterostructures have attracted much attention for their scientific and technological importance appropriate for optoelectronic devices such as laser diodes (LDs) and light-emitting diodes (LEDs) operating in the blue-green range. The ZnSe-based quantum well structures are among the most extensively studied heterostructures. Great progress has been made during the past two years with the demonstration of blue laser action and electroluminescence from (Zn,Cd)Se/ZnSe quantum well devices.[1–3] This has stimulated increasing activities in the study of the all-binary strained CdSe/ZnSe system due to its possible application in blue-green light emission devices and large optical nonlinearity.[4–9] Unlike other strained II-VI systems such as ZnSe/ZnS and CdTe/ZnTe, the CdSe/ZnSe system is grown utilizing two materials with differing crystal structures in bulk form. Although the normal crystal structure of CdSe is hexagonal wurtzite instead of cubic zinc-blende, single-crystal zinc-blende CdSe and CdZnSe alloy thin films can be grown on (100) GaAs substrates by molecular beam epitaxy (MBE).[10,11] Therefore CdSe/ZnSe heterostructures in the cubic phase are expected to be grown by MBE on zinc-blende substrates such as GaAs.

In this paper we present the results of a study on the optical properties of CdSe/ZnSe quantum wells (QWs) grown by MBE on GaAs substrates. A variety of CdSe/ZnSe QWs with different well widths were prepared for the study. Photoluminescence (PL), photoluminescence excitation (PLE), and photoreflectance (PR) measurements were performed at low temperatures to characterize quantum confinement effects of these samples and to evaluate sample quality by monitoring the excitonic emissions from the QWs. The PL emission intensity is found to drop drastically as the CdSe well width is increased beyond three monolayers and the PL linewidth is found to narrow as the well width decreases. Significant discrepancy in the energy positions of the PL emission between single quantum wells (SQWs) and multiple quantum wells (MQWs) with the same well widths is also observed. Low-temperature pressure-dependent PL measurements were also performed on some samples in order to obtain some additional information to give more insight into these problems. We found that the pressure coefficient of the PL emission associated with transitions between the lowest confined states is quantum-well width dependent. Our results suggest that the linewidth narrowing of PL spectra with the well width can be attributed to alloy formation at the interface due to lateral interface diffusion; the dependence of the PL signal intensity and the pressure coefficients on the well width can be explained in terms of strain relaxation induced misfit dislocations and critical thickness in the system. The critical thickness for CdSe layers coherently grown on ZnSe is suggested to be less than four monolayers.

II. EXPERIMENTS AND RESULTS

All CdSe/ZnSe QS samples used in this study are grown by MBE using GaAs substrates. A ZnSe buffer layer (approximately 2 μm) was first grown on a (100) GaAs substrate under optimal growth conditions,[12] then followed by the quantum well structures. A $\sim$1000 Å ZnSe clading layer was deposited to cap the quantum well structures. Three groups of quantum well structures were prepared: (i) four single quantum well (SQW) samples with a CdSe well width of 1, 2, 3, and 4 monolayers (MLs), respec-

[a]On leave from Shanghai Institute of Technical Physics, Chinese Academy of Sciences, Shanghai, P. R. China.

 0021-8979/93/74(9)/5699/6/$6.00

tively; (ii) two multiple quantum well (MQWs) samples with the well width of 1 ML [CdSe (3 Å)/ZnSe (163 Å)×50 periods] and 2 MLs [CsSe (7 Å)/ZnSe (167 Å)×25 periods], respectively; and (iii) a so-called "fractional" SQW sample with a series of submonolayer CdSe wells. This sample was prepared by depositing less than one monolayer of CdSe on the ZnSe surface and subsequently following the growth of 1000 Å ZnSe to form a nominal CdSe/ZnSe fractional SQW. The deposition times for CdSe onto the ZnSe surface were 1, 2, 3, and 4 s under the MBE growth condition, corresponding to form quantum wells with 1/4-, 1/2-, 3/4-, and 1-ML CdSe, respectively. The well thicknesses of MQWs were measured by x-ray diffraction. High-resolution x-ray rocking curves confirmed that the true well thicknesses controlled by the MBE shutter times with the thermal flux transient taken into account are in good agreement with the designed ones. As for the SQWs, in addition, the experimentally measured emission energies as a function of number of monolayers were compared with theoretical calculations. The results indicate the true well thicknesses are with an error of less 1 ML. Photoluminescence measurements were performed using the 3250 Å line from a HeCd laser as the excitation source. Samples were attached to a cold finger in a closed-cycle cryostat. The PL signals were detected by a GaAs photomultiplier with a photon counting electronic system through a 0.85 m double-grating spectrometer. Continuous light from a halogen tungsten lamp dispersed by a 0.5 m monochromator was used as a tunable excitation source for PLE and as the probe beam for PR measurements. The detection positions for PLE measurements were set at the corresponding PL peak positions for the given samples. A chopped HeCd laser beam was used in PR measurements to provide a repetitive modulation to the samples. The luminescence and reflectance signals were detected by a UV-enhanced Si photodiode followed by a lock-in amplifier and data acquisition system.

In all samples used in this work, the PL signals were found to exhibit a single excitonic emission line except the sample with four submonolayer SQWs. In Fig. 1, the PL spectra from 1-, 2-, 3-, and 4-ML SQWs at 10 K are shown. It has been reported by several authors[6,9] that PL spectra of CdSe/ZnSe samples show a decrease of signal intensity and an increase of the full width at half maximum (FWHM) with increasing CdSe layer thickness. We have made a similar observation in our samples. For example, under the same excitation condition the PL intensity of the 4-ML SQW sample decreases by a factor of 10 compared to the other three with narrower wells. The FWHM of the PL emission is about 15 meV for the 1-ML SQW sample and about 35–40 meV for the other three. In Fig. 2 we show the PL spectrum taken from the "fractional" SQW sample with nominal submonolayer quantum wells. Although the emission lines from the four wells in the sample overlap, the PL spectral structures associated with 1/4- and 1-ML wells can be well resolved. We note that the FWHM is only about 5 meV for the PL line corresponding to the nominal 1/4-ML well in the ample. The differences in relative intensities from different wells in this sample are qualitatively

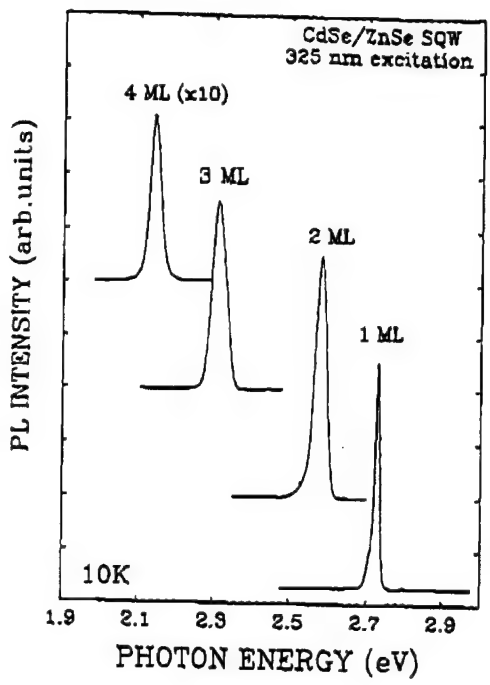

FIG. 1. Photoluminescence spectra taken from CdSe/ZnSe SQWs with different well widths. The curves are vertically displaced for clarity.

due to the attenuation of exciting radiation by absorption of the wider wells closer to the surface as well as the ZnSe barriers as the light penetrates the sample and reabsorption of the photoluminescence. Thus the PL emission intensity depends on the distance between the sample surface and each individual quantum well in the sample.

Shown in Fig. 3 are the spectra of PL and PR at 80 K obtained from CdSe (3 Å)/ZnSe (163 Å) MQWs. The FWHM of the PL emission lines observed in the MQW samples are more than twice as broad as that from the SQW samples with the same well widths, mainly due to layer-thickness fluctuations in the MQWs. In these two MQWs the PL energy positions are significantly lower than their counterparts in the SQWs. A comparison is presented in Fig. 4, where the experimentally observed PL energy positions from the all samples studied in this work are plotted as a function of the well width (number of mono-

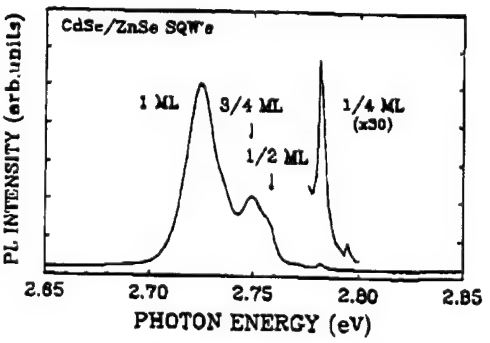

FIG. 2. PL spectral structures of the SQW sample with nominal submonolayer CdSe wells.

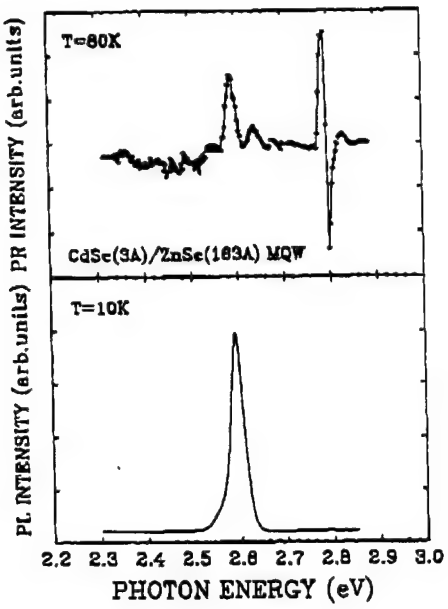

FIG. 3. Photoreflectance (top) and photoluminescence (bottom) spectra from CdSe (3 Å)/ZnSe (163 Å) MQWs. The spectral structures at higher energy around 2.8 eV are transitions associated with the ZnSe barriers and the buffer layer.

layers). As shown in the figure, the difference in energy positions between the PL peaks from SQWs and MQWs with identical CdSe layer thickness is quite large. From the figure one can also see that the experimentally obtained PL spectral range (450–577 nm) from the CdSe/ZnSe quantum wells used in this work covers virtually the entire blue-green region as the CdSe layer thickness varies from nominal 1/4 ML to 4 MLs. This suggests that the all-binary CdSe/ZnSe system is also promising in the development of optoelectronic devices operating at the short-wavelength range of the visible region.

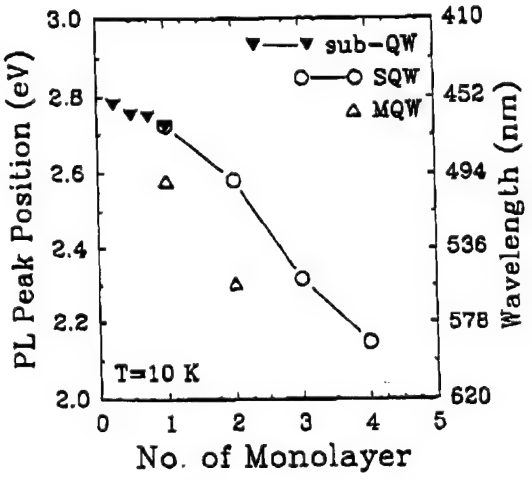

FIG. 4. Experimentally obtained PL emission peak positions as a function of the number of monolayers for the CdSe well.

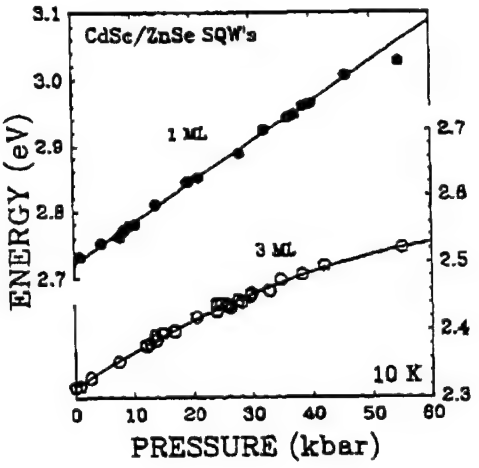

FIG. 5. Pressure dependence of direct interband transitions in 1-ML and 3-ML SQWs measured by PL at 10 K. The strong sublinear pressure dependent behavior of the 3-ML SQW sample is considered to be caused by strain relaxation under applied pressure.

III. DISCUSSIONS

So far there have been several reports on the study of the CdSe/ZnSe quantum well structures mainly concerning sample preparation and optical characterization.[4–9] In these studies a decrease of the PL signal intensity with increasing well width was commonly observed. We also observed a considerable decrease of the PL emission intensity in the 4-ML SQW sample. The other SQW samples with narrower well widths (1, 2, and 3 MLs) exhibit more or less the same emission intensity. It is well known that the decrease of the PL intensity in a quantum well, particularly in a strained quantum well, usually indicates poor sample quality. Since the CdSe/ZnSe is a highly lattice-mismatched strain system, the decrease of the PL intensity in the 4-ML SQW sample is most likely to result from both the built-in strain partially relaxed and misfit dislocations generated when the CdSe layer thickness exceeds the critical limit for pseudomorphically strained layer growth.

We have studied the effect of hydrostatic pressure on the energy levels in the SQW samples at 10 K to give more insight to the problem. Shown in Fig. 5 is the effect of pressure on the direct gap transitions in the 1- and 3-ML SQWs. The 1 ML SQW sample shows a typically linear dependence of the direct band gap transition on pressure, which can be described by a least-squares fit to the experimental data using the linear function

$$E(P)=E(0)+\alpha P, \tag{1}$$

where $E(0)$ is the interband transition energy at ambient pressure and α, the pressure coefficient. This phenomenon has been well documented in various studies of the effect of pressure on the direct band gap transitions in a variety of quantum well systems.[13–19] For the 3-ML SQW sample, an appreciably smaller pressure dependence with considerably strong sublinear behavior was obtained. This is a real effect beyond the experimental uncertainty. The function

$$E(P)=E(0)+\alpha P+\beta P^2 \tag{2}$$

TABLE I. Pressure dependence of the excitonic emission from CdSe/ZnSe SQWs. The pressure coefficients of cubic ZnSe and hexagonal CdSe bulks are also listed.

Samples	$E(0)$	$\alpha = dE/dP$ (meV/kbar)	$\beta = d^2E/dP^2$ (10^{-2} meV/kbar^2)
1 ML	2.723	6.1	...
3 ML	2.316	5.6	−3.3
ZnSe	2.821[a]	7.2[b]	−1.5[b]
CdSe	1.738[c]	5.8[c]	...

[a]Reference 20.
[b]Reference 21.
[c]Reference 22.

was used to make a least-squares fit in order to derive the liner (α) and quadratic (β) pressure coefficients from the data. In Table I we show the comparison of the pressure coefficients in these two samples with the counterparts of zinc-blende ZnSe and wurtzite CdSe in bulk form.[20–22] The direct band gap transition energies at ambient pressure are also given in the table. It has been reported by several authors[15,16,19] that the values of pressure coefficients of quantum transitions obtained by fitting Eq. (1) are slightly dependent on the quantum well width with a variation in a frame of about 1%–2%. The difference in the linear pressure coefficients for the 1- and 3-ML SQW samples, however, is quite large ($>8\%$). Moreover, the significant sublinear pressure dependence for the 3-ML SQW sample is not comparable to that for the 1-ML SQW sample. The explanation to such a phenomenon is that three monolayers is the critical thickness for CdSe to be pseudomorphically grown on ZnSe to form a coherent quantum well. The built-in strain which elastically accommodates the lattice of CdSe to that of ZnSe starts relaxing when external pressure is applied on the 3-ML SQW sample since the highly strained CdSe layer is at the margin of critical value and cannot sustain any extra stress, although the stress is hydrostatic. Dislocations then appear at the heterointerfaces as a result of applied pressure induced lattice relaxation. The short-range potentials of the dislocations will perturb the wave functions of quantum states confined to the well and give rise to variations of the pressure dependence of those states. This results in a reduction of the pressure coefficient of the direct interband transition and produces a significantly strong sublinear pressure dependence in the 3-ML SQW sample.

Another interesting result is the PL linewidth narrowing with decreasing well width observed in SQWs and the so-called fractional SQW sample with submonolayer wells as shown in Fig. 6. In general, at low temperature and low excited carrier concentrations the principal linewidth broadening mechanism associated with excitonic transitions in semiconductor quantum well structures arises from inhomogeneous origins such as structural or compositional fluctuations.[23–25] The linewidths of excitonic emission in quantum well structures are strongly influenced by the potential fluctuations induced by interface roughness and broadens as the well thickness decreases in the moderate range of well width (>10 Å).[26,27] However, for the

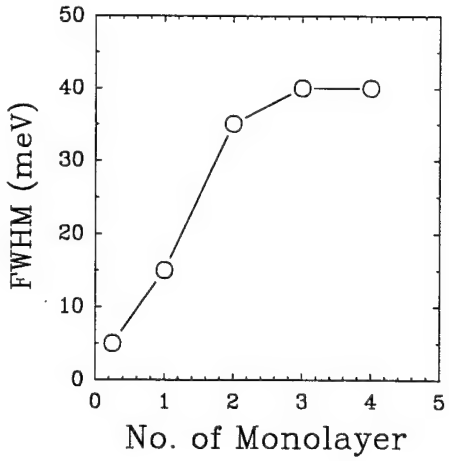

FIG. 6. The full width at half maximum (FWHM) of PL spectra from SQWs as a function of the CdSe layer thickness (number of monolayers).

samples with very thin wells (<10 Å) the linewidth narrows with decreasing well thickness as observed in this study and reported by some authors.[9,27] Zhu *et al.* have suggested that interfacial alloy formation due to lateral interdiffusion in such ultrathin wells as submonolayer CdSe has to be taken into account to explain the linewidth narrowing.[28] A 2-ML-thick $Cd_xZn_{1-x}Se$ alloy layer will be formed when CdSe is deposited on the surface of ZnSe as a result of interlayer diffusion because of the formation of CdSe islands and valleys. The alloy concentration can be estimated depending on the nominal thickness of submonolayers. For example, 1/4 monolayer is equivalent to $x=0.125$ and one monolayer equivalent to $x=0.5$. Therefore the linewidth of excitonic emission considerably depends on the alloy concentration due to inhomogeneous broadening by the alloy scattering potential rather than interface roughness. That is because as a quantum well layer is reduced to very thin layer approaching to zero, the spatial confinement of two-dimensional exciton in the well will diminish. Consequently, the linewidth broadening of exciton emission due to well width fluctuations will be very much reduced because the changes in the thicknesses of very thin well layers have little effect on exciton energies which will converge asymptotically to that of three-dimensional exciton.[29]

Finally, we also note that the interband transition energies obtained from both MQWs are about 100 meV lower than those from SQW counterparts. Similar observations were reported in Ref. 9. It is known that for strained superlattice and quantum well structures to be coherent with the substrate or buffer layer the individual layers must be thinner than their own critical thicknesses and the overall thickness of the structure as a whole must be lower than some critical value.[30,31] When a well layer thickness or the thickness of the whole structure is greater than the critical value, the built-in strain will relax and arrays of dislocations will appear. As a result, a red shift of the photoluminescence peak can be observed with respect to the completely strained system. Since CdSe/ZnSe is a highly strained system with about a 7% lattice mismatch, the

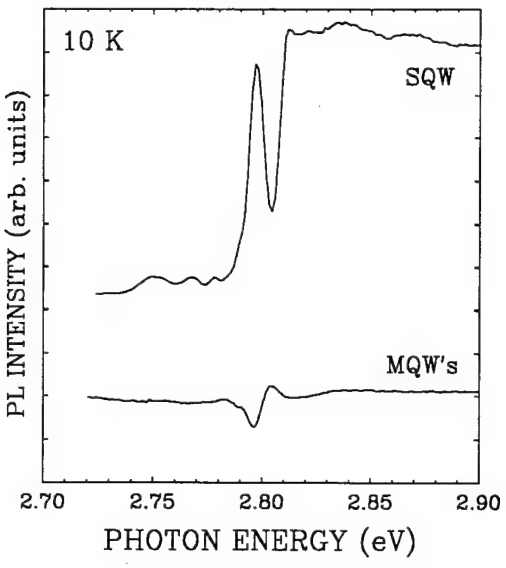

FIG. 7. Photoluminescence excitation spectra obtained near the ZnSe band gap for 1-ML SQW and 1-ML MQW [CdSe (3 Å)/ZnSe (163 Å) with 50 periods] samples. The detection wavelengths were set to the respective PL peak positions of the samples.

whole MQW thickness might be over the critical limit for a coherently strained structure. The lower PL emission position observed in MQWs compared to SQWs suggests that the MQW samples are at least partially relaxed. This can be qualitatively demonstrated by the PLE spectra in the energy region of the ZnSe band gap as shown in Fig. 7, where a comparison of 1-ML MQWs with 1-ML SQW is given. The increase of photoluminescence from the SQW when the excitation photon energy is above the ZnSe band gap is almost completely washed out in the MQWs because the diffusion of the carriers created in the buffer layer toward the MQW region and into wells making ultimate contribution to the luminescence is severely decreased by numerous nonradiative defects such as dislocations at and near the interface between the MQW structure and the ZnSe buffer layer.

IV. CONCLUSIONS

We have studied the optical properties of a variety of MBE-grown highly strained CdSe/ZnSe QW samples using low-temperature PL, PLE, and PR measurements. In general, the direct interband transitions from samples with the well widths from 1/4 to four monolayers are found to vary in energy from 2.15 to 2.78 eV, which cover almost the entire blue-green color range useful for optoelectronic device operation. The critical thickness for CdSe layers to be coherently grown on ZnSe is suggested to be around three monolayers ($\sim$10 Å) according to the experimental results. The experimentally observed PL linewidth narrowing is explained in terms of the alloy formation in the vicinity of CdSe due to lateral interfacial diffusion and the asymptotical convergence of the energies of two-dimensional excitons to that of three-dimensional excitons as the well width decreases. The discrepancy in the energy positions of interband transitions between the SQW and MQW samples with the same CdSe layer thickness is attributed to the strain relaxation occurring from the overall thickness of the MQW structure as a whole surpassing the critical limit for pseudomorphic growth of coherent strained MQWs.

ACKNOWLEDGMENTS

We thank Dr. J. Li and J. Jacob for helpful discussions. The OSU part of this work was supported by ONR, DARPA, and OCAST.

[1] M. A. Haase, J. Qiu, J. M. DePuydt, and H. Cheng, Appl. Phys. Lett. **59**, 1272 (1991).
[2] H. Jeon, J. Ding, W. Patterson, A. V. Nurmikko, W. Xie, D. C. Grillo, M. Kobayashi, and R. L. Gunshor, Appl. Phys. Lett. **59**, 3619 (1991).
[3] H. Jeon, J. Ding, A. V. Nurmikko, W. Xie, M. Kobayashi, and R. L. Gunshor, Appl. Phys. Lett. **60**, 892 (1992).
[4] P. J. Parbrook, P. J. Wright, B. Cockayne, A. G. Cullis, B. Henderson, and K. P. O'Donnell, J. Cryst. Growth **106**, 503 (1990).
[5] F. Yang, P. J. Parbrook, B. Henderson, K. P. O'Donnell, P. J. Wright, and B. Cockayne, J. Lumin. **53**, 427 (1992).
[6] S. Fujita, Y. H. Wu, Y. Kawakami, and S. Fujita, J. Appl. Phys. **72**, 5233 (1992).
[7] Z. L. Peng, J. Li, W. H. Yao, L. He, X. Y. Cheng, and S. X. Yuan, Jpn. J. Appl. Phys. **11B**, 31 (1992).
[8] P. Juza, H. Zajicek, H. Sitter, M. Helm, W. Faschinger, and K. Lischka, Appl. Phys. Lett. **61**, 3133 (1992).
[9] H. Zajicek, P. Juza, E. Abramof, O. Pankratov, H. Sitter, M. Helm, G. Brunthaler, W. Faschinger, and K. Lischka, Appl. Phys. Lett. **62**, 717 (1993).
[10] N. Samarth, H. Luo, J. K. Furdyna, S. B. Qadri, Y. R. Lee, A. K. Ramdas, and N. Otsuka, Appl. Phys. Lett. **54**, 2680 (1989).
[11] N. Samarth, H. Luo, J. K. Furdyna, R. G. Alonso, Y. R. Lee, A. K. Ramdas, S. B. Qadri, and N. Otsuka, Appl. Phys. Lett. **56**, 1163 (1990).
[12] T. Yao, M. Fujimoto, S. K. Chang, and Tanino, J. Cryst. Growth **111**, 823 (1991).
[13] D. J. Wolford, T. F. Kuech, J. A. Bradley, M. A. Gell, D. Ninno, and M. Jaros, J. Vac. Sci. Technol. B **4**, 1043 (1986).
[14] U. Venkateswaran, M. Chandrasekhar, H. R. Chandrasekhar, B. A. Vojak, F. A. Chambers, and J. M. Meese, Phys. Rev. B **33**, 8416 (1986).
[15] H. Q. Hou, L. J. Wang, R. M. Tang, and J. M. Zhou, Phys. Rev. B **42**, 2926 (1990).
[16] W. Shan, X. M. Fang, D. Li, S. Jiang, S. C. Shen, H. Q. Hou, W. Feng, and J. M. Zhou, Phys. Rev. B **43**, 14615 (1991).
[17] V. A. Wilkinson, A. D. Prins, D. J. Dunstan, L. K. Howard, and M. T. Emeny, J. Electron. Mater. **20**, 509 (1991).
[18] K. Reimann, M. Holtz, K. Syassen, Y. C. Lu, and E. Bauser, Phys. Rev. B **44**, 2985 (1991).
[19] R. J. Thomas, H. R. Chandrasekhar, M. Chandrasekhar, N. Samarth, H. Luo, and J. Furdyna, Phys. Rev. B **45**, 9505 (1992).
[20] K. Shahzad, D. J. Olego, and D. A. Cammack, Phys. Rev. B **39**, 13016 (1989).
[21] S. Ves, K. Strossner, N. E. Christensen, C. K. Kim, and M. Cardona, Solid State Commun. **56**, 479 (1985).
[22] J. R. Mei and V. Lemos, Solid State Commun. **52**, 785 (1984).
[23] D. F. Welch, G. W. Wicks, and L. F. Eastman, Appl. Phys. Lett. **46**, 991 (1985).
[24] J. Singh and K. K. Bajaj, Appl. Phys. Lett. **48**, 1077 (1986).
[25] S. Hong and J. Singh, J. Appl. Phys. **62**, 1994 (1987).
[26] C. Weisbuch, in *Semiconductors and Semimetals,* edited by R. Dingle (Academic, New York, 1987), Vol. 24, p. 58.
[27] D. Bimberg, J. Christen, T. Fukunaga, H. Nakashima, D. E. Mars, and

J. N. Miller, J. Vac. Sci. Technol. B **5**, 1191 (1987).
[28] Z. Q. Zhu, H. Yoshihara, K. Takebayashi, and T. Yao, Appl. Phys. Lett. (unpublished).
[29] E. S. Koteles, D. A. Owens, D. C. Bertolet, and K. M. Lau, Phys. Rev. B **38**, 10139 (1988).
[30] J. Cibert, Y. Gobil, L. S. Dang, S. Tatarenko, G. Feuillet, P. H. Jouneau, and K. Saminadayar, Appl. Phys. Lett. **56**, 292 (1990).
[31] J. Y. Marzin, J. M. Gerard, P. Voisin, and J. A. Brum, in *Semiconductors and Semimetals*, edited by T. P. Pearsall (Academic, New York, 1990), Vol. 32, p. 55.

Determination of the fundamental and split-off band gaps in zinc-blende CdSe by photomodulation spectroscopy

W. Shan* and J. J. Song
Department of Physics and Center for Laser Research, Oklahoma State University, Stillwater, Oklahoma 74078

H. Luo and J. K. Furdyna
Department of Physics, University of Notre Dame, Notre Dame, Indiana 46556
(Received 22 February 1994; revised manuscript received 6 May 1994)

We present the results of experimental determination of the fundamental band gap (E_0) and the spin-orbit split-off energy gap (Δ_0) of zinc-blende CdSe using photomodulation spectroscopy. The single-crystal CdSe film was grown by molecular-beam epitaxy on a (100) GaAs substrate with a ZnTe buffer layer. Photoreflectance (PR) measurements were performed on the sample at various temperatures from 10 K to room temperature. The sharp derivativelike spectral features associated with the interband Γ_8^V-Γ_6^C and Γ_7^V-Γ_6^C transitions in PR spectra allow us to determine the E_0 and $E_0+\Delta_0$ band-gap energies. We found that zinc-blende CdSe has a fundamental band gap E_0 of 1.661 eV and a spin-orbit split-off gap Δ_0 of 0.42 eV at room temperature (295 K). The fundamental band gap E_0 of zinc-blende CdSe has been mapped out as a function of temperature and the Varshni thermal coefficients have been determined for this material. The results yield $E_0(T)=1.766-6.96\times10^{-4}\,T^2/(281+T)$ eV.

In recent years, much effort has been devoted to the study of wide band-gap II-VI compound semiconductors and their multilayer heterostructures for optoelectronic device applications, such as laser diodes and light-emitting diodes operating in the blue-green range. The $Cd_xZn_{1-x}Se$/ZnSe quantum-well and superlattice structures are among the most extensively studied heterostructure materials. The ternary II-VI compound $Cd_{1-x}Zn_xSe$ with zinc-blende structure has been grown by molecular-beam epitaxy (MBE) over the entire range of compositions by Samarth *et al.*[1] Blue laser action and electroluminescence have been successfully achieved from the ZnSe-based quantum-well devices using $Cd_{1-x}Zn_xSe$ as quantum-well materials.[2–4] The success of these developments has partially been attributed to the quality and properties of $Cd_xZn_{1-x}Se$ alloys which proved to be particularly useful for electron-hole pair confinement in the $Cd_xZn_{1-x}Se$/ZnSe heterostructures.[5,6] However, there has been relatively little work on the electronic band structure of the binary zinc-blende CdSe itself (which is one of the end points of the alloy just mentioned), especially for such important parameters as the fundamental band gap E_0 and the spin-orbit split-off band gap Δ_0.

In this paper we present the results of a photomodulation spectroscopy study of optical transitions between the bottom of the Γ_6^C conduction band and the tops of the Γ_8^V valence band and the Γ_7^V spin-orbit split-off band in a zinc-blende CdSe single-crystal epilayer. Photoreflectance (PR) measurements were performed on the sample at different temperatures from 10 K to room temperature (295 K). The sharp spectral features related to Γ_8^V-$\Gamma_6^C(E_0)$ and $\Gamma_7^V-\Gamma_6^C(E_0+\Delta_0)$ transitions due to the derivative nature of photoreflectance spectra allow us to determine the transition energies precisely. The fundamental band gap E_0 of zinc-blende CdSe is found to be 1.661 eV at room temperature (295 K). The spin-orbit split-off band gap Δ_0 is determined to be $\sim$0.42 eV. The dependence of the fundamental band gap E_0 on temperature has been mapped out by fitting the experimental data to the Varshni empirical equation,[7] yielding $E_0(T=0)=1.766\pm0.003$ eV, and Varshni thermal coefficients $\alpha=6.96\times10^{-4}$ eV/K and $\beta=281$ K.

The CdSe epilayer used in this work was grown by MBE on a semi-insulating (100) GaAs substrate. The substrate was pretreated by chemical etching using H_2SO_4:H_2O_2:H_2O (5:1:1) mixture at room temperature for 1 min. Before the growth of CdSe film, a ZnTe buffer layer with a thickness of 1 μm was deposited on the GaAs substrate at the growth temperature of 315 °C to provide a clean and defect-free surface for CdSe deposition. The CdSe epilayer of $\sim$1 μm was then grown at 300 °C. It has been previously demonstrated that, although the normal (i.e., bulk) crystal structure of CdSe is hexagonal (wurtzite), CdSe single-crystal epilayers with cubic (zinc blende) structure can be formed by MBE growth on zinc-blende substrates.[1,8,9] The zinc-blende crystal structure of the CdSe epilayer used in this study was verified by x-ray double-crystal rocking curves. The lattice parameter of the MBE-grown CdSe directly on GaAs substrate was previously determined to be 6.077 Å,[8] very close to the ZnTe lattice constant of 6.099 Å.[10] The CdSe epilayer may thus be considered to be nearly lattice matched to the ZnTe buffer.

PR spectroscopy was carried out on the CdSe sample at a temperature range from 10 K up to room temperature (295 K). The sample was attached to a cold finger of a closed-cycle refrigerator by vacuum grease and cooled down to the desired temperatures for PR measurements. Quasimonochromatic light dispersed by a 0.5-m monochromator from a halogen tungsten lamp was focused on the sample as the probe beam, and a chopped HeCd laser beam was used to provide the photomodulation. The reflectance signals were detected by a Si photodiode using

lock-in amplification and computer-controlled data acquisition.

Photoreflectance spectroscopy is a differential method utilizing modulation of the built-in electric field through photoinjected carriers by a periodically modulated light beam, such as the chopped laser beam used in this work. A change in reflectivity $\Delta R/R$ due to the modulation may be expressed as[11]

$$\Delta R/R = a\Delta\epsilon_1 + b\Delta\epsilon_2 , \tag{1}$$

where a and b are referred to as Seraphin coefficients and are related to the unperturbed dielectric function $\epsilon=\epsilon_1+i\epsilon_2$, while $\Delta\epsilon_1$ and $\Delta\epsilon_2$ are the changes in the real and the imaginary parts of the modulated dielectric function.[11] The differential changes in the reflectance appear as sharp derivativelike line shapes in the modulated reflectance spectrum, corresponding to specific transitions in the Brillouin zone. In this work, the photoreflectance spectra obtained on the CdSe epilayer at various temperatures consist of two derivativelike spectral signatures in the visible range, as illustrated in Fig. 1.

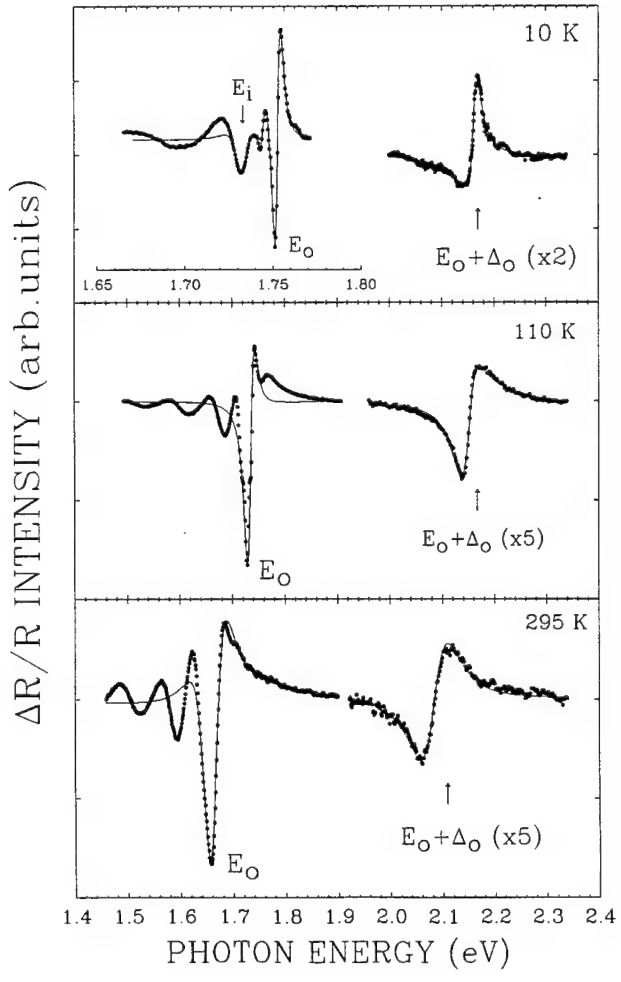

FIG. 1. Photoreflectance spectra taken at 10, 110, and 295 K. The E_0 spectral feature at 10 K is horizontally expanded for clarity. Solid circles are experimental data and solid lines represent the least-squares fit to the data.

The features marked by E_0 and $E_0+\Delta_0$ correspond to the Γ_8^V-Γ_6^C and Γ_7^V-Γ_6^C transitions, respectively. The oscillations at the energy below the Γ_8^V-$\Gamma_6^C(E_0)$ transition are interference effects caused by the heterointerface.

In order to determine the energy positions associated with the optical transitions, the PR spectra are fitted to the functional form[11-13]

$$\Delta R/R = Re[Ce^{i\theta}(E-E_0+i\Gamma)^{-n}] , \tag{2}$$

where C and θ are the amplitude and phase of the line shape, and E_0 and Γ are the energy and the empirical broadening parameter of the transitions, respectively. The exponent n is a characteristic parameter which depends on the type of the critical point and the order of the derivative. The values of $n=\frac{5}{2}$ and 2, which correspond to the three-dimensional interband and excitonic transitions, respectively,[11,14] are used to fit the derivativelike spectral structures. We found that the line positions and widths of the PR spectra taken at low temperatures (≤ 140 K) could be fit using $n=2$ due to the excitonic nature of these features. The $n=\frac{5}{2}$ (which simulates band-to-band line shapes) was found to be more appropriate for fitting the spectra obtained at high temperatures (≥ 150 K), where excitons are expected to dissociate via strong exciton-phonon coupling and inhomogeneous perturbations.[11] The broadening parameter Γ was indeed found to increase significantly with temperature in the numerical fits to the spectra taken at temperatures higher than 150 K. The solid lines in Fig. 1 are the least-squares fits to the experimental data using Eq. (2).

As shown in Fig. 1, the portion of PR spectra at 10 K in the region of the Γ_8^V-$\Gamma_6^C(E_0)$ transition is quite complicated even excluding the interference effect. It is necessary to fit the experimental data with two oscillators using a first-derivative line shape for the spectral feature E_0 and a third-derivative line shape for the feature denoted by E_i. The excellent agreement between the theoretical fit and the observed spectrum indicates that the E_i feature corresponds to a real transition rather than an oscillatory interference signature. The transition energies for E_0 and E_i are 1.752 and 1.732 eV, respectively. While the E_0 feature can be identified as the excitonic Γ_8^V-Γ_6^C transition for its predominant feature in the PR spectra taken at various temperatures, the origin of the E_i feature is not immediately clear. It is known that for such a heterostructure as CdSe epilayer grown on ZnTe, although the two constituents are nearly lattice matched, the difference in the thermal expansion coefficients of lattice constants could introduce an additional temperature-dependent built-in strain. The strain will shift the center of gravity of the entire Γ_8^V band and split the fourfold degeneracy of the top of the Γ_8^V band into two twofold degenerate $|\frac{3}{2},\pm\frac{3}{2}\rangle$ and $|\frac{3}{2},\pm\frac{1}{2}\rangle$ states, i.e., the heavy-hole band and the light-hold band. As a result, two distinct spectral features associated with these two states could be observed if the strain-induced splitting is large enough. It seems that this could be a plausible interpretation for the E_i feature as it is an excitonic transition associated with either the heavy-hole or the light-hole band edge. However, this is not the case in this

study, as can be elucidated from studying temperature dependence of the relative intensity and energy separation between the E_i and E_0 features. If the strain induced by the difference in thermal expansion were used to account for the 20-meV separation between the E_i and E_0 features at 10 K, one would expect the relative intensity of the E_i and E_0 features to be insensitive to temperature and the energy separation of these two features to change with temperature. But the intensity of the E_i feature was found to decrease much faster than that of the E_0 feature as temperature increases, and completely disappear with temperature above 100 K. The energy separation between two features was found to be temperature independent while the E_i feature is still observable. Thus, the aforementioned interpretation for the E_i feature can be ruled out since it is inconsistent with the experimental observations. We find that, provided the CdSe epilayer is thick enough, the built-in strain induced by the overall lattice mismatch between CdSe and ZnTe including the effect of different thermal expansions is fully relaxed in the CdSe layer, so that the maxima of the heavy- and light-hole valence bands remain degenerate, and the optical response of the sample is essentially that of unperturbed bulk CdSe. The photoluminescence spectrum of a zinc-blende CdSe sample cut from the same wafer as the samples used in this work exhibits a strong dominant emission peak at 1.73 eV at 10 K (Ref. 9), which is very close to the transition energy of the E_i feature observed in this work. Note that low-temperature PL spectra are generally dominated by radiative recombinations associated with impurity states.[15] The carriers trapped by impurities can recombine through interaction with free carriers and carriers bound to other impurities, and excitons can be bound to those impurities before annihilation. The E_i feature therefore can be attributed to a near band-edge impurity transition due to its significant decrease in intensity caused by thermal ionization with increasing temperature. It also needs to use two oscillators to fit the line shape of spectral features corresponding to the Γ_7^V-$\Gamma_6^C(E_0+\Delta_0)$ transition at 10 K though the spectrum does not explicitly exhibit that. The best fit yields a 2.168 eV for the transition at 10 K. The fitting also indicates that the second oscillator has an energy position $\sim$10 meV below the $E_0+\Delta_0$ transition, which suggests that there might be an impurity state closely associated with the Δ_0 band edge.

For the fitting to the PR spectra taken at temperatures ≥ 80 K, all line shapes can be fit well using only one oscillator in Eq. (2), except the oscillatory shoulder on the high-energy side of the E_0 feature (see Fig. 1). The oscillatory line shape is most likely due to a Franz-Keldysh oscillation induced by a built-in electric field.[16,17] It is well known that the mechanism of photoreflectance, whether in the low-field regime or the Franz-Keldysh regime, depends on the presence of a built-in electric field. Usually, the appearance of Franz-Keldysh oscillations is the indication of the presence of a built-in field which is above the low-field limit. As a result, PR line shapes are related to the magnitude of the field and to the interband effective mass along the field direction.[11,16] Equation (2) used to fit PR line shapes is, strictly speaking, only valid in the low-field limit, where the PR line shapes are independent of electric field.[11] However, the fact that there is only one small Franz-Keldysh oscillatory signature on the high-energy side of the E_0 feature suggests that it is just above the low-field limit, and therefore Eq. (2) can still be used to fit the PR line shapes in this case. The direct band-to-band transitions E_0 and $E_0+\Delta_0$ at room temperature (295 K) are evaluated by using $n=\frac{5}{2}$ (the third-derivative line shape), since they are of three-dimensional interband nature, to be 1.661 and 2.082 eV, respectively. As a result, we can determine that in zinc-blende CdSe the Γ_7^V split-off valence band has an energy gap Δ_0 of 0.42 eV below the Γ_8^V valence band at the center of the Brillouin zone.

The change of the fundamental band gap E_0 with temperature is of considerable importance both for basic science and for technological applications. It is well known that the temperature dependence of the fundamental band gap in a semiconductor can be described by the Varshni empirical equation[7]

$$E_0(T)=E_0(0)-\alpha T^2/(\beta+T)\ , \tag{3}$$

where $E_0(0)$ is the band-gap value at 0 K, and α and β are constants (referred to as Varshni thermal coefficients). In Fig. 2 we plot the values of the E_0 band gap of zinc-blende CdSe as a function of temperature. The solid line represents the best fit to the data using Eq. (3). The parameters obtained from the fit are $E_0(0)=1.766$ eV, $\alpha=6.96\times10^{-4}$ eV/K, and $\beta=281$ K. To the best of our knowledge, these are the first values ever reported for zinc-blende CdSe. A free exciton binding energy of 13 meV has been added to Γ_8^V-Γ_6^C transition energies obtained at low temperatures (<150 K), as plotted in Fig. 2, due to the excitonic origin of the spectral features associated with the transition observed in that temperature range. The exciton effect has to be taken into account so as to obtain the temperature dependence of the actual fundamental band gap E_0 (band-to-band transition instead of excitonic transition). The exciton binding energy was estimated using the effective masses for zinc-blende

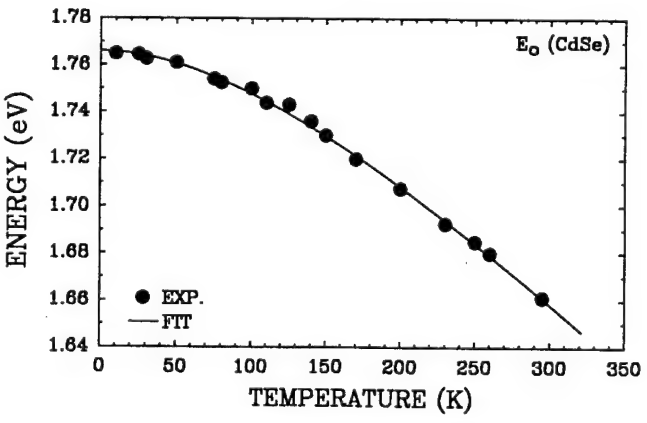

FIG. 2. Variation of the E_0 energy gap with temperature, with the exciton binding energy taken into account. The curve represents the best fit to the Varshni equation.

CdSe at the Γ point calculated by Kim *et al.*[18] ($m_n=0.12m_0$ and $m_p\approx 1.16m_0$) and an average dielectric constant of wurtzite CdSe (Ref. 19) [$\epsilon(0)\approx 9.5$], because this value for zinc-blende CdSe is not available at present. The uncertainty in this estimate of the exciton binding energy is ~ 3 meV, primarily coming from the value of the dielectric constant. At higher temperatures, since the E_0 band gap is directly determined by fitting Eq. (2) to the experimental data due to the PR spectral features originating from band-to-band transition rather than excitonic transition, the uncertainty in determination of E_0 mainly results from the fitting to the complicated line shape at the lower energy side of the E_0 feature, where the spectral structure related to the Γ_8^V-Γ_6^C transition overlaps with the interference oscillations. The largest deviation of E_0 energy obtained by using different amplitude and phase parameters in the fittings is found to be around 3 meV in the fit to the experimental data of room temperature (295 K). We have also fitted the energies of $E_0+\Delta_0$ (the Γ_7^V-Γ_6^C transition) at different temperatures to Eq. (3), obtaining Varshni coefficients $\alpha=5.63\times 10^{-4}$ eV/K and $\beta=288$ K, respectively. The result suggests that Δ_0 is weakly temperature dependent.

Finally, we note that recently Kim *et al.* reported $E_0=1.66$ eV and $\Delta_0=0.39$ eV for zinc-blende CdSe obtained from their room-temperature ellipsometric measurements of the dielectric function of $Zn_xCd_{1-x}Se$ single-crystal films, from which the band structure of cubic CdSe was calculated using a nonlocal empirical pseudopotential method.[18] Compared with these values, the energy of E_0 obtained in this work is in excellent agreement, whereas there is a ~ 30-meV deviation in the energy of Δ_0. Since the E_0 and $E_0+\Delta_0$ are the lowest direct band gaps located at the center of the Brillouin zone, with a relatively small density of states in ellipsometric measurements, they appeared only as small spectral features sitting on a slowly varying large background of the dielectric function.[18] By contrast, the spectral features associated with these two transitions are greatly enhanced in PR measurements, appearing as sharp peaks on a featureless background in the modulated spectrum. This results in a much better spectral resolution and allows a more precise determination of the actual transition energy. We therefore regard $\Delta_0=0.42$ eV as a more accurate result.

In summary, the E_0 and $E_0+\Delta_0$ band-gap energies of zinc-blende CdSe were measured as a function of temperature using photomodulation spectroscopy. The room-temperature value of the fundamental band gap E_0 of zinc-blende CdSe obtained from these measurements is 1.661 eV, and the spin-orbit split-off gap Δ_0 is 0.42 eV. By fitting the temperature-dependent energy value of E_0 to the Varshni empirical relation, we have determined the fundamental band gap $E_0=1.766\pm 0.003$ eV at 0 K, with the thermal coefficients $\alpha=6.96\times 10^{-4}$ eV/K and $\beta=281$ K.

The work at OSU was supported by ONR, ARPA, and OCAST. The University of Notre Dame work was supported by NSF Grant No. DMR 92-21390 and ONR Grant No. N00014-90-J-1782.

*On leave from Shanghai Institute of Technical Physics, Chinese Academy of Sciences, Shanghai 200083, People's Republic of China.

[1]N. Samarth, H. Luo, J. K. Furdyna, R. G. Alonso, Y. R. Lee, A. K. Ramdas, S. B. Qadri, and N. Otsuka, Appl. Phys. Lett. **56**, 1163 (1990).

[2]M. A. Haase, J. Qui, J. M. DePuydt, and H. Cheng, Appl. Phys. Lett. **59**, 1272 (1991).

[3]H. Jeon, J. Ding, W. Patterson, A. V. Nurmikko, W. Xie, D. C. Grillo, M. Kobayashi, and R. L. Gunshor, Appl. Phys. Lett. **59**, 3619 (1991).

[4]H. Jeon, J. Ding, A. V. Nurmikko, W. Xie, M. Kobayashi, and R. L. Gunshor, Appl. Phys. Lett. **60**, 892 (1992).

[5]J. Ding, N. Pelekanos, A. V. Nurmikko, H. Luo, N. Samarth, and J. K. Furdyna, Appl. Phys. Lett. **57**, 2885 (1990).

[6]N. T. Pelekanos, J. Ding, M. Hagerott, A. V. Nurmikko, H. Luo, N. Samarth, and J. K. Furdyna, Phys. Rev. B **45**, 6037 (1992).

[7]V. P. Varshni, Physica **34**, 149 (1967).

[8]N. Samarth, H. Luo, J. K. Furdyna, S. B. Qadri, Y. R. Lee, A. K. Ramdas, and N. Otsuka, Appl. Phys. Lett. **54**, 2680 (1989).

[9]H. Luo, N. Samarth, F. C. Zhang, A. Pareek, M. Dobrowolska, J. K. Furdyna, K. Mahalingam, N. Otsuka, W. C. Chou, A. Petrou, and S. B. Qadri, Appl. Phys. Lett. **58**, 1783 (1991).

[10]T. Yao, in *The Technology and Physics of Molecular Beam Epitaxy,* edited by E. H. C. Parker (Plenum, New York, 1985), p. 313.

[11]D. E. Aspnes, in *Optical Properties of Solids,* edited by M. Balkanski (North-Holland, Amsterdam, 1980), Chap. 4A.

[12]O. J. Glembocki and B. V. Shanabrook, Superlatt. Microstruct. **3**, 235 (1987).

[13]F. H. Pollak and O. J. Glembocki, Proc. SPIE **946**, 2 (1988).

[14]H. Shen, S. C. Shen, F. H. Pollak, and R. N. Sacks, Phys. Rev. B **36**, 3487 (1987).

[15]M. Voos, R. F. Leheny, and J. Shah, in *Optical Properties of Solids,* edited by M. Balkanski (North-Holland, Amsterdam, 1980), Chap. 6.

[16]O. J. Glembocki, Proc. SPIE **1286**, 2 (1990).

[17]F. H. Pollak and H. Shen, Mater. Sci. Eng. **R10**, 275 (1993).

[18]Y. D. Kim, M. L. Klein, S. F. Ren, Y. C. Chang, H. Luo, and J. K. Furdyna, Phys. Rev. B **49**, 7262 (1994).

[19]I. Broser, R. Broser, and A. Hoffmann, in *Semiconductors: Physics of II-VI and I-VII Compunds, Semimagnetic Semiconductors,* edited by O. Madelung, Landolt-Börnstein, New Series, Group III, Vol. 17, Pt. b (Springer-Verlag, Berlin, 1982).

Above room temperature near ultraviolet lasing from an optically pumped GaN film grown on sapphire

X. H. Yang, T. J. Schmidt, W. Shan, and J. J. Song
Center for Laser Research and Department of Physics, Oklahoma State University, Stillwater, Oklahoma 74078

B. Goldenberg
Honeywell Technology Center, Bloomington, Minnesota 55420

(Received 9 August 1994; accepted for publication 1 November 1994)

Optically pumped near ultraviolet lasing from single-crystal GaN grown by metalorganic chemical vapor deposition has been achieved over a temperature range from 10 K to over 375 K by using a side-pumping geometry on small barlike samples. The laser emission threshold was measured as a function of temperature and the threshold was found to show weak temperature dependence: ~500 kW/cm^2 at 10 K and ~800 kW/cm^2 at room temperature (295 K) for one particular sample studied. The longitudinal lasing modes were clearly observed. The characteristics of the temperature dependence of the laser emission threshold suggests that GaN is a suitable material for the development of optoelectronic devices required to operate at high temperatures. © *1995 American Institute of Physics.*

Recently, III–V nitrides have attracted much attention because of their large energy band gaps, great physical hardness, high thermal conductivities, and high melting temperatures.[1] These properties make III–V nitrides promising for high-temperature electronic and optoelectronic device applications. In particular, GaN has been the most extensively studied material because its large direct band gap of 3.41 eV at room temperature is appropriate for short wavelength (blue-ultraviolet) light emitting diodes and laser diodes.[1–3] With the advancement of growth techniques, high quality GaN crystals have been grown and room-temperature optically pumped stimulated emission has been reported by several groups.[4–10] Also, a commercial light-emitting diode based on an InGaN/AlGaN double-heterostructure has been successfully fabricated by Nichia Chemical Company in Japan.[11] However, thus far clear evidence of lasing from prepared cavities has not been reported from GaN, nor from other nitrides, except an early report by Dingle *et al.*, showing Fabry–Pérot modes superimposed on top of a broad emission background from as-grown GaN needle samples.[8] This can be partially attributed to difficulties associated with sample preparation and processing. In particular, suitable cavity end mirrors are difficult to obtain when the single-crystal epilayer films are grown on such a hard substrate as sapphire. This makes the observation of laser emission and the resultant longitudinal cavity modes difficult.[6]

In this letter we report the experimental results of optically pumped lasing from single-crystal GaN samples over a temperature range from 10 K to over 375 K. The GaN samples were grown on sapphire substrates by low-pressure metalorganic chemical vapor deposition (MOCVD). By cutting the large sample wafer into small barlike specimens and employing a side-pumping geometry we were able to produce strong near-UV laser emissions from the GaN samples over a temperature range from 10 K to over 375 K. The longitudinal cavity modes of the laser emission could be clearly observed without the need for fine polishing or reflective coating of the samples edge facets. The lasing threshold pumping power density has been measured in detail as a function of temperature. The characteristics of the temperature dependence of the lasing threshold suggests that this wide band gap material can be used for the development and fabrication of light-emitting devices required to operate at high temperatures. To our knowledge, this is the best experimental evidence of optically pumped near-UV lasing of GaN ever observed.

The GaN samples used in this study were cut from a nominally undoped single-crystal grown by low-pressure MOCVD. The 4.2 μm thick GaN epilayer was grown on a 1.75 in. (0001) sapphire substrate at 1040 °C. Before the deposition of the GaN film a 50 nm AlN buffer layer was grown on the substrate at 775 °C. The large wafer was cut into small barlike specimens of various thicknesses, ranging from 150 to 1000 μm. Extreme care was taken to ensure that the quality and parallelness of the cut edge facets were as good as possible. The barlike samples were then mounted on a sapphire heat sink which was then attached to a copper sample holder inside a cryostat. The optical pumping system is very similar to that used in our previous ZnSe lasing work.[12,13] A tunable dye laser pumped by a frequency-doubled pulsed Nd:YAG laser was used as the primary optical pumping source. The output of the dye laser was then frequency doubled to achieve a near UV pumping frequency. Side-pumping geometry was used in this study. The emission signal from one facet of the GaN sample was collected into a Spex 1.0 m spectrometer and recorded by either a charge coupled device (CCD) camera or a photomultiplier tube used in conjunction with a boxcar averager.

Strong near-UV laser actions from the GaN samples were observed over the broad temperature range from 10 K to over 375 K under the conditions of high-excitation power densities. The laser emission light was found to be transverse electric (TE) polarized (along the direction of the bar). As the temperature was increased, the lasing peak shifted to longer wavelength, from 362 nm at 10 K to 381 nm at 375 K. The room-temperature (295 K) laser emission peak position was

 0003-6951/95/66(1)/1/3/$6.00

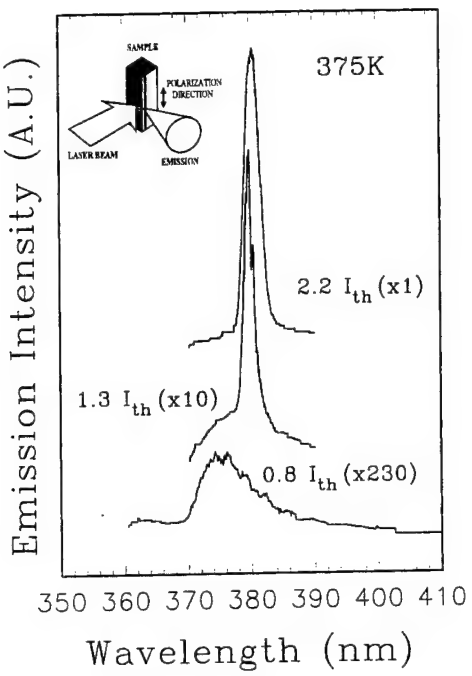

FIG. 1. Emission spectra from a GaN sample with a cavity length of 330μm under pump power densities of 2.2 I_{th}, 1.3 I_{th}, and 0.8 I_{th}. The curves are vertically displaced for clarity. The threshold pump power density I_{th} was determined to be 1.2 MW/cm^2 at 375 K. The insert shows the excitation and emission configuration.

found to be 373 nm. The full width at half-maximum (FWHM) of the lasing peak is ~1 nm at 10 K and broadens slightly with increasing temperature. In Fig. 1 we show the emission spectra taken at a temperature well above room temperature (375 K), for pumping power densities above and below the estimated threshold pumping power density. Under the condition of low pump power intensities, only a broad emission spectral structure with an approximate peak position of 376 nm could be observed (lower curve). Its emission intensity was found to be linearly proportional to the pumping power density, indicating that the broad emission structure is of the typical nature of spontaneous emission. As pumping power density increases, a new emission feature with a much narrower line shape appears at the low-energy shoulder of the spontaneous emission structure. The emission intensity of this new spectral feature becomes predominant as the pumping power density is increased to slightly above the lasing threshold (middle curve). The strong, narrow emission exhibits a superlinear increase and the broad emission background is totally suppressed as the pumping power density is increased further, indicating the occurrence of laser action in the sample. For example, the emission intensity increased by almost three orders of magnitude when the pumping power density was increased by less than a factor of 3 (upper curve). Meanwhile, the laser emission peak shifts to a longer wavelength as the pumping power density is increased. In addition, some longitudinal cavity modes could be recognized in the emission spectra shown in Fig. 1. In order to better resolve the longitudinal cavity modes in the emission spectra, a sample with a 200 μm cavity length was used and different spectra were captured using a CCD camera with a very short integration time (0.1 s). Mode hopping was observed. Figure 2 shows two typical spectra captured at 295 and 375 K. The irregular appearance of the spectra shown in Fig. 2 is primarily a result of imperfections in the samples edge facets. Spectral quality is expected to improve greatly after the samples edge facets are fine polished and reflective coated. The mode spacing caused by the 200 μm long Fabry–Pérot resonant cavity is about 0.2 nm, which is consistent with the calculated value of the mode spacing determined by the formula[14,15]

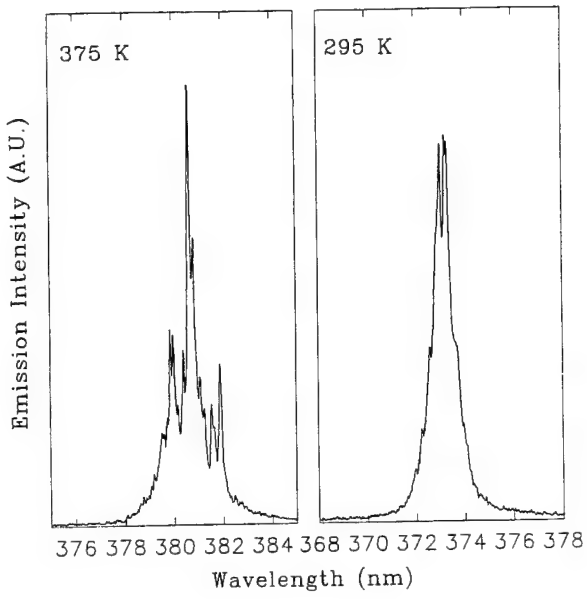

FIG. 2. Lasing spectra taken at two different temperatures from a sample with a cavity length of 200 μm. The longitudinal modes are clearly resolved.

$$\Delta\lambda = \frac{\lambda_0^2}{2L(n - \lambda_0 dn/d\lambda)},$$

where L is the cavity length, λ_0 is the wavelength of one mode, $\Delta\lambda$ is the spacing of an adjacent mode, n is the index of refraction at λ_0, and $dn/d\lambda$ is the variation of the index of refraction with wavelength.

Figure 3 demonstrates the change in the laser emission intensity for a sample at 10 K and at room temperature (295 K) as the pumping power density is increased. The emission intensity was measured by integrating the area under the emission peak. The lasing threshold of pumping power density for these two different temperatures is well defined by the onset of the increase in slope of the emission intensity versus pumping power intensity curve. The lasing threshold was found to be ~0.5 MW/cm^2 at 10 K and ~0.8 MW/cm^2 at room temperature. One interesting finding of the study is that the lasing threshold was relatively insensitive to the temperature change. The variation of the lasing threshold as a function of temperatures is plotted in Fig. 4. We note that over the temperature range from 10 to 120 K the lasing threshold is not very dependent on temperature. As the temperature increases further, the lasing threshold increases slowly. The threshold increases by about three times when

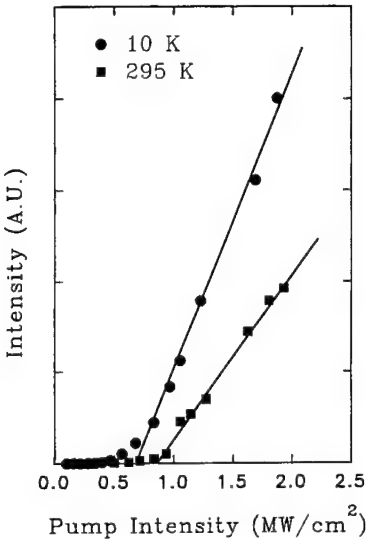

FIG. 3. Emission output vs optical pumping power densities at 10 and 295 K.

the temperature is increased from 10 to 375 K. The solid line in Fig. 4 represents the best fit of the experimental data to the empirical form[16]

$$I_{th}(T)=I_0 \exp(T/T_0)$$

for the temperature dependence of the lasing threshold. The characteristic temperature T_0 was estimated to be 230 K over the temperature range from 120 to 375 K for this sample. This value of T_0 is about two times larger than that of II–VI lasers (T_0=~120 K for II–VI lasers), indicating that the lasing threshold is less sensitive to changes in temperature.[17,18] It is well known that high-temperature sensitivity of the lasing threshold usually limits the performance of a laser under high-temperature operation.[16] On the other hand, a weak temperature dependence for the lasing threshold implies that the high-temperature performance limit for

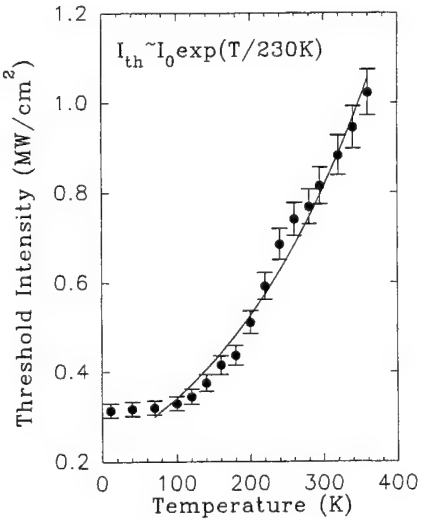

FIG. 4. Variation of the lasing threshold as a function of temperature. The error bars indicate the fluctuations in pump power density. The solid line is the best fit to the experimental data using the formula $I_{th}=I_0 \exp(T/230\ \text{K})$.

laser operation can be significantly expanded. Therefore, our results suggest that GaN-based laser diodes will have a much higher temperature tolerance. We should also mention that laser action was observed at temperatures as high as 425 K. However, due to our current systems limitations, lasing could not be studied in detail at these higher temperatures. Further investigation is underway to study higher temperature lasing effects.

In summary, optically pumped near-UV laser action in single-crystal MOCVD grown GaN samples has been successfully achieved for the first time without reflective coating at temperatures ranging from 10 to over 375 K. The laser action was evidenced by the spectral narrowing of the emission peak, the suppression of the broad emission background, the drastic increase in emission output for pump power intensities above threshold, and the clearly resolved longitudinal lasing modes. This work demonstrates that the laser cavity can be formed by simply cutting the sample into a barlike structure without a need for polishing or reflective coating. The laser emission threshold of pumping power density was measured as a function of temperature and was found to exhibit a weak temperature dependence. The characteristics of the temperature dependence of the lasing threshold suggests that GaN is not only a suitable material for the development of UV light emitters, but that it is also suitable for the development of optoelectronic devices required to operate at high temperature.

The work at OSU was supported by AFOSR, ONR, ARPA, and OCAST. One of the authors (BG) would like to acknowledge the technical assistance of Maurice Hitchell. A portion of this work was presented at the Rare Earth Doped Optoelectronic Materials Workshop held in Malibu, CA, June, 1994.

[1] S. Strite and H. Morkoc, J. Vac. Sci. Technol. B **10**, 1237 (1992), and references therein.
[2] T. Kawabata, T. Matsuda, and S. Koike, J. Appl. Phys. **56**, 2367 (1984).
[3] J. I. Pankove, Mater. Res. Soc. Symp. Proc. **162**, 515 (1990), and references therein.
[4] M. A. Khan, D. T. Olson, J. M. Van Hove, and J. N. Kuznia, Appl. Phys. Lett. **58**, 1515 (1991).
[5] K. Yung, J. Yee, J. Koo, M. Rubin, N. Newman, and J. Ross, Appl. Phys. Lett. **64**, 1135 (1994).
[6] H. Amano, T. Asahi, and I. Akasaki, Jpn. J. Appl. Phys. **29**, L205 (1990).
[7] H. Amano, T. Asahi, M. Kito, and I. Akasaki, J. Lumin. **48&49**, 889 (1991).
[8] R. Dingle, K. L. Shaklee, R. F. Leheny, and R. B. Zetterstrom, Appl. Phys. Lett. **19**, 5 (1971).
[9] I. M. Catalano, A. Cingolani, M. Ferrara, M. Lugara, and A. Minafra, Solid State Commun. **25**, 349 (1978).
[10] C. D. Wang and M. Gershenzon, Bull. APS **24**, 343 (1979).
[11] S. Nakamura, T. Mukai, and M. Senoh, Appl. Phys. Lett. **64**, 1678 (1994).
[12] X. H. Yang, J. Hays, W. Shan, W. Shan, E. Cantwell, and J. Aldridge, Appl. Phys. Lett. **59**, 1681 (1991).
[13] X. H. Yang, J. Hays, W. Shan, J. J. Song, E. Cantwell, and J. Aldridge, Appl. Phys. Lett. **60**, 926 (1992).
[14] J. J. Song and W. C. Wang, J. Appl. Phys. **55**, 660 (1984).
[15] M. Voos, R. F. Leheny, and J. Shah, in *Optical Properties of Solids*, edited by M. Balkanski (North-Holland, Amsterdam, 1980), Chap. 6.
[16] See, for example, G. P. Agrawal and N. K. Dutta, in *Semiconductor Lasers* (Van Nostrand Reinhold, New York, 1993), p. 132.
[17] A. M. Glass, K. Tai, R. B. Bylsma, R. D. Feldman, D. H. Olson, and R. F. Austin, Appl. Phys. Lett. **53**, 834 (1988).
[18] K. Nakanishi, I. Suemune, Y. Fujii, Y. Kuroda, and M. Yamanishi, Appl. Phys. Lett. **59**, 1401 (1991).

Optical studies of GaN and GaN/AlGaN heterostructures on SiC substrates

W. Shan,[a] A. J. Fischer, and J. J. Song
Center for Laser Research and Department of Physics, Oklahoma State University, Stillwater, Oklahoma 74078

G. E. Bulman, H. S. Kong, and M. T. Leonard
Cree Research, Inc., Durham, North Carolina 27713

W. G. Perry, M. D. Bremser, and R. F. Davis
Department of Materials Science and Engineering, North Carolina State University, Raleigh, North Carolina 27695

(Received 22 April 1996; accepted for publication 29 May 1996)

We present the results of spectroscopic studies on GaN based epitaxial materials on SiC substrates by metalorganic chemical vapor deposition. A variety of techniques has been used to study the optical properties of GaN epilayers and GaN/AlGaN heterostructures. Sharp spectral structures associated with the intrinsic free excitons were observed by photoluminescence and reflectance measurements from GaN based materials grown on SiC substrates. The residual strain was found to have a strong influence in determining the energies of exciton transitions. Picosecond relaxation studies of exciton decay dynamics suggest that an AlGaN cladding layer with a small mole fraction of AlN can be relatively effective in enhancing the radiative recombination rate for excitons by reducing the density of dislocations and suppressing surface recombination velocity in the GaN active layer for the GaN/AlGaN heterostructure samples. © *1996 American Institute of Physics.* [S0003-6951(96)04532-9]

GaN based wide band-gap III–V nitride semiconductors have been extensively studied for their device applications, such as high-power amplifiers, UV, blue, green, and yellow light-emitting diodes (LED's), and short-wavelength laser diodes.[1–3] Observation of optically pumped stimulated emission in GaN epifilms has led to increased interest in the development of efficient nitride UV-visible light emitters.[4,5] In fact, superbright high-efficiency blue LED's have recently been commercialized and current-injection laser diodes based on nitride heterostructures have been reported by the Nichia group.[6,7] So far, the majority of research activities, including the assessment of material properties and the development of devices, has concentrated on nitrides grown on sapphire substrates, although its lattice parameter and coefficient of thermal expansion are significantly different from that of any III nitrides. An alternative substrate material for III-nitride epitaxial growth is SiC. It has many advantages over sapphire in terms of nitride epitaxy deposition and device fabrication: close match of lattice parameters and coefficient of thermal expansion to that of III nitrides; higher thermal conductivity of SiC offers greater power handling and improved reliability; and both *n*- and *p*-type electrical conductivity can be achieved allowing vertical device structure. In this report, we present the results of optical studies of the properties of GaN epilayers and GaN/AlGaN heterostructures grown by metalorganic chemical vapor deposition (MOCVD) on 6H–SiC (0001) substrates. The effects of strain on the exciton transitions in the GaN epitaxial materials on SiC were examined and compared with those observed in the GaN epilayer on sapphire samples. The dynamics of photoexcited excess carriers in the region of near-band-edge excitonic emissions were investigated by transient luminescence spectroscopy in the picosecond regime.

Samples used in this study were all nominally undoped single-crystal films grown on (0001) 6H–SiC substrates by MOCVD. AlN buffers were deposited on the substrates before the growth of GaN. GaN layers were deposited at 1050 °C directly on the AlN buffers. The GaN/AlGaN heterostructures used in this work included both double heterostructure (DH) samples and separate confinement heterostructure (SCH) samples. The DH and SCH structures were deposited on GaN epilayers with the thickness typically around three microns. The particular DH structure under discussion has an ~800 Å thick GaN active layer, surrounded by a few thousand Å $Al_{0.1}Ga_{0.9}N$ cladding layers. The SCH structure consists of a 100 Å thick GaN quantum well, with an $Al_xGa_{1-x}N$ cladding layer and a lower mole fraction $Al_xGa_{1-x}N$ waveguide layer symmetrically locating on each side. The nominal Al compositions are 11% and 6%, respectively. Conventional photoluminescence (PL) spectra were measured with either a cw HeCd laser (325 nm) or a frequency-doubled Ar^+ laser (244 nm) as the excitation source and a 1-M double-grating monochromator connected to a photon-counting system. For reflectance measurements, the quasimonochromatic light dispersed by a $\frac{1}{2}$-M monochromator from a xenon lamp was focused on the sample, and the reflectance signals were detected using a lock-in amplification system. Time-resolved photoluminescence (TRPL) measurements were performed using a frequency tunable pulsed laser (2 ps pulse duration, 76 MHz) as an excitation source and a streak camera (2 ps resolution), in conjunction with a $\frac{1}{4}$-M monochromator as a detection system.

The GaN based samples studied in this work exhibit strong near-band-edge exciton luminescence. Results of PL spectroscopy from a 3.7-μm GaN epilayer sample are shown in Fig. 1 at selected temperatures. The intensity of the strongest emission line marked by BX in Fig. 1 was found to decrease much faster than that labeled FX as the temperature

[a]Electronic mail: wshan@osuunx.ucc.okstate.edu

 0003-6951/96/69(6)/740/3/$10.00

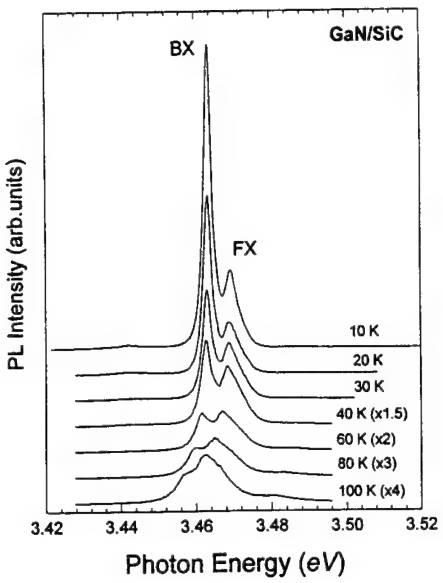

FIG. 1. Near-band-edge exciton luminescence spectra taken from a 3.7-μm GaN epilayer on SiC at selected temperatures.

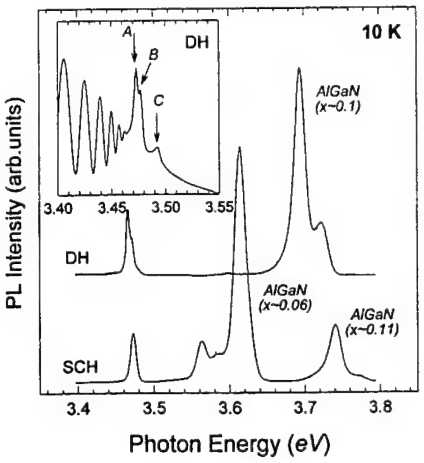

FIG. 3. 10-K PL spectra of a DH and a SCH sample grown on SiC. The inset illustrates the exciton transition signatures of the GaN active layer in the DH sample measured by reflectance spectroscopy.

increased. It became hardly resolvable at the temperatures higher than 100 K (not shown). Such variations of the luminescence intensity as a function of temperature indicate that the emission line can be attributed to the radiative recombination of excitons bound to neutral donors. The second strongest luminescence structure, together with the weak emission feature on the higher energy side, can be assigned to intrinsic free-exciton emissions. Figure 2 shows a reflectance spectrum taken from the sample at 10 K. Three exciton resonances associated with the transitions referred to as the *A*, *B*, and *C* exciton transitions[8,9] between the bottom of the conduction band (Γ_7^C) and three topmost valence band edges ($\Gamma_9^V+\Gamma_7^V+\Gamma_7^V$) are indicated by vertical arrows. The energy positions of these transitions are 3.470, 3.474, and 3.491 eV, respectively. We note that the values of the transition energies obtained here are lower than those reported in the literature,[9–11] for example, 3.485, 3.493, and 3.518 eV, for GaN on sapphire substrates.[10] Such discrepancy can be attributed to the effects of residual strain in the epilayers due to the mismatch of lattice parameters and coefficients of thermal expansion between GaN and the substrate materials.[11,12] Because of the inevitable occurrence of strain relaxation by the formation of a large density of dislocations, it is generally difficult to separate the strain effects caused by lattice-parameter mismatch from the ones involving thermal-expansion mismatch so as to exactly determine their influences on the optical properties of GaN epitaxial layers. However, by comparing the observed exciton transition energies in GaN epilayers deposited on sapphire and SiC to the values (3.4751, 3.4815, and 3.503 eV) obtained from virtually strain-free bulk GaN reported in Ref. 9, one can infer that the overall effects of residual strain generated in GaN on sapphire is compressive, which results in an increased band gap, while the stress induced in GaN on SiC is tensile, which leads to a decrease in measured exciton transition energies. Therefore, we conclude that residual strain induced by thermal-expansion mismatch in GaN based epitaxial layers has the prevailing influence on the energy variations of exciton transitions, since lattice-mismatch induced strain has a completely opposite effect on the variation of the GaN band gap.

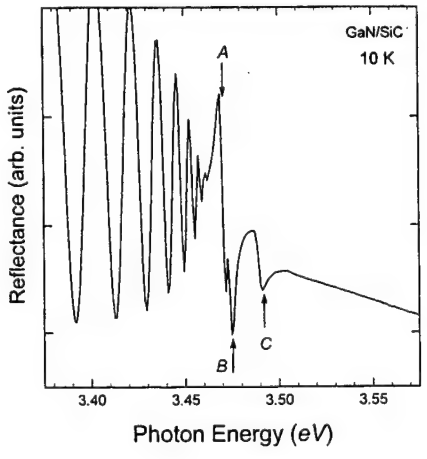

FIG. 2. Reflectance spectrum of the exciton transition region of the MOCVD GaN/SiC sample at 10 K. The oscillatory structures at lower energy are interference effects caused by the heterointerface.

Figure 3 shows the 10 K PL spectra of the DH and SCH samples. The inset highlights the signatures of intrinsic free exciton transitions observed by reflectance measurements from the GaN active layer of the DH structure. The emission peaks at the energy position around 3.47 eV in the PL spectra are exciton luminescence from the GaN active layers in these two heterostructures. The peak position of the SCH GaN active layer was found to be ~10 meV higher than that of the DH GaN layer. The blue shift might be due to quantum confinement effects. By using the envelope function approximation approach,[13] the lowest confinement energy can be readily calculated, with electron the effective mass $m^* \sim 0.2m_0$ and the hole effective mass $m^* \sim 0.8m_0$,[14] to be ~10 meV for electrons and ~3 meV for holes in a 100-Å single GaN quantum well with $Al_{0.06}Ga_{0.94}N$ barriers. This estimation is consistent with the experimental observation. The strong and relatively broad emission structures at higher

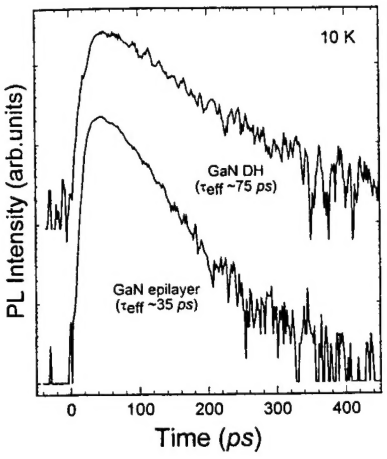

FIG. 4. Comparison of PL decay of exciton emissions in the GaN DH sample and an epilayer sample. The curves are vertically displaced for clarity.

energies are luminescence associated with AlGaN layers as labeled in the figure. The doublet spectral feature related to AlGaN alloys in the DH sample presumably arises from a small alloy concentration difference between two AlGaN cladding layers. If this is the case, the observed energy separation of ~25 meV suggests that slightly less than a 1% alloy concentration fluctuation occurred during the preparation of DH structure by MOCVD growth. However, the rather complicated spectral structure on the lower energy side of the main emission peak exhibited by the alloy waveguiding layers in the SCH sample cannot be simply assigned to the deviation in Al compositions between the two layers. This is an issue requiring further study.

We have also performed time-resolved PL measurements to study the dynamics of exciton luminescence in the GaN active layer of the DH structure. In order to avoid generating carriers in the AlGaN cladding layers and to prevent the profound effects of carrier diffusion from barrier layers into the active layer, the photon energy of the picosecond pulsed laser was tuned to very closely to the band gap of GaN with an excitation wavelength at ~345 nm. Figure 4 presents the time evolution of bound-exciton emission observed in the GaN/AlGaN DH sample, where a typical PL time-decay curve from a GaN epitaxial film taken under the same experimental conditions is also given for comparison. Both samples were deposited on SiC substrates under similar growth conditions except that the DH structure was deposited on top of one of them. As shown in the figure, the measured decay time for the bound exciton emission in the DH sample was found to be (~75 ps) twice as longer as that in the GaN epilayer (~35 ps). Recent exciton dynamic studies have revealed that the capture of excitons and trapping of carriers by nonradiative centers at defects and impurities play a major role in the recombination processes responsible for the exciton population decay in GaN samples.[15] However, it is unclear whether or not dislocations behave like nonradiative recombination centers. The results presented here suggest that dislocations most likely involve the nonradiative recombination processes. The increase in the exciton PL decay time observed in the DH sample indicates that the density of nonradiative recombination centers in the GaN active layer of the DH sample is smaller than that of the bare GaN epilayer. The AlGaN cladding layers could be a factor in the enhancement of the radiative recombination rate by reducing the density of dislocations in the GaN active layer, since it is known that a heterostructure system with built-in strain can significantly reduce the density of defects such as dislocations.[16] In addition, the deposition of a cladding layer on top of the GaN active layer could have passivated the surface states resulting in a reduction in the nonradiative recombination velocity of the photoexcited carriers on the bare surface and in its vicinity.

In conclusion, strong, sharp spectral structures associated with exciton transitions in GaN epitaxial layers and GaN/AlGaN heterostructures grown on 6H–SiC substrates by MOCVD were observed in photoluminescence and reflectance spectra. The observation of exciton transitions with lower energies in the epitaxial GaN based materials grown on SiC compared to that on sapphire substrates suggests that the GaN based epilayers on SiC substrates are subject to tensile strain, while those on sapphire substrates are under compression. The residual strain induced by lattice-parameter and thermal-expansion mismatch plays an important role in determining the exciton transition energies. In addition, our picosecond relaxation study of exciton decay dynamics suggests that for the GaN/AlGaN heterostructure samples, an AlGaN cladding layer with a small mole fraction AlN can be relatively effective in enhancing the radiative recombination rate for excitons as a result of reducing the density of dislocations and suppressing surface recombination velocity in the GaN active layer.

This work at OSU was supported by AFOSR, DARPA, ONR, and ARO. The work at CREE was supported by DARPA under Contract No. MDA972-95-C-0016. The work at NCSU was supported by ONR under Contract No. N00014-92-J-1477.

[1] J. I. Pankove, Mater. Res. Soc. Symp. Proc. **162**, 515 (1990), and references therein.
[2] S. Strite and H. Morkoç, J. Vac. Sci. Technol. B **10**, 1237 (1992), and references therein.
[3] H. Morkoç, S. Strite, G. B Gao, M. E. Lin, B. Sverdlov, and M. Burns, J. Appl. Phys. **76**, 1363 (1994).
[4] X. H. Yang, T. Schmidt, W. Shan, J. J. Song, and B. Goldenberg, Appl. Phys. Lett. **66**, 1 (1995).
[5] A. S. Zubrilov, V. I. Nikovlaev, V. A. Dmitriev, K. G. Irvine, J. A. Edmond, and C. H. Carter, Jr., Inst. Phys. Conf. Ser. **141**, 525 (1995).
[6] S. Nakamura, M. Senoh, S. Nagahama, N. Iwasa, T. Yamada, T. Matsushita, H. Kiyoku, and Y. Sugimoto, Jpn. J. Appl. Phys. **35**, L74 (1996).
[7] S. Nakamura, M. Senoh, S. Nagahama, N. Iwasa, T. Yamada, T. Matsushita, H. Kiyoku, and Y. Sugimoto, Appl. Phys. Lett. **68**, 2105 (1996).
[8] R. Dingle and M. Ilegeme, Solid State Commun. **9**, 175 (1971).
[9] B. Monemar, Phys. Rev. B **10**, 676 (1974).
[10] W. Shan, T. J. Schmidt, X. H. Yang, S. J. Hwang, J. J. Song, and B. Goldenberg, Appl. Phys. Lett. **66**, 985 (1995).
[11] B. Gil, O. Briot, and R.-L. Aulombard, Phys. Rev. B **52**, R17028 (1995).
[12] W. Rieger, T. Metzger, H. Angerer, R. Dimitrov, O. Ambacher, and M. Stutzmann, Appl. Phys. Lett. **68**, 970 (1996).
[13] G. Bastard, Phys. Rev. B **25**, 7584 (1982).
[14] *Landolt-Bornstein*, edited by O. Madelung, New Series, Group 3, Vol. 17a (Springer, Berlin, 1982).
[15] W. Shan, X. C. Xie, J. J. Song, and B. Goldenberg, Appl. Phys. Lett. **67**, 2512 (1995).
[16] Z. Liliental-Weber, H. Sohn, and J. Washburn, in *Semiconductors and Semimetals*, edited by E. R. Weber (Academic, Boston, 1993), Vol. 38, Chap. 9.

Room-temperature stimulated emission in GaN/AlGaN separate confinement heterostructures grown by molecular beam epitaxy

T. J. Schmidt, X. H. Yang, W. Shan,[a] and J. J. Song
Center for Laser Research and Department of Physics, Oklahoma State University, Stillwater, Oklahoma 74078

A. Salvador, W. Kim, Ö. Aktas, A. Botchkarev, and H. Morkoç[b]
Coordinated Science Laboratory, University of Illinois at Urbana-Champaign, Urbana, Illinois 61801

(Received 13 November 1995; accepted for publication 29 January 1996)

Strong near-ultraviolet stimulated emission was observed at room temperature in GaN/AlGaN separate confinement heterostructures (SCH) grown by molecular beam epitaxy (MBE) on sapphire substrates. The MBE grown GaN/AlGaN SCH samples exhibited stimulated emission threshold pumping powers as low as 90 kW/cm^2 at room temperature under the excitation of a frequency-tunable nanosecond laser system with a side-pumping configuration. This represents an order of magnitude reduction over bulklike GaN. Our results suggest that the carrier confinement and waveguiding effects of the SCH samples result in a substantial decrease in the stimulated emission threshold. © *1996 American Institute of Physics.* [S0003-6951(96)01913-9]

GaN based wide-band-gap group III–V nitride semiconductors have attracted a good deal of attention recently because of their potential applications in electronic and optoelectronic devices, such as high power-high efficiency amplifiers, UV, blue, green, and yellow LEDs, and, as yet to be demonstrated, short wavelength laser diodes.[1–3] With rapid progress in nitride epitaxial growth technology, high quality nitride single crystalline epitaxial layers can now be grown on sapphire and SiC substrates. Recent demonstration of superbright high-efficient violet, blue, green, and yellow LEDS based on nitride heterostructures by the Nichia group[4] and the reports on the observation of optically pumped stimulated emission in GaN epitaxial layers[5–10] have fueled an intense interest in the development of nitride based UV-visible light emitters. However, pivotal issues pertinent to optical processes in lasers have not been fully explored. In this report, we discuss our investigation of the optically pumped stimulated emission in GaN/AlGaN separate confinement heterostructures (SCH) at room temperature. The stimulated emission phenomena in the GaN/AlGaN SCH samples were investigated using a high-power pulsed laser system. Strong near-violet stimulated emissions were achieved at room temperature using a "side pumping" geometry. We observed that the pumping power required for stimulated emission is significantly lowered due to the quantum confinement and waveguiding effects of the SCH structure compared to bulklike epitaxial GaN layers.

The GaN/AlGaN separate confinement heteorstructures used in this work were grown on (0001) sapphire substrates by a modified reactive MBE at a substrate temperature near 800 °C. The particular structure under discussion has a 600 Å thick AlN layer, directly grown on sapphire, followed by a GaN buffer layer, an AlGaN cladding layer, a lower mole fraction AlGaN waveguide layer, a 70 Å thick GaN quantum well, which is capped by a low mole fraction AlGaN waveguide, and an AlGaN cladding layer. The quantum well was doped with Si to a level of 5×10^{17} cm^{-3}. Samples having a size of 3×1 mm^2 were cut and mounted on a sapphire heat sink, and then attached to a copper sample holder for optical pumping experiments. The primary optical pumping source of the experimental system consists of a frequency-tunable dye laser pumped by the second harmonic laser beam (532 nm) of a pulsed Nd:YAG laser with ~10 ns pulse width and 10 Hz repetition rate. The output of the dye laser was then frequency doubled to achieve a near-UV pumping wavelength. The laser beam was focused on the sample surface using a cylindrical lens to form a rectangular excitation spot on the sample for uniform pumping. The excitation intensity of the laser light on the sample was varied continuously using a variable neutral density filter, and the pumping power densities were recorded by a power meter. The emission signal was collected from the edge of the GaN/AlGaN SCH samples into a 1-M monochromator then detected by either a CCD camera or a photomultiplier tube in conjunction with a boxcar averager.

Figure 1 shows the room-temperature emission spectra of the GaN/AlGaN SCH samples taken at different excitation power densities. Under the conditions of low-excitation power densities, the observed spectra exhibit a relatively weak and broad emission feature with the peak position around 365 nm, and the emission intensities linearly increase with the excitation power density, showing the typical characteristic of spontaneous emission. As the excitation power density increases, a sharp, narrow emission feature appears on the higher energy side of the spontaneous emission peak. The position of the maximum of this new emission feature is ~361.5 nm. Its emission intensity increases superlinearly with the excitation power. This new emission structure becomes the dominant feature as the pumping power density is further increased. Under the conditions of high-excitation power densities, the output of the emission from the GaN SCH samples was very intense. The observations of spectral narrowing, a superlinear increase in intensity with the exci-

[a]Electronic mail: wshan@osuunx.ucc.okstate.edu
[b]On sabbatical leave at Wright Laboratories.

 0003-6951/96/68(13)/1820/3/$10.00

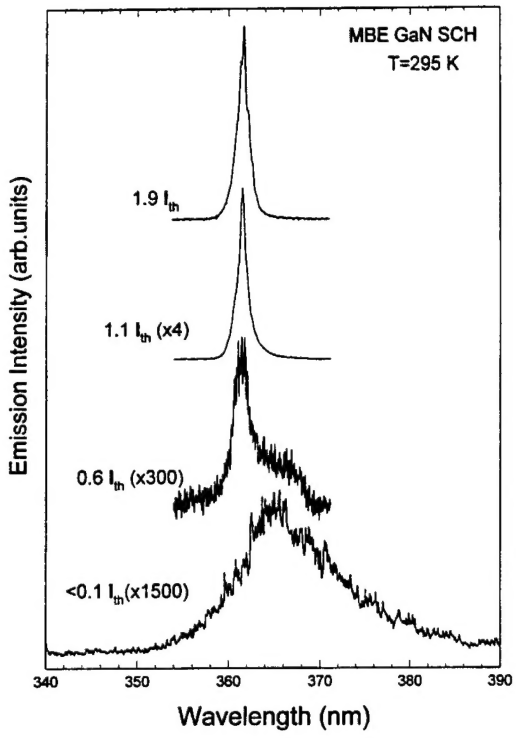

FIG. 1. Emission spectra taken from a GaN/AlGaN SCH sample at different pumping power densities. The spectra were vertically displaced for the clarification. I_{th} (=90 kW/cm^2) represents the pumping threshold for stimulated emission.

tation power density, as well as the complete suppression of the broad emission background, are of the typical characteristics of the occurrence of stimulated emission.

The onset of the steep rise of the emission intensity plotted as a function of pumping power density, shown in Fig. 2, can be defined as the threshold for stimulated emission. The inset in Fig. 2 details the drastic change in the emission intensity against excitation power density in the vicinity of the onset of stimulated emission. The pumping threshold for stimulated emission was determined to be ~90 kW/cm^2 for the GaN/AlGaN SCH samples. The measured threshold

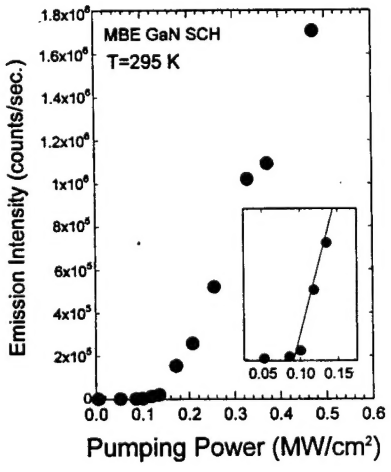

FIG. 2. The change of emission intensity as a function of pumping power density. The onset of the superlinear increase of emission intensity is defined as the pumping threshold as shown in the inset. The solid line in the inset is for guiding the eyes.

value is approximately one order of magnitude less than our previously reported value for the GaN bulklike epifilms grown by metalorganic chemical vapor deposition.[9] Generally, the threshold value can be affected by parameters which are dependent on the pumping source and sample. For a given optical pumping source, the most important influence on the threshold is from the sample itself with the threshold varying from sample to sample. This can be classified into two groups: one is associated with material properties, such as impurities, crystallinity, and defects; the other is related to the sample preparation such as, in the case of lasing studies, laser cavity length and the quality of sample edge facets. The specimens used in this optical pumping experiment were small pieces simply cut off from the large GaN/AlGaN SCH wafer with no attempt to finesse the cut surfaces. The difficulties associated with forming high quality facets with these types of materials grown on sapphire are well known. This provides a basis for our optimism that the pumping power threshold for stimulated emission and lasing in these samples can be further reduced with improved facets.

We also note that the peak position of the stimulated emission is located at a shorter wavelength compared to that of the spontaneous emission, which is contrary to the commonly observed redshift of stimulated emission in undoped bulklike epilayer materials.[5–10] The broad spontaneous emission spectral feature located at lower energy presumably corresponds to the radiative recombination processes associated with the presence of Si dopants in the GaN confinement layer. The binding energy of Si in GaN can be estimated using the hydrogenic model based on the effective mass approximation. By using the electron effective mass of $\sim 0.22 m_0$ and the dielectric constant of 9–10,[11,12] a binding energy of ~30±5 meV can be obtained. The spontaneous emission is most likely associated with the transition from the Si impurity level to the top of the valence band. At high pumping power levels, the available density of impurity levels is saturated, and the radiative combination process for the majority of photogenerated carriers will be dominated by the transition from the conduction band to the valence band. Therefore, the observed blueshift indicates that the stimulated emission indeed originates from band-to-band transitions in the GaN/AlGaN SCH samples. We should note that the band edge emission does not exhibit any discernible redshift indicative of reduced coupling to the lattice in these samples.

In summary, the pumping power threshold for stimulated emission in MBE grown GaN/AlGaN separate confinement heterostructures was found to be ~90 kW/cm^2 at room temperature, representing an order of magnitude reduction over the reported value of 800 kW/cm^2 for bulklike GaN epitaxial films. The optical pumping experiments were conducted using a frequency-tunable nanosecond laser system with a side-pumping configuration. The observed stimulated emission was evidenced through spectral narrowing and the superlinear increase of emission intensity with increased pumping power, as well as the complete suppression of spontaneous emission background. The results suggest that the carrier confinement and waveguiding effects substantially decrease the stimulated emission threshold in the GaN/AlGaN SCH samples.

This work at OSU was supported by AFOSR, ONR, ARO, and ARPA. The work at UIUC was supported by grants from ONR, AFOSR, and BMDO. H. M. is funded by a University President Research Program funded by AFOSR.

[1] J. I. Pankove, Mater. Res. Soc. Symp. Proc. **162**, 515 (1990).
[2] S. Strite and H. Morkoç, J. Vac. Sci. Technol. B **10**, 1237 (1992).
[3] H. Morkoç, S. Strite, G. B. Gao, M. E. Lin, B. Sverdlov, and M. Burns, J. Appl. Phys. **76**, 1363 (1994).
[4] S. Nakamura, J. Vac. Sci. Technol. A **13**, 705 (1995).
[5] H. Amano, T. Asahi, and I. Akasaki, Jpn. J. Appl. Phys. **29**, L205 (1990).
[6] H. Amano, T. Asahi, M. Kito, and I. Akasaki, J. Lumin. **48&49**, 889 (1991).
[7] M. A. Khan, D. T. Olson, J. M. Van Hove, and J. N. Kuznia, Appl. Phys. Lett. **58**, 1515 (1991).
[8] K. Yung, J. Yee, J. Koo, M. Rubin, N. Newman, and J. Ross, Appl. Phys. Lett. **64**, 1135 (1994).
[9] X. H. Tang, T. Schmidt, W. Shan, J. J. Song, and B. Goldenberg, Appl. Phys. Lett. **66**, 1 (1995).
[10] A. S. Zubrilov, V. I. Nikovlaev, V. A. Dmitriev, K. G. Irvine, J. A. Edmond, and C. H. Carter, Jr., Inst. Phys. Conf. Ser. **141**, 525 (1995).
[11] *Landolt-Bornstein*, edited by O. Madelung, New Series, Group 3, Vol. 17a (Springer, Berlin, 1982).
[12] D. C. Reynolds, D. C. Look, W. Kim, Ö. Aktas, A. Botchkarev, A. Salvador, H. Morkoç, and D. N. Talwar (unpublished).